On model and measurement uncertainty in predicting land surface carbon fluxes

Hanna Post

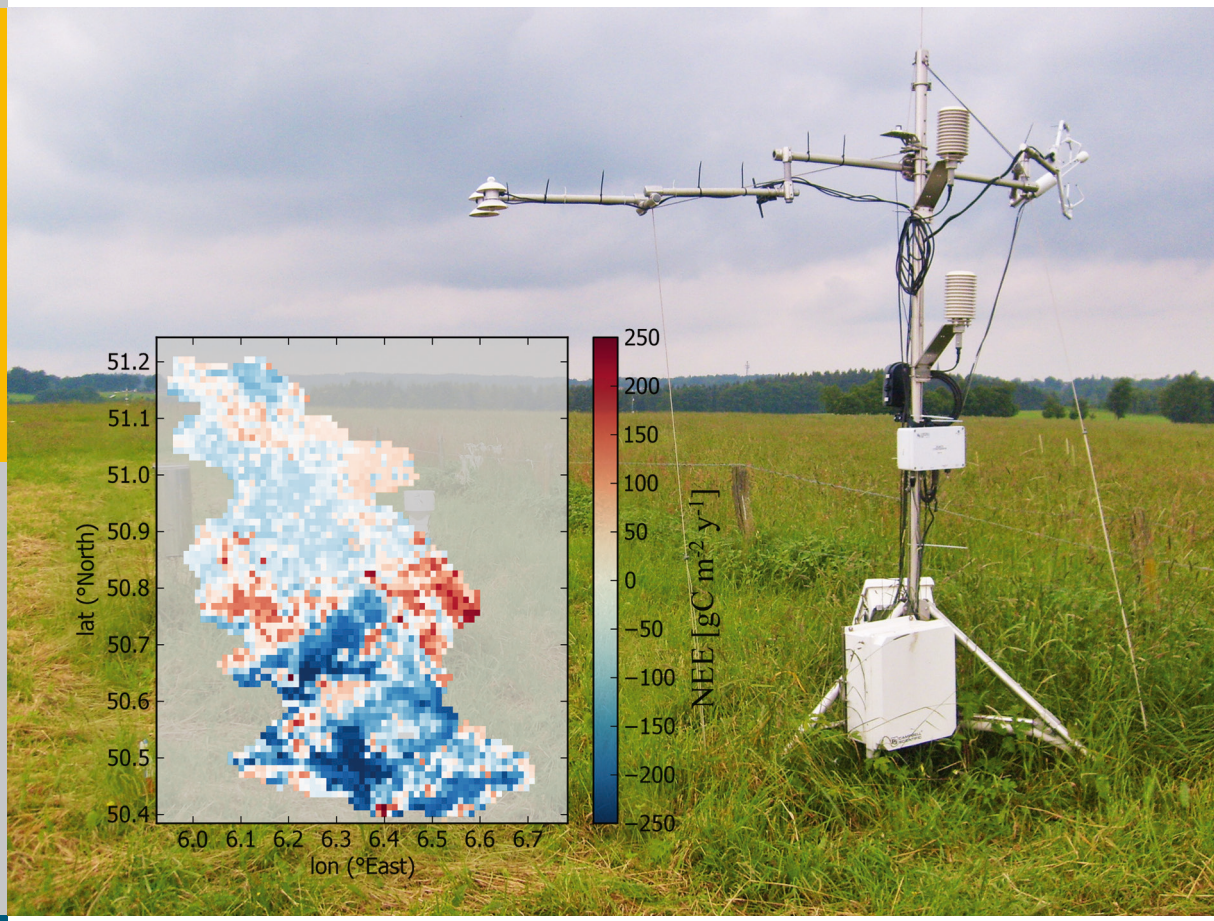

Member of the Helmholtz Association

Energie & Umwelt / Energy & Environment
Band / Volume 347
ISBN 978-3-95806-190-3

JÜLICH
FORSCHUNGSZENTRUM

Schriften des Forschungszentrums Jülich
Reihe Energie & Umwelt / Energy & Environment Band / Volume 347

Forschungszentrum Jülich GmbH
Institute of Bio- and Geosciences
Agrosphere (IBG-3)

On model and measurement uncertainty in predicting land surface carbon fluxes

Hanna Post

Schriften des Forschungszentrums Jülich
Reihe Energie & Umwelt / Energy & Environment Band / Volume 347

ISSN 1866-1793 ISBN 978-3-95806-190-3

Bibliographic information published by the Deutsche Nationalbibliothek.
The Deutsche Nationalbibliothek lists this publication in the Deutsche
Nationalbibliografie; detailed bibliographic data are available in the
Internet at http://dnb.d-nb.de.

Publisher and Distributor: Forschungszentrum Jülich GmbH
Zentralbibliothek
52425 Jülich
Tel: +49 2461 61-5368
Fax: +49 2461 61-6103
Email: zb-publikation@fz-juelich.de
www.fz-juelich.de/zb

Cover Design: Grafische Medien, Forschungszentrum Jülich GmbH

Printer: Grafische Medien, Forschungszentrum Jülich GmbH

Schriften des Forschungszentrums Jülich
Reihe Energie & Umwelt / Energy & Environment, Band / Volume 347

D 82 (Diss. RWTH Aachen University, 2016)

ISSN 1866-1793
ISBN 978-3-95806-190-3

The complete volume is freely available on the Internet on the Jülicher Open Access Server (JuSER)
at www.fz-juelich.de/zb/openaccess.

Contents

List of Tables

List of Figures

List of Acronyms

CLM	Community Land Model
DREAM	DiffeRential Evolution Adaptive Metropolis
DE-Gri	Grillenburg (FLUXNET site in Germany)
DE-Hai	Hainich (FLUXNET site in Germany)
DE-Kli	Klingenberg (FLUXNET site in Germany)
EBD	energy balance deficit
EC	eddy covariance
FR-Fon	Fontainebleau site (FLUXNET site in France)
LAI	leaf area index
LSMs	land surface models
MAD	mean absolute difference
MAPs	maximum a posteriori estimates
MCMC	Markov Chain Monte Carlo
ME	Merzenhausen (EC tower site in Germany)
NDVI	Normalized Differenced Vegetation Index
NEE	Net Ecosystem Exchange of CO_2 between the land surface and the atmosphere
NEE_{corr}	NEE corrected for systematic flux differences to estimate the NEE uncertainty with the extended two-tower approach
RMSE	root mean square error
RO	Rollesbroich (EC tower site in Germany)
s-	season-based
PAR	photosynthetically active radiation
pdf	probability distribution function
PFT	plant functional type
PPFD	photosynthetically active photon flux density
SE	Selhausen (EC tower site in Germany)
sfd	systematic flux differences
SI	solar irradiance
WÜ	Wüstebach (EC tower site in Germany)

Abstract

The Net Ecosystem Exchange (NEE) of CO_2 between the land surface and the atmosphere refers to the difference of photosynthetic CO_2 uptake and CO_2 release via ecosystem respiration. NEE is an important indicator for the net carbon source or sink function of an ecosystem and a crucial variable for understanding and predicting feedback mechanisms between climate and ecosystem change. NEE is typically measured by micrometeorological methods like eddy covariance (EC). At continental or global scales, land surface models (LSMs) such as the Community Land Model (CLM) are commonly used to predict NEE and other fluxes by simulating the coupled carbon, nitrogen, water and energy cycle of the land surface. In order to support future decision making in climate politics and environmental planning, it is important to improve LSM carbon flux predictions at regional scales. A central goal of this PhD work was therefore to combine measured EC data and CLM to estimate NEE for the Rur catchment area.

For the last decade, model-data fusion approaches like parameter estimation have increasingly been applied to reduce the uncertainty of carbon flux estimates, because both EC measurements and LSM predictions are uncertain. In order to use EC data in meaningful model-data fusion or LSM evaluation approaches, an estimate of the measurement uncertainty is required. Thus, in the first part of the thesis, the NEE measurement uncertainty was studied for one grassland site in Germany located in the Rur catchment. At present, many uncertainty estimation approaches exist, but none are generally accepted and applied. The classical two-tower approach, which is based on the standard deviations of the fluxes measured simultaneously at two nearby EC towers, is one of the most well-known approaches. It provides linear regression functions between the flux magnitude and the random error, which are commonly adopted by scientists for a fast estimation of the random error. In previous studies, the (classical) two-tower approach has yielded robust uncertainty estimates, but care must be taken to meet the often competing requirements of statistical independence (non-overlapping footprints) and ecosystem homogeneity when choosing an appropriate tower distance. Thus, an extension of the classical two-tower approach is proposed here that corrects systematic differences of the NEE fluxes measured synchronous at the two EC tower stations. The role of the tower distance was investigated with help of a roving station separated between 8 m and 34 km from a permanent EC grassland station. For evaluation, uncertainty estimates obtained from a different, raw-data based method were used as reference. The herein introduced correction for systematic flux differences applied to weather-filtered data substantially reduced the overestimation of the two-tower based NEE measurement uncertainty for all distances (except 8 m) by 79% (34 km distance) to 100% (95 m distance). Results indicated that the sensitivity of the two-tower approach to the tower distance was reduced, which enhances the applicability of the extended two-tower approach.

In the second part, NEE data measured at EC sites inside or close to the Rur catchment were used to estimate eight key ecological CLM parameters with the Markov Chain Monte Carlo (MCMC) method DREAM (DiffeRential Evolution Adaptive Metropolis). Parameters were estimated separately for four sites of different land use types: C3-grass, C3-crop, broadleaf deciduous trees, and evergreen needleleaf trees. These are the most widespread plant functional types (PFTs) in the Rur catchment. Five of the estimated parameters are PFT-specific, the other three are constants in the model. Parameters were estimated separately for a one year period and for the single seasons within that year. For the one year period, an additional experiment was conducted where four multiplication factors for the initial model states (carbon-nitrogen pools and leaf area index LAI), were estimated jointly with the eight parameters. The parameter estimates were evaluated with measured NEE from four additional sites located in about 600 km distance to the original sites. It was shown that parameters varied seasonally, which was related to the finding of correlations between the CLM parameters and the initial state factors.

The new parameter values considerably improved simulated NEE, especially if estimated on seasonal basis. In that case, the relative difference of the annual NEE sum (modeled versus observed, averaged over all sites) was 50% lower than for the reference run with default parameters. A major conclusion was that parameter estimates were most robust for the forest PFTs (in time and in space), but also compensated for model structural errors, particularly in case of C3-grass and C3-crop.

In the third and final part of this thesis, new CLM ecosystem parameters were estimated and evaluated for the Rur catchment. A difference to the former study was that now only five PFT-specific parameters were estimated. The parameters were then applied to all grid cells in the Rur catchment, which are covered by at least one of the four PFTs. The parameter estimates were evaluated using measured NEE data from seven EC sites within the Rur catchment. In addition, LAI predictions were evaluated using RapidEye data. A central result was that DREAM-CLM parameter estimates reduced the difference between the observed and simulated NEE sum of the evaluation period (Dec. 2012 – Nov. 2013) by 23% compared to the default parameters. Therefore, it was concluded that parameter estimates can provide a more reliable CLM estimate of the annual NEE balance for the catchment than global default parameters. Besides, the consistency of observed and modeled LAI data was on average 59% higher with estimated parameters. This work highlights how strongly CLM parameters, model states like LAI and the predicted carbon fluxes are linked. It was shown that for C3-grass and C3-crop, predicted LAI and NEE values were much more sensitive to perturbed initial conditions and perturbed atmospheric input data compared to forest. This resulted in substantial standard deviations (STD) of the modeled annual NEE sum ranging between 24.1 and 225.9 gC m^{-2} y^{-1}, compared to STD = 0.1 – 3.4 gC m^{-2} y^{-1} (effect of parameter uncertainty only, without additional perturbation of initial states and meteorological forcings). In contrast, the STD for the coniferous forest sites was < 3.1 gC m^{-2} y^{-1} in both cases. In this respect it is suggested to further investigate the effect of the length of the perturbed spin-up with uncertain parameters (and uncertain initial states). It was concluded that a better model representation of PFT-specific processes such as plant phenology and crop management is required to further enhance parameter estimation results and the reliability of CLM carbon flux predictions for this catchment, which is representative for many agriculturally dominated regions in central-west Europe.

Zusammenfassung

Der netto CO_2-Austausch zwischen terrestrischen Ökosystemen und der Atmosphäre (NEE) ist die Differenz von der CO_2-Aufnahme durch Photosynthese und der CO2-Emission durch Respiration. NEE ist ein wichtiger Indikator für die Ökosystemfunktion als Kohlenstoffquelle oder –senke und eine zentrale Variable für das Verständnis und die Vorhersage von Rückkopplungseffekten zwischen Klima- und Ökosystemveränderungen. NEE wird üblicherweise durch mikrometeorologische Methoden wie Eddy-Kovarianz (EC) gemessen. Auf kontinentalen oder globalen Skalen werden Landoberflächenmodelle (LSMs) wie das Community Land Model (CLM) für die Vorhersage von NEE und anderen Flüssen angewendet, unter Simulation des gekoppelten Kohlenstoff-, Stickstoff-, Wasser-, und Energiekreislaufes der Landoberfläche. Die Verbesserung von NEE-Vorhersagen auf regionalen Skalen ist wichtig für die Unterstützung der zukünftigen Entscheidungsfindung in Klimapolitik und Umweltplanung. Ein zentrales Ziel dieser Dissertation war daher die Abschätzung von NEE-Flüssen für das Rureinzugsgebiet, welches repräsentativ ist für viele Agrarland-dominierte Regionen in Mittelwesteuropa, durch Kombination von gemessenen EC Daten und CLM. Da sowohl EC-Messungen als auch LSM-Vorhersagen unsicher sind, werden seit einer Dekade zunehmend „model-data fusion“ Methoden wie Parameterabschätzung verwendet, um die Unsicherheiten von Kohlenstoffflüssen zu verringern. Um EC-Daten im Bereich „model-data fusion“ oder für die Bewertung von Landoberflächenmodellen sachgemäß anzuwenden, ist eine Abschätzung der Messunsicherheit erforderlich.

Dementsprechend wurde im ersten Teil der Dissertation die NEE-Messunsicherheit für einen Graslandstandort im Rureinzugsgebiet untersucht. Es gibt zwar viele Ansätze zur Abschätzung dieser Messunsicherheit, jedoch hat sich bislang keiner für eine breite Anwendung durchgesetzt. Die klassische „two-tower“ Methode, die auf der Standardabweichung der simultan an zwei benachbarten Türmen gemessenen Flüsse basiert, ist einer der bekanntesten Ansätze. Diese Methode liefert lineare Regressionsfunktionen zwischen der Flussmagnitude und dem Zufallsfehler, die üblicherweise von Wissenschaftlern für eine schnelle Abschätzung der Messunsicherheit übernommen werden. In vorherigen Studien hat die (klassische) „two-tower“ Methode robuste Ergebnisse geliefert. Aufgrund der häufig widersprüchlichen Voraussetzungen von statistischer Unabhängigkeit (nicht überlappender Footprint) und homogenen Bedingungen ist jedoch Vorsicht geboten in Bezug auf die Wahl einer angemessenen Distanz der zwei Türme. Aus diesem Grund wird hier eine Erweiterung der klassischen „two-tower“ Methode vorgeschlagen, die systematische Unterschiede des synchron von zwei EC-Stationen gemessenen NEE-Flusses korrigiert. Der Einfluss der Distanz zwischen den Stationen wurde mittels einer variablen Station untersucht, welche in Abständen von 8 m bis 34 km von der permanenten EC-Station auf Grasland installiert wurde. Für die Evaluierung wurden Unsicherheitswerte von einer rohdatenbasierenden Referenzmethode verwendet. Die hier eingeführte Korrektur von systematischen Flussdifferenzen, angewendet auf wettergefilterte Daten, hat für alle Distanzen (außer 8 m) deutlich die Überschätzung der „two-tower“ basieren NEE-Messunsicherheit vermindert (79% bei 34 km Distanz bis 100% bei 95 m Distanz). Die Ergebnisse haben gezeigt, dass die Sensitivität der „two-tower“ Methode gegenüber der Distanz reduziert wurde, welches mit einer verbesserten Anwendbarkeit der erweiterten Methode verbunden ist.

Im zweiten Teil wurden NEE-Daten verwendet, die an EC-Standorten innerhalb oder nahe des Rureinzugsgebietes gemessen wurden, um acht ökologische CLM-Schlüsselparameter abzuschätzen. Dazu wurde die Markov Chain Monte Carlo (MCMC) Methode DREAM (DiffeRential Evolution Adaptive Metropolis) verwendet. Die Parameter wurden separat für vier EC-Standorte mit unterschiedlichen Landnutzungen abgeschätzt: C3-Gras, C3-Getreide,

Laubwald und Nadelwald. Dies sind die weitverbreitetsten Pflanzenfunktionstypen (PFTs) im Rureinzugsgebiet. Fünf der abgeschätzten Parameter sind PFT-spezifisch, die anderen drei sind Modelkonstanten. Die Parameter wurden separat für eine Einjahresperiode durchgeführt, sowie für die einzelnen Jahresseiten innerhalb dieses Jahres. Im Falle der Einjahresperiode wurde ein zusätzliches Experiment durchgeführt, bei dem Multiplikationsfaktoren für CLM-Anfangsbedingungen (Kohlenstoff-Stickstoff-Pools und Blattflächenindex, LAI) gemeinsam mit den Parametern abgeschätzt wurden. Die abgeschätzten Parameter wurden mit gemessenen NEE-Daten von vier weiteren EC-Standorten evaluiert, die etwa 600 km von den Ursprungsstandorten entfernt waren. Es wurde gezeigt, dass die Parameter saisonal variieren, welches mit den ermittelten Korrelationen zwischen CLM-Parametern und den Anfangszustandsfaktoren zusammenhängt. Die neuen Parameterwerte haben die NEE-Vorhersagen deutlich verbessert, insbesondere wenn sie auf saisonaler Basis abgeschätzt wurden. In diesem Fall war die relative Differenz der NEE-Jahressumme (modelliert vs. beobachtet, gemittelt über alle Standorte) 50% geringer im Vergleich zum Referenzlauf mit Standardparametern. Eine wesentliche Schlussfolgerung war, dass die abgeschätzten Parameter im Falle der Wald-PFTs (in Zeit und im Raum) robust waren, aber auch strukturelle Modellfehler kompensiert haben, insbesondere im Falle von C3-Gras und C3-Getreide.

Im dritten und letzten Teil dieser Dissertation wurden neue CLM-Ökosystemparameter abgeschätzt und für das Rureinzugsgebiet evaluiert. Ein Unterschied zur vorherigen Studie war, dass diesmal nur die fünf PFT-spezifischen Parameter abgeschätzt wurden. Die Parameter wurden anschließend auf alle Rasterzellen des Rureinzugsgebietes angewendet, in welchen mindestens eine der vier PFTs vorkam. Die abgeschätzten Parameter wurden mit NEE-Daten evaluiert, die auf sieben EC Standorten im Rureinzugsgebiet gemessen wurden. Zusätzlich wurden LAI-Vorhersagen mittels RapidEye-Daten evaluiert. Ein zentrales Ergebnis war, dass die abgeschätzten DREAM-CLM-Parameter die Differenz zwischen der beobachteten und der simulierten NEE-Summe der Evaluierungsperiode (Dez. 2012 – Nov. 2013) um 23% reduziert haben, verglichen zu den Standardparametern. Daher wurde geschlussfolgert, dass die CLM-Abschätzung der NEE-Jahresbilanz mit den abgeschätzten Parametern verlässlicher ist als mit globalen Standardparametern. Außerdem war die Übereinstimmung von beobachteten und modellierten LAI-Daten mit abgeschätzten Parametern durchschnittlich 59% höher. Diese Arbeit verdeutlicht, wie stark CLM-Parameter, Modellzustände wie LAI und Kohlenstoffflussvorhersagen verknüpft sind. Es wurde gezeigt, dass die LAI- und NEE-Vorhersagen für C3-Gras und C3-Getreide wesentlich sensitiver gegenüber unsicherer Anfangszustände und atmosphärischer Inputdaten waren im Vergleich zu Wald. Dies führte zu deutlichen Standardabweichungen (STD) der modellierten NEE-Jahressumme, welche zwischen 24.1 und 225.9 gC m^{-2} y^{-1} schwankte, im Vergleich zu STD = 0.1 – 3.4 gC m^{-2} y^{-1} (nur Effekt der Parameterunsicherheit, ohne zusätzliche Störung von CLM Anfangszuständen und meteorologischen Inputdaten). Es wurde geschlussfolgert, dass eine bessere Modeldarstellung PFT-spezifischer Prozesse wie Pflanzenphänologie und landwirtschaftliches Management notwendig ist, um Ergebnisse der Parameterabschätzung und die Verlässlichkeit der CLM-Kohlenstoffflussvorhersagen für das Einzugsgebiet weiter zu verbessern.

Chapter 1: Introduction

Reliable estimates of net ecosystem exchange (NEE) are essential for environmental research and political decision making, e.g. to reduce the uncertainty of predicted climate trends. NEE, the net CO_2 flux between terrestrial ecosystems and the atmosphere, is the difference between the CO_2 release by ecosystem respiration and the CO_2 uptake by plants during photosynthesis or gross primary production (GPP) (Baldocchi, 2003). In the field, NEE is measured by eddy covariance (EC) stations along with the sensible and the latent heat flux and various meteorological variables. The global EC tower network FLUXNET comprises over 650 sites of different land cover types (http://fluxnet.ornl.gov/). Eddy covariance flux measurements are prone to various error sources. For example, one basic assumption of the EC method is a fully developed turbulence in the lower atmospheric boundary layer (Baldocchi, 2001). This assumption is not always met, particularly during night when wind velocities are low, such that nighttime data is often rejected for further analysis (Barr et al., 2006). For this and other reasons, measured NEE time series usually contain many gaps. However, the estimated annual NEE sums and net carbon balances require complete NEE time series. Thus, various studies applied and enhanced gap filling techniques including non-linear regression methods (e.g. Falge et al., 2001; Hollinger et al., 2004) or artificial neural networks (ANNs) (Papale and Valentini, 2003; Moffat et al., 2007). While most of those methods succeed in generating consistent estimates of annual NEE sums, the reliability of nighttime data remains low (Moffat et al., 2007). In terms of measured EC fluxes, a distinction is made between systematic errors, which are mostly corrected during EC data processing, and random errors or uncertainties, which can be quantified and characterized by probability distribution functions but are impossible to correct (Dragoni et al., 2007; Aubinet et al., 2011; Richardson et al., 2012). Depending on the height of the measurement devices and other factors such as wind velocities and atmospheric stability, the along-wind distance of an EC flux footprint ranges from about 500 m to more than 1.5 km (Rannik et al., 2012). Thus, EC flux measurements are usually limited to a relatively small area. Chen et al. (2012) showed that the 90% cumulative annual footprint area of 12 EC towers located at Canadian sites (with different land cover including grassland and forest) varied between 1.1 km^2 to 5.0 km^2, and that the representativeness of EC fluxes strongly depends on the land surface heterogeneity. Because the effect of the different environmental drivers on biogeochemical fluxes is spatially and temporally highly variable and nonlinear, conventional interpolation methods are not suited to upscale NEE from the EC footprint scale to larger areas (Chen et al., 2009; Stoy et al., 2009). Errors in measured EC time series and the low spatial

density of EC stations further limit the possibilities to upscale NEE with sorely data-based approaches. In order to obtain complete time series of spatially distributed NEE data for larger areas, terrestrial ecosystem models or land surface models are crucial.

Land surface models (LSMs) such as the Community Land Model CLM (Oleson et al., 2013) simulate the coupled carbon, nitrogen, water and energy cycles of the land surface, and with it key processes which determine carbon, latent heat (LE) and sensible heat (H) fluxes between terrestrial ecosystems and the atmosphere, including transpiration, evaporation, photosynthesis and respiration. LSMs are a critical component of larger integrated models (Earth system models, prognostic global climate models), which are used to predict future changes of the earth system, including land, ocean, and atmosphere (IPCC, Stocker et al., 2013). CLM for example is the land component of the Community Earth System Model (CESM). Thus, LSMs are essential to understand and predict climate-ecosystem interactions and feedbacks as well as the effect of land use change. In this context a major question to be answered is how the land carbon sink – including vegetation dynamics and soil carbon stocks – changes with climate and land use change (e.g. Quéré et al., 2012; Arora et al., 2013; Brovkin et al., 2013; Todd-Brown et al., 2014). In contrast to several other LSMs, CLM is an open source model, sponsored by the National Science Foundation and the U.S. Department of Energy. It is maintained by the National Center for Atmospheric Research (NCAR), and embedded in a continuous development process of a large user community. At present, CLM and other LSM have mainly been applied at global or continental scales with a coarse spatial resolution between about 0.25° and 1.5° (e.g. Stöckli et al., 2008; Bonan et al., 2011; Lawrence et al., 2012). In case of CLM, the respective standardized input data are available online. The estimation of carbon fluxes for single regions is essential to improve the understanding and predictability of CO_2 dynamics and their drivers (Desai et al., 2008). However, regional scale applications of LSMs are very rare, not least because high resolution input data is often not available, and, because the implementation of a new model set-up to a specific region is relatively time consuming. Han et al. (2014) for example applied CLM on a regional scale in a data assimilation study with focus on soil moisture using synthetic data. Regional studies with focus on carbon fluxes are not published yet.

LSM predictions of carbon fluxes and stocks are still subject to a high degree of uncertainty due to (i) model structural deficits related to an imperfect and incomplete model representation of the biogeochemical processes (Todd-Brown et al., 2012; Foereid et al., 2014), (ii) poorly constrained model parameters (Abramowitz et al., 2008; Beven and Freer, 2001; Todd-Brown et al., 2013), (iii) errors in the representation of initial states which are generated via the model

spin-up (Carvalhais et al., 2010; Kuppel et al., 2012), as well as (iv) errors in both atmospheric and land surface input data. Equifinality, i.e. multiple optimal parameter sets that generate equally good model outputs, was identified as a major source of errors in simulated land surface fluxes including NEE (Schulz et al., 2001; Williams et al., 2009; Luo et al., 2009; Todd-Brown et al., 2013). Equifinality increases with model complexity and increasing number of model parameters, and is therefore common in land surface models (Beven and Freer, 2001; Santaren et al., 2007).

In order to reduce the impact of uncertainties in both models and observed data, model-data fusion approaches have increasingly been applied since a decade to study "terrestrial carbon fluxes at different scales" (Wang et al., 2009) and to reduce the uncertainty of carbon flux predictions. The major model-data fusion approaches that have been used to improve modeled land surface fluxes with EC data are (i) Bayesian global search algorithms based on a random generator such as the Markov Chain Monte Carlo (MCMC) Method (Braswell et al., 2005; Knorr and Kattge, 2005; Richardson et al., 2010b; Keenan et al., 2012b; Hararuk et al., 2014), (ii) approaches based on gradient descent algorithms including variational data assimilation methods (Wang et al., 2001; Wang, 2007; Santaren et al., 2007; Verbeeck et al., 2011; Kuppel et al., 2012), and (iii) sequential data assimilation methods (Williams et al., 2005; Mo et al., 2008; Hill et al., 2012). In contrast to the other two methods, sequential data assimilation approaches such as the ensemble Kalman filter method (Evensen, 2003) assimilate the observed data sequentially and accordingly update the model state vector, which may or may not include parameters. Only the gradient-based studies estimated parameters for more complex LSMs similar to CLM, while most of the model-data fusion studies constrained simple ecosystem models. Wang et al. (2001) estimated three or four parameters of the CSIRO Bioshere Model (CBM), including the maximum rate of carboxylation and electron transport at 25°C (V_{cmax25}, and j_{max25}, respectively) using NEE, LE and ground heat flux data of several weeks measured at six EC sites. The approach by Wang (2007) is very similar. They found that V_{cmax25} and j_{max25} vary seasonally for deciduous forest and that CBM with optimized parameters predicted NEE and LE fluxes "quite well". Santaren et al. (2007), Verbeeck et al. (2011) and Kuppel et al. (2012) estimated parameters of the ORCHIDEE model (Krinner et al., 2005), also using EC data and a gradient-based algorithm that minimizes a cost function, i.e. the model-data misfit. Santaren et al. (2007) optimized 12 ORCHIDEE parameters for a pine forest site in France and found that parameters related to photosynthesis and energy balance can be robustly inferred from the EC flux data, while biological parameters controlling respiration are poorly constrained and remain strongly sensitive to the initial carbon pools settings. Verbeeck et al.

(2011) estimated parameters for one site in the Amazon forest and found that soil depth and root profile parameters significantly improved both simulated NEE and LE. Kuppel et al. (2012) estimated 21 ORCHIDEE parameters with measured NEE and LE data from twelve temperate deciduous broadleaf forest sites, comparing a "multi-site" (MS)-optimization, i.e. assimilating data from several sites simultaneously, and a "single-site" optimization conducted separately for each site. They show that MS-optimization reduces model-data misfit as well as single site optimization. Kuppel et al. (2014) extended this optimization approach to seven groups of PFTs in order to improve global scale NEE and LE predictions with ORCHIDEE. They found largest reductions of the model-data misfit for temperate and boreal broadleaf forests, and in case of temperate needleleaf forest and C3-grass, single-site optimization reduced the misfit more than MS-optimization. Kuppel et al. (2013) explored the structure of the observation error (defined here as sum of the model error and the measurement error) on simulated land surface fluxes with parameter optimized with NEE data of 12 temperate deciduous broadleaf forest sites. Santaren et al. (2013) assimilated several years of NEE and LE for the temperature beach forest site Hesse in France, to estimate ORCHIDEE parameters. They compared a gradient-based algorithm and a generic stochastic search algorithm and showed that single site model-data fusion provided better results with the generic Monte Carlo-based method. The different studies show that complex LSMs can be successfully constrained with EC data. However, it is highlighted that only a few model parameters can be well constrained and substantially reduce misfit between observed and simulated NEE and LE fluxes (Wang et al., 2001; Verbeeck et al., 2011). Most model-data fusion studies for carbon flux estimation focus on single forest ecosystems (Braswell et al., 2005; Williams et al., 2005; Santaren et al., 2007; Keenan et al., 2012b; Mo et al., 2008; Verbeeck et al., 2011; Kato et al., 2012; Kuppel et al., 2012, 2013; Rosolem et al., 2013; Santaren et al., 2013). Regional scale model-data fusion approaches to improve carbon flux estimates are very rare. Xiao et al. (2014) applied a simple ecosystem model at the regional scale and used a MCMC method to estimate the effect of parameter uncertainty on the modeled carbon fluxes for different plant functional types. Similar parameter estimation approaches for CLM have not been published yet.

Several attempts have been made to estimate the uncertainty of modeled carbon fluxes or stocks by combining different land surface models (Huntzinger et al., 2012; Piao et al., 2013; Fisher et al., 2014). However, attempts to analyze and quantify the uncertainty of carbon flux estimates for single LSMs under consideration of the different model error sources are very rare. Most of the cited model-data fusion approaches sorely consider parameter uncertainty, which leads to

an underestimation of the total model uncertainty. It was shown that LSM parameter estimates are not constant over time but vary seasonally and inter-annually (Wang et al., 2007; Mo et al., 2008; Rosolem et al., 2013). This highlights that uncertainty of parameters is related to deficits in the model structure and uncertain model states (Carvalhais et al., 2010; Kuppel et al., 2012). Therefore, single contributions of different error sources to the overall uncertainty in predicted NEE are difficult to quantify. For example, Keenan et al. (2012b) showed that the leaf area index (LAI) and the parameter V_{cmax25} are closely linked in the forest ecosystem model "FöBAAR". In CLM, V_{cmax25} is also a key parameter for both carbon flux predictions and the prognostic simulation of the LAI , and was found to be highly uncertain (Bonan et al., 2011; Göhler et al., 2013). Williams et al. (2009) show that the discussed model error sources (parameter uncertainty, initial states, spatial and temporal variations of parameters, etc.) are major challenges also when improving land surface models with EC data using model-data fusion techniques.

Against this background, this work is aiming at combining the Community Land Model (CLM) and measured EC data in order to obtain regional NEE estimates for the Rur catchment under consideration of both measurement and model uncertainty. Therefore, CLM version 4.5 in active biogeochemistry (BGC) mode (CLM4.5BGC) was applied. The Rur catchment is located in the Belgian-Dutch-German border region. Like many areas in Europe, the catchment is predicted to encounter an increase of mean annual temperature and a decrease of freezing days in the future. Associated with climate change, vegetation periods are expected to start earlier and to prolong later ("Regionaler Klimaatlas Deutschland.," 2015). This would also affect the regional carbon balance (e.g. higher CO_2 uptake by GPP versus extra CO_2 emissions due to increased respiration rates) and imply feedbacks on meteorological and hydrological processes (e.g. evapotranspiration). Accordingly, reliable estimates of present carbon balances at regional scales are crucial for environmental management and political decision making. Because global default parameters in LSMs are uncertain and cannot be assumed valid for specific locations or regions, they require careful estimation if the model is applied for new sites or areas. A suitable parameter estimation approach, which has been successfully applied in many research fields including ecohydrology (Dekker et al., 2012), and biogeochemistry (e.g. Dumont et al., 2014; Scharnagl et al., 2010), is the "DiffeRential Evolution Adaptive Metropolis" DREAM (Vrugt and Robinson, 2007; Ter Braak and Vrugt, 2008; Laloy and Vrugt, 2012; Vrugt, 2016). DREAM is a multi-chain MCMC method. Because high dimensional nonlinear models like CLM are likely to suffer from complex posterior multivariate parameter distributions (Beven

and Freer, 2001; Williams et al., 2009; Vrugt, 2016), DREAM has several crucial advantages compared to e.g. gradient-based methods, for example because it is much less prone to become stuck in a local minimum during the optimization process (Santaren et al., 2007; Williams et al., 2009). Sequential data assimilation methods have only been successfully applied yet to estimate carbon fluxes with simple ecosystem models (Williams et al., 2005; Mo et al., 2008; Hill et al., 2012) or to estimate model states like soil moisture with complex LSMs, including CLM (Han et al., 2014). The Data Assimilation Research Testbed DART (Anderson et al., 2009) provided by NCAR is coupled to CLM and allows for the estimation of model states with EC data. However, for climate applications it is important to estimate the uncertain and unknown ecosystem parameters in order to correct long-term projections of NEE. Besides, as highlighted e.g. by Hill et al. (2012), sequential data assimilation benefits from longer measurement time series in order to obtain stable estimates, while MCMC-based estimates are less dependent on the length of the time series. The fact that long measurement time series were not available for the EC sites in the Rur catchment was another reason why DREAM was considered most suited to estimate CLM parameters for the Rur catchment. A main reason, why MCMC-based approaches have not been applied yet to estimate LSM parameters is the high computational demand of this method.

The objectives of this work were to:

1. determine and increase the reliability of the uncertainty estimates of eddy covariance NEE measurements, which is an important prerequisite for using EC data in a model-data fusion approach;
2. Couple DREAM with CLM, i.e. develop a new (and probably the first) parameter estimation framework for CLM to constrain important ecosystem model parameters and reduce the model-data misfit under consideration of parameter uncertainty;
3. Identify key ecological CLM parameters and estimate those parameters with DREAM for single sites of different PFTs using measured NEE data, and evaluate parameter estimates and test their transferability to other sites. The role of uncertain initial model states is evaluated in this context;
4. Evaluate the feasibility of upscaling NEE data to the catchment scale with CLM and updated DREAM parameter estimates under additional consideration of different sources of model uncertainty (atmospheric input data and initial model conditions).

Chapter 2 briefly summarizes the relevant theory of the eddy covariance method, CLM and DREAM. Chapter 3 is dedicated to the uncertainty estimation of eddy covariance NEE data and introduces an extension of the classical two-tower approach (Hollinger et al., 2004; Hollinger

and Richardson, 2005; Richardson et al., 2006). Random error estimates of measured NEE obtained from the two-tower approach are based on the standard deviations of the fluxes measured simultaneously at two nearby EC towers. Basic underlying assumptions of this method are (i) statistical independence of the measured data, i.e. non-overlapping footprints, and (ii) identical or very similar environmental conditions in the footprint of both EC towers. Those competing requirements challenge the applicability of the method and hamper the definition of an appropriate tower distance. The proposed extension removes systematic differences of measured NEE, which should not be attributed to the random error estimate. The role of the tower distance was investigated with help of a roving station, which was separated in five distances between 8 m and 34 km from a permanent EC tower. Moreover, the effect of an additional filter for similar weather conditions applied to the NEE dataset was tested. The two-tower based NEE random error estimates were compared to the corresponding random error determined with a different, raw-data based approach presented in Mauder et al. (2013).

Chapter 4 presents how NEE data measured at single EC tower sites were used to estimate eight key ecological CLM parameters, which were previously selected by means of a simple sensitivity analysis. The first main objective was to improve CLM NEE predictions for different plant functional types (PFTs) in the central-west region of Europe including the Rur catchment. Therefore, parameters were estimated with DREAM separately for four sites of different land use: (1) grassland, (2) C3-crop, (3) evergreen coniferous forest, and (4) broadleaf deciduous forest. Those are the four most widespread PFTs in the Rur catchment. In order to evaluate the transferability of the parameter estimates to other sites and thus the potential of upscaling EC carbon flux measurements with DREAM-CLM, NEE data of four additional FLUXNET sites were used. Each evaluation site was located about 600 km away from the corresponding parameter estimation site of the same PFT. In order to test how strongly the parameter estimates vary seasonally, parameters were estimated based on a complete one year time series of NEE data, and also individually for each season in that year. Related to that, in order to test how strongly parameter estimates depend on / correlate with the initial model states, an additional experiment was conducted, where the eight parameters were estimated jointly with four multiplication factors for the initial model states (carbon-nitrogen pools and LAI).

Chapter 5 focusses on the evaluation of CLM4.5BGC carbon flux and LAI predictions for the Rur catchment at a spatial resolution of 1 km^2 when applying DREAM parameter estimates. New posterior probability distribution functions (pdfs) were determined, this time only for the five PFT-specific parameters, using the same DREAM-CLM set-up and the same one year NEE time series of the four sites as in chapter 4. Based on the results of chapter 4 and other studies

(e.g. Keenan et al., 2012b) the hypothesis was that the NEE-based parameters estimates strongly affect and potentially improve simulated LAI. This was tested here. Half-hourly NEE data of seven sites within the Rur catchment and LAI data obtained from RapidEye were used for the evaluation of the model outputs with and without updated parameters. In addition, the uncertainty of modeled NEE and LAI was explicitly evaluated with a second CLM ensemble where not only parameters were uncertain (sampled from the posterior pdfs estimated by DREAM), but also initial states and atmospheric input data.

Finally, chapter 6 provides a summary of the main results and chapter 7 an outlook for future research.

Chapter 2: Theory and Methods

2.1. THE EDDY COVARIANCE (EC) METHOD

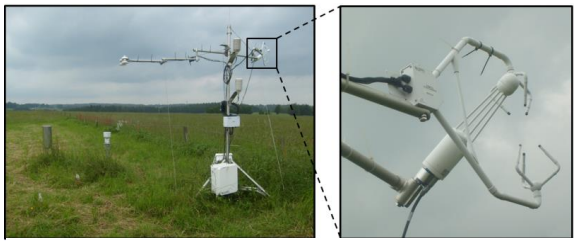

Figure 2.1: Eddy covariance station.

The vertical energy fluxes (latent heat, sensible heat) and NEE fluxes between the land surface and the atmosphere are measured by the eddy covariance method. Eddy covariance stations (Figure 2.1) measure the wind speed in three dimensions and simultaneously the gas concentration with an infrared gas analyzer (Pumpanen et al., 2009) at a temporal resolution of e.g. 10 or 20 Hz. EC measurement devices are located above canopy, usually in about 1-3 m height at grassland or agricultural sites and in about 20-40 m at forest sites (e.g. Chen et al., 2012). In the lowest atmospheric boundary layer close to the land surface turbulent flow predominates. Accordingly, the eddy covariance method determines the turbulent mass transfer assuming that all vertical mass transport within this part of the boundary layer is determined by turbulent flow (so called "eddies"). The EC-method assumes that horizontal divergence of flow and advection are negligible. Therefore, the terrain where EC stations are located is ideally flat and the land surface homogeneous (Baldocchi, 2001). The EC method is amongst others based on the mass conservation principle, which requires the assumption of steady state conditions of the meteorological variables (Baldocchi, 2003). By sampling both wind speed in three dimensions and the CO_2 concentration over time, the vertical net flux density F of CO_2 [mmol m^{-2} s^{-1}] across the canopy-atmosphere interface can be calculated as a function of the dry air molar density ρ_a [mmol m^{-3}], the CO_2 mixing ratio c [mmol (CO^2) / mmol (dry air)] and the vertical wind velocity ω [m s^{-1}]:

$$F = \overline{\rho_a} \cdot \overline{\omega' \cdot c'} \tag{2.1}$$

The prime denotes fluctuations around the mean; the bar the average over the measurement interval (e.g. half hour), i.e.:

$$\overline{c' \cdot \omega'} = \sum_{k=0}^{n} \frac{[(\omega_k - \bar{\omega})(c_k - \bar{c})]}{n-1} \quad (2.2)$$

with n being the number of measurements during the measurement interval. The CO_2 mixing ratio c is equal to the ratio of the CO_2 molar density ρ_c to the dry air molar density ρ_a, implying the necessity of a correction (Webb et al., 1980) if CO_2 concentration was originally measured per unit volume.

The correction for systematic measurement errors and the quantification of the measurement uncertainty is a prerequisite to model-data fusion (Richardson et al., 2006, 2008). Before the measured EC data can be used for scientific purposes, it requires careful post processing and undergoes various correction steps. The TK3.1 software (Mauder and Foken, 2011) for example was used for the processing of the EC data measured in the Rur catchment. This software also provides a standardized flagging system, which classifies the data into high, moderate or low quality. The final NEE flux data provided after processing is still subject to systematic and random errors, which are briefly summarized in the following.

2.1.1. Systematic errors

Recent studies identified two main types of systematic errors in eddy covariance CO_2 flux measurements:

1. During night, respiration is often underestimated due to low wind conditions and a temperature inversion which hinders the upward transport (Baldocchi, 2003). Hence, nighttime data is commonly rejected for further analysis (Barr et al., 2006). Goulden et al. (1996) introduced a friction velocity threshold as disqualifier. This threshold however is not universal for CO_2 fluxes but ranges from 0.1 to 0.6 m s^{-1} (Baldocchi, 2003).

2. The sum of measured energy fluxes (latent heat, sensible heat and ground heat flux) is often found to be 10-30% smaller than the measured net radiation, which refers to an energy closure problem (Wilson et al., 2002; Foken et al., 2006; Foken, 2008). Possible reasons for this energy balance deficit (EBD) are (a) the underestimation of turbulent energy fluxes and/or a overestimation of the available energy (Wilson et al., 2002), (b) the negligence or incorrect estimation of the energy storage in the canopy and the soil (Kukharets et al., 2000) and, probably most important, (c) the land surface heterogeneity which can even on flat terrain induce advection (Panin et al., 1998; Foken et al., 2006; Liu et al., 2006; Finnigan, 2008). The latter is closely linked to (d) an omission of low or high frequency turbulent

fluxes (Wilson et al., 2002; Foken et al., 2006). Commonly, measured energy fluxes are corrected for EBD. However, the correction method used and the ratio to which EBD accounts for the sensible and latent heat correction remains controversial. Often the Bowen Ratio is used for the correction (e.g. Todd et al., 2000; Twine et al., 2000), but alternative approaches have been proposed (e.g. Hendricks Franssen et al., 2010). Some of the most recent studies apply H post closure methods (Gayler et al., 2013; Imukova et al., 2015), e.g. letting the latent heat flux unaltered and adding the gap fully to the measured sensible heat flux (H). Because atmospheric CO_2 transport processes are very similar to those of the energy fluxes and because their calculation with the eddy covariance method is based on the same physical assumptions, the energy balance closure problem probably also results in systematic errors of the CO_2 flux measurements (Twine et al., 2000; Wilson et al., 2002; Mauder et al., 2010). For example, Wilson et al. (2002) found that nocturnal respiration was significantly less when the energy balance deficit was larger. However, the correction of measured CO_2 fluxes with EBD is not widely accepted, because the connection between energy- and CO_2 deficits has not been firmly proven and depends on the actual reason for the imbalance (Wilson et al., 2002; Barr et al., 2006; Foken et al., 2006).

2.1.2. Random errors

The random error is the remaining uncertainty after the measured data has been corrected for systematic errors and originates e.g. from instrumentation or calibration errors, flux footprint heterogeneity and turbulence sampling errors (Flanagan and Johnson, 2005). The uncertainty cannot be corrected or predicted like systematic errors due to the random character but can be quantified by statistical analysis and characterized by probability distribution functions (Richardson et al., 2012). The most common methods that have been proposed to estimate the uncertainty of CO_2 flux eddy covariance measurements are:

1. The “two-tower” or “paired-tower” approach, where simultaneous flux measurements of two towers with non- overlapping footprints (several hundred meters to several kilometers distance) are analyzed (Hollinger et al., 2004). It is assumed that environmental conditions for both towers are similar. The difference of the measured flux values then allows for the uncertainty estimation.
2. The “one- tower” or “24-h differencing” method is based on the two-tower approach, but in this case fluxes measured on two following days with “similar” environmental conditions (wind speed, temperature, photosynthetic active radiation) of only one EC tower are compared (Richardson et al., 2006). The definition of “similar environmental conditions” is

arbitrary but should guarantee that flux differences are not arising from varying boundary conditions. Because most often environmental condition are not the same on two sequential days (Liu et al., 2006), the applicability of this method suffers from a lack of data.

3. With the model residual approach CO_2 fluxes are simulated with a simple model. The method is based on the assumption that the model error is negligible. The model residual is then attributed to the random measurement error (Hollinger and Richardson, 2005; Dragoni et al., 2007; Moffat et al., 2007; Richardson et al., 2008)

4. Recently, Mauder et al. (2013) introduced to EC data processing an operational, independent quantification of the instrumental noise and of the stochastic error by calculating the auto- and cross-covariances of the measured fluxes. This method was adapted from Finkelstein and Sims (2001). In contrast to the previous approaches this method uses the high-frequency raw-data. The advantage of this approach is that it is independent of measurements by a second tower or measurement from the next day. Moreover, the raw-data based uncertainty estimate is not affected by not fulfilled underlying assumptions such as a correct simulation model or similar environmental conditions. Because many data users do not have access to the raw-data but to processed data only, the applicability of the raw-data based approach is restricted to those responsible for the initial data processing.

2.2. The Community Land Model (CLM) and its representation of the land carbon cycle

Figure 2.2 illustrates the main processes of the coupled carbon, energy and water cycles represented by the Community Land Model (CLM) and other land surface models. The simulated land surface fluxes (carbon, latent heat, sensible heat) are driven by the meteorological input data and are determined by the land surface conditions (e.g., land cover distribution, soil texture) as well as model states (e.g., carbon and nitrogen pools, soil moisture). The initial states are

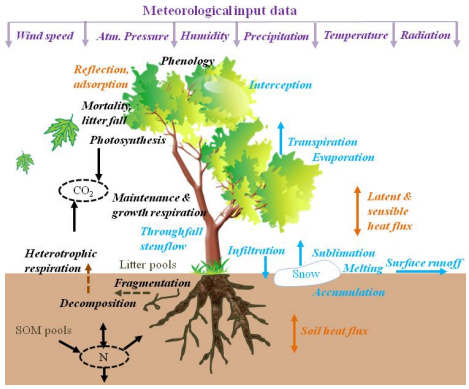

Figure 2.2: Land biogeophysical and biogeochemical processes simulated with CLM.

generated by a model spin-up. In this study, the Community Land Model version 4.5 (CLM4.5) was used in the dynamic carbon-nitrogen mode (BGC). CLM4.5BGC comprises a biogeochemical model that is based on the terrestrial biogeochemistry model Biome-BGC (Thornton et al., 2002; Thornton and Rosenbloom, 2005; Thornton et al., 2009) and is characterized by a fully prognostic carbon and nitrogen dynamic (Oleson et al., 2013).

The net exchange of CO_2 between the land surface and the atmosphere (NEE) is the sum of gross primary production (GPP), i.e. the photosynthetic CO_2 uptake, and ecosystem respiration (ER) through which CO_2 is released from ecosystems into the atmosphere. In CLM, photosynthesis is calculated at the leaf scale separately for sunlit and shaded canopy fractions (Dai et al., 2004; Thornton and Zimmermann, 2007) and is upscaled via the leaf area index. The leaf stomatal resistance is calculated based on the Ball-Berry conductance model (Ball and Berry, 1982; Collatz et al., 1991), which was implemented by Sellers et al. (1996) for global climate model applications. Photosynthesis in C_3 and C_4 plants is calculated based on the models by Farquhar et al. (1980) and Collatz et al. (1992) respectively, which were implemented by Bonan et al. (2011) in CLM. As outlined in Oleson et al. (2013), leaf net photosynthesis (A_n) is

$$A_n = \min\left(A_c, A_j, A_p\right) - R, \tag{2.3}$$

with R= respiration [µ mol CO_2 m^{-2} s^{-1}], A_c= RuBP carboxylase (Rubisco) limited rate of carboxylation [µ mol CO_2 m^{-2} s^{-1}], A_j = light limited carboxylation rate [µ mol CO_2 m^{-2} s^{-1}], and A_p = the product-limited carboxylation rate (C_3 plants) and the PEP (phosphoenolpyruvate) carboxylase-limited rate of carboxylation (C_4-plants). A_c, A_j, A_p are all a function of the internal leaf CO_2 partial pressure (Pa). A_p is also a function of the the Michaelis-Menten constants (Pa) for CO_2 and oxygen (O_2). A_p and A_c are both determined by the maximum rate of carboxylation V_{cmax} [µmol m^{-2} s^{-1}]. V_{cmax} is dependent on the maximum rate of carboxylation at 25°C (V_{cmax25}):

$$V_{\mathrm{cmax25}} = \frac{\mathrm{fl_{NR}}\ \mathrm{F_{NR}}\ a_{R25}}{\mathrm{CN_L}\ \mathrm{sla_{top}}} \tag{2.4}$$

where $\mathrm{fl_{NR}}$= fraction of leaf N in Rubisco enzyme [g N Rubisco g^{-1} N], $\mathrm{F_{NR}}$= mass ratio of total Rubisco molecular mass to nitrogen in Rubisco [g Rubisco g^{-1} N in Rubisco], a_{R25} = specific activity of Rubisco [µmol CO_2 g^{-1} Rubisco s^{-1}], $\mathrm{CN_L}$ = leaf carbon-to-nitrogen ratio [gC g^{-1}N] and $\mathrm{sla_{top}}$=specific leaf area at the canopy top [m^2 g^{-1} C]). V_{cmax25} is modified with a function of variations in daylength, which introduces seasonal variations to V_{cmax}. For further details see Oleson et al. (2013).

The total ecosystem respiration (ER) in CLM includes both heterotrophic respiration (HR) and autotrophic respiration, the sum of maintenance respiration (MR) and growth respiration (GR). MR and GR are treated separately in CLM. As outlined in Oleson et al. (2013) "maintenance respiration is defined as the carbon cost to support the metabolic activity of existing live tissue, while growth respiration is defined as the additional carbon cost for the synthesis of new growth". CLM distinguishes between living vegetation pools (roots, stem, and leaves) and dead carbon-nitrogen (CN) pools (litter, coarse wood debris, soil organic matter). The maintenance respiration (MR) is the sum of MR separately calculated for leaves (MR_{leaf}), fine roots (MR_{froot}), live stem ($MR_{livestem}$) and live coarse roots ($MR_{livecroot}$). The individual MR contribution for leaves is calculated as follows:

$$\mathrm{MR}_{\mathrm{leaf}} = NS_{\mathrm{leaf}}\, mr_{\mathrm{b}}\, Q_{10}{}^{(T_{2\mathrm{m}}-20)/10} \tag{2.5}$$

where NS_{leaf} [gN m^{-2}] is leaf nitrogen content, mr_b [gC gN^{-1} s^{-1}] is the base rate of maintenance respiration per unit nitrogen content, Q_{10} is the temperature sensitivity for maintenance respiration and T_{2m} [°C] is the air temperature at 2m height. The contributions $MR_{livestem}$ and $MR_{livecroot}$ are accordingly calculated (with $NS_{livestem}$ and $NS_{livecroot}$ instead of NS_{leaf}). MR_{froot} is the sum of MR_{froot} separately calculated for different soil layers j using the soil temperature at level j instead of T_{2m} and including the fraction of fine roots present at soil level j. Growth respiration is calculated individually for each allocation pathway based on the growth respiration factor (g_R), which is multiplied with the carbon allocated to each individual living vegetation pool at a given time step (Oleson et al., 2013).

Decomposition of fresh litter material, the gradual transition of labile dead organic matter into more recalcitrant forms, is represented as the carbon transfer from one pool to another:

$$\frac{\partial C_i}{\partial t} = CP_i + \sum_{j \neq i} (i - r_j) T_{ji} k_j C_j - k_i C_i \tag{2.6}$$

where C_i is the carbon content of pool i, CP_i are the direct carbon inputs from plant tissues to i (only non-zero for coarse woody debris and litter pools), k_i is the decay constant of pool i, T_{ji} is the fraction of carbon directed from pool j to pool i, and r_j is the carbon fraction lost as the respiration flux (HR).

CLM4.5 contains both the old CLM4 decomposition structure based on CLM-CN (Thornton et al., 2002; Thornton and Rosenbloom, 2005) and the BGC structure, which is based on the CENTURY model (Parton et al., 1988, 1993) and contains a different pool structure and slower decomposition rates. In a 10 year multi-site field experiment executed for 27 sites across North and Central America (Bonan et al., 2013), the parameterization of the litter and soil organic

matter pools in CLM-CN, originally based on laboratory incubation experiments (Thornton and Rosenbloom, 2005), was found to differ strongly from real conditions. In particular the litter decomposition was found to be too high in CLM-CN, which caused a too rapid CN cycle and an underestimation of the remaining carbon mass. Thus, the BGC decomposition module is now standard in CLM4.5 and was also used in this study. CLM4.5 also includes a new vertically resolved soil biogeochemistry scheme and decomposition structure (Koven et al., 2013). In this scheme, decomposition decreases exponentially with soil depth (Jenkinson and Coleman, 2008). The decomposition base rates are modified by environmental variables including soil temperature and soil moisture. The temperature scalar is calculated based on the temperature coefficient Q_{10} for each soil layer. The influence of the soil water potential is calculated separately for each soil layer based on Andrén and Paustian (1987). They formulated a relationship that includes the soil water potential in layer j, the lower limit for soil water control on the deposition rate (set to -10 MPa), and the saturated soil water potential [MPa]. The latter is calculated with a multivariate regression model by Cosby et al. (1984), which is a function of the volume percentages of sand and clay content in each individual soil layer. In case of the vertically resolved model (Koven et al., 2013), which was applied here, two additional environmental modifiers are calculated: the depth scalar, and an oxygen scalar, which is enabled with the CH_4 submodel and limits decomposition if the oxygen supply is insufficient. In addition, heterotrophic respiration can be limited by the available mineral nitrogen (N) in soil. CLM resolves the competition between plant and microbial nitrogen demand. Accordingly, all carbon fluxes depend on the soil nitrogen content, which is altered by atmospheric N deposition, biological nitrogen fixation, nitrification, denitrification and leaching (as well as losses in fire, but the fire module was switched off in this application as fires are very rare in the Rur catchment).

As outlined in Oleson et al. (2013), CLM4.5BGC is fully prognostic with respect to the seasonal timing of vegetation growth and litterfall. The day length, the soil and air temperature as well as the soil water content are the main determinants of plant phenology. Plant phenology representation follows three different schemes depending on the particular plant functional type (PFT): 1. Evergreen phenology, 2. Seasonal deciduous phenology, and 3. Stress deciduous phenology. The four most widespread CLM-PFTs in the Rur catchment are: (1) temperate evergreen needleleaf trees, (2) temperate broadleaf deciduous trees, (3) C3 non-arctic grass, and (4) C3-crop. Evergreen coniferous trees follow phenology scheme 1, deciduous broadleaf trees follow scheme 2, and both C3-grass and C3-crop follow scheme 3. The LAI and all carbon and

nitrogen state variables in the vegetation, litter, and soil organic matter are calculated prognostically.

The definition of land use cover in CLM follows a nested sub-grid hierarchy structure (Oleson et al., 2013). The main land units (defined as percentage coverage per grid cell) are: glacier, wetland, vegetated land, lake and urban area. Each land unit follows a different sub model scheme to calculate the respective carbon, water and energy fluxes for a certain grid cell. Each vegetated land unit has 15 soil columns and can include different plant functional types. The PFTs are also defined as percentage area of the vegetated area within the grid cell.

2.3. PARAMETER ESTIMATION WITH DREAM

DREAM is an adaptive Markov Chain Monte Carlo (MCMC) method for statistical inference of the posterior probability density function (pdf) of the model parameters (Vrugt et al., 2008, 2009; Vrugt, 2016). The concept of Markov Chain Monte Carlo simulations is to approximate the posterior probability distribution of parameters (and states) according Bayes theorem without restricting assumptions on the shape of the probability density function of parameters and states. The Bayes Theorem is given by:

$$p(\mathbf{x}|\tilde{\mathbf{Y}}) = \frac{p(\mathbf{x})p(\tilde{\mathbf{Y}}|\mathbf{x})}{p(\tilde{\mathbf{Y}})} \tag{2.7}$$

where $\mathbf{x}$ are the model parameters to be estimated, $\tilde{\mathbf{Y}} = \{\tilde{y}_1, \dots, \tilde{y}_n\}$ is a n-vector of measured data, $p(\mathbf{x}|\tilde{\mathbf{Y}})$ signifies the posterior probability density function (pdf), $L(\mathbf{x}|\tilde{\mathbf{Y}}) \equiv p(\tilde{\mathbf{Y}}|\mathbf{x})$ is the likelihood function, $p(\mathbf{x})$ the prior distribution and $p(\tilde{\mathbf{Y}})$ the normalizing constant. In practice, $p(\tilde{\mathbf{Y}})$ needs not be computed, and all statistical inferences about $p(\mathbf{x}|\tilde{\mathbf{Y}})$ can be made from its unnormalized density, $p(\mathbf{x}|\tilde{\mathbf{Y}}) \propto p(\mathbf{x})L(\mathbf{x}|\tilde{\mathbf{Y}})$.

It is assumed herein that the prior distribution is uniform (non-informative) using ranges of the predefined upper and lower bounds for each parameter. The likelihood function quantifies in probabilistic terms the level of agreement between the simulated n-vector, $\mathbf{Y}(\mathbf{x})$ and the corresponding observed data, $\tilde{\mathbf{Y}}$. Under the assumption of uncorrelated and normally distributed error residuals, $\mathbf{E}(\mathbf{x}) = \tilde{\mathbf{Y}} - \mathbf{Y}(\mathbf{x}) = \{\mathrm{e}_1(\mathbf{x}), \dots \mathrm{e}_n(\mathbf{x})\}$, the likelihood function can be written as follows:

$$L\left(\mathbf{x}\middle|\widetilde{\mathbf{Y}},\boldsymbol{\sigma}^{\mathbf{2}}\right)=\prod_{1}^{n}\frac{1}{\sqrt{2\pi\sigma_t^2}}\exp\left[-\frac{1}{2}\left(\frac{e_t(\mathbf{x})}{\sigma_t}\right)^2\right] \tag{2.8}$$

where $\boldsymbol{\sigma} = \{\sigma_1,\ldots,\sigma_n\}$ is a n-vector with standard deviations of the measurement error of the observations. If homoscedasticity of the measurement errors is anticipated, then the likelihood function of Equation 2.8 can be simplified to

$$L\left(\mathbf{x}\middle|\widetilde{\mathbf{Y}}\right)\propto\sum_{t=1}^{n}|e_t(\mathbf{x})|^{-n} \tag{2.9}$$

using

$$s^2=\frac{1}{n-1}\sum_{t=1}^{n}(e_t(\mathbf{x}))^2 \tag{2.10}$$

as sufficient statistic of the measurement error variance σ^2. This sum of squared error type likelihood function is used herein for posterior inference. For reasons of numerical stability, the log-formulation, $\mathcal{L}\left(\mathbf{x}\middle|\widetilde{\mathbf{Y}}\right)$ of Equation 2.9 is used herein:

$$\mathcal{L}\left(\mathbf{x}\middle|\widetilde{\mathbf{Y}}\right)=-\frac{1}{2}n\log\left\{\sum_{t=1}^{n}e_t(\mathbf{x})^2\right\}. \tag{2.11}$$

Now the prior distribution and likelihood function have been defined, what is left is to summarize the posterior distribution, $(\mathbf{x}|\widetilde{\mathbf{Y}})$ of the model parameters. For complex, nonlinear models like CLM, this posterior distribution of parameters cannot be obtained by analytical means or by analytical approximation. Thus, an iterative method is required that approximate the posterior pdf, which in case of DREAM is Markov chain Monte Carlo (MCMC) simulation (Metropolis et al., 1953). The basis of MCMC simulation is a Markov chain that generates a random walk through the search space and successively visits solutions with stable frequencies stemming from a stationary distribution.

The DREAM multi-chain MCMC simulation algorithm automatically tunes the scale and orientation of the proposal distribution in route to the target distribution, and exhibits excellent sampling efficiencies on complex, high-dimensional, and multi-modal target distributions. The use of multiple chains offers a robust protection against premature convergence, and opens up the use of a wide arsenal of statistical measures to test whether convergence to a limiting distribution has been achieved.

In short, in DREAM N different Markov chains are run simultaneously in parallel. If the state of a single chain is given by the d-vector $\mathbf{x}$, then at each generation t - 1 the N chains define a

population, $\mathbf{X}_{t-1} = \{\mathbf{x}_{t-1}^1, \ldots, \mathbf{x}_{t-1}^N\}$ which corresponds to a $N \times d$ matrix, with each chain as row. If A is a subset of d^*-dimensions of the original parameter space, $\mathbb{R}^{d^*} \subseteq \mathbb{R}^d$ then a jump ($\mathrm{d}\mathbf{X}^i$) in the ith chain, $i = \{1, \ldots, N\}$ at iteration $t = \{2, \ldots, T\}$ is calculated from $\mathbf{X}_{t-1}$ using

$$\mathrm{d}\mathbf{X}_{\mathrm{A}}^i = \boldsymbol{\zeta}_{d*} + (1_{d^*} + \boldsymbol{\lambda}_{d^*})_{\mathrm{Y}(\delta,d^*)} \sum_{j=1}^{\delta} (\mathbf{X}_{\mathrm{A}}^{\mathbf{a}_j} - \mathbf{X}_{\mathrm{A}}^{\mathbf{b}_j}) \tag{2.12}$$

$$\mathrm{d}\mathbf{X}_{\neq \mathrm{A}}^i = 0,$$

where $\gamma = 2.38/\sqrt{2\delta d^*}$ denotes the jump rate, δ is the number of chain pairs used to generate the jump, and **a** and **b** are vectors consisting of δ integers drawn without replacement from $\{1, \ldots, i-1, i+1, \ldots, N\}$. The values of $\boldsymbol{\lambda}$ and $\boldsymbol{\zeta}$ are sampled independently from a multivariate uniform distribution $\mathcal{U}_{d*}(-c, c)$ and normal distribution $\mathcal{N}_{d*}(0, c_*)$, respectively, and, with typically c = 0.1 and c_* small compared to the width of the target distribution (e.g. c_*=10^{-6}). To enable direct jumps between disconnected posterior nodes, the value of γ is set to unity with a 20% probability, otherwise the default value of γ is used. The d^*-members of the subset A are sampled from the entries $\{1, \ldots, d\}$ (without replacement) and define the dimensions of the parameter space to be sampled by the proposal.

The proposal point of chain i at iteration t then becomes:

$$\mathbf{X}_p^i = \mathbf{X}^i + \mathrm{d}\mathbf{X}^i \tag{2.13}$$

and the Metropolis acceptance ratio α is used to determine whether to accept this proposal or not:

$$P_{\mathrm{accept}}\left(\mathbf{x}_{t-1}^i \to \mathbf{X}_p^i\right) = \min\left[1, \frac{p(\mathbf{X}_p^i)}{p(\mathbf{x}_{t-1}^i)}\right]. \tag{2.14}$$

If the candidate point is accepted, then the i^{th} chain moves to the new position, that is $\mathbf{x}_{t-1}^i = \mathbf{X}_p^i$, otherwise $\mathbf{x}_t^i = \mathbf{x}_{t-1}^i$ (Vrugt, 2016). After a burn-in period, the Markov chains have become independent of their initial value and convergence is defined and monitored with the univariate $\hat{R}$-convergence diagnostic of Gelman and Rubin (1992). The $\hat{R}_j$-statistic of Gelman is computed for each dimension as the ratio of variance within one chain and the variance between different chains. Because every point in the parameter space is hit with a frequency proportional to its probability, the random walk allows to iteratively find a stable target distribution. Hence, after convergence, the density of the acceptance points in the parameter space approximates the posterior pdf according to Bayes theorem.

Herein, a simple adaptation of DREAM is used, called the DREAM$_{(zs)}$ algorithm which creates the jumps in Equation 2.12 from an "archive" of past states of the joint chains rather than their current states only (Vrugt, 2016). This reduces the required number of Markov chains to just a few. Moreover, DREAM$_{(zs)}$ uses a "snooker update" as well (Ter Braak and Vrugt, 2008) to increase diversity of the sampled proposals. It is assumed that convergence of the DREAM$_{(zs)}$ algorithm to a limiting distribution has been achieved if the $\hat{R}$ −statistic is smaller than the threshold value of 1.2 for all d model parameters. The least-squares parameter values (also referred to as maximum a posteriori [MAP] solution) are found by locating the sample of the posterior distribution with highest posterior density

$$\text{MAP} = \underset{\mathbf{x} \in \mathbb{R}^d}{\text{argmax}} \left(p\left(\mathbf{x} \middle| \widetilde{\mathbf{Y}}\right) \right). \tag{2.15}$$

A full description of the DREAM and DREAM$_{(zs)}$ algorithms can be found in Ter Braak and Vrugt (2008), Vrugt et al., (2008, 2009) and (Vrugt, 2016). This chapter was adapted from Post et al. (2016).

Chapter 3: Uncertainty analysis of eddy covariance net carbon flux measurements for different EC tower distances

*adapted from: Post, H., Hendricks Franssen, H.J., Graf, A., Schmidt, M., Vereecken, H., 2015. Uncertainty analysis of eddy covariance CO 2 flux measurements for different EC tower distances using an extended two-tower approach. Biogeosciences 12, 1205–1221.

3.1. INTRODUCTION

The net ecosystem exchange of CO_2 between the land surface and the atmosphere (NEE) can be determined with the eddy covariance (EC) method. Eddy covariance CO_2 flux measurements are commonly used to analyze the interactions between terrestrial ecosystems and the atmosphere, which is important for the understanding of climate-ecosystem feedbacks. In this regard reliable EC data with appropriate uncertainty estimates are crucial for many application fields, such as the evaluation and improvement of land surface models (e.g. Braswell et al., 2005; Hill et al., 2012; Kuppel et al., 2012).

The term ‘uncertainty’ is here referring to the random error following the definition in Dragoni et al. (2007). It differs from the systematic error in that it is unpredictable and impossible to correct (but can be quantified). Uncertainty doesn’t accumulate linearly but “averages out” and can be characterized by probability distribution functions (Richardson et al., 2012). Systematic errors are considered to remain constant for a longer time period (> several hours). Ideally they can be corrected, but in case of EC measurements this is still limited by either our understanding of various error sources or insufficient background data. Systematic errors arise not only from instrumental calibration and data processing deficits, but also from unmet underlying assumptions about the meteorological conditions (Richardson et al., 2012). A main assumption is that turbulence is always well developed in the lowest atmospheric boundary layer and responsible for the mass transport while horizontal divergence of flow and advection are assumed to be negligible (Baldocchi, 2001). Moreover, the EC method is based on the mass conservation principle, which requires the assumption of steady state conditions of the meteorological variables (Baldocchi, 2003). In case of CO_2 fluxes, night-time respiration is

often underestimated due to low wind velocities conditions and a temperature inversion which hinders the upward carbon dioxide transport (Baldocchi, 2001). Hence, night-time data are commonly rejected for further analysis (Barr et al., 2006).

After a possible correction of the EC flux data for systematic errors a random error will remain, which can arise from different sources such as (a) the assumption of a constant footprint area within a measurement interval and the negligence of flux footprint heterogeneity (e.g. due to temporal variability of wind direction, wind speed and atmospheric stability, which cause temporal variations of the footprint area); (b) turbulence sampling errors which are related to the fact that turbulence is a highly stochastic process and especially the sampling or not sampling of larger eddies is associated with considerable random fluctuations of fluxes, even if they are already averaged over a 30-minutes period; and (c) instrumentation deficits that can e.g. cause random errors in the measured variables (such as the CO_2 mixing ratio and the vertical wind velocity) used to calculate the net CO_2 flux (Flanagan and Johnson, 2005; Aubinet et al., 2011, p.179).

Within the past decade, several approaches have been proposed to quantify the uncertainty of eddy covariance CO_2 flux measurements. With the “two-tower” or “paired tower” approach simultaneous flux measurements of two EC towers are analyzed (Hollinger et al., 2004; Hollinger and Richardson, 2005). For the uncertainty quantification with the two-tower approach, it is necessary that environmental conditions for both towers are nearly identical (Hollinger et al., 2004; Hollinger and Richardson, 2005). However, most eddy covariance sites do not have a nearby second EC tower to provide nearly identical environmental conditions. Therefore, Richardson et al. (2006) introduced the “one-tower” or “24-h differencing” method, which is based on the two-tower approach. The main difference is that the uncertainty estimate is based on differences between fluxes measured on subsequent days if environmental conditions were similar on both days. Because most often environmental conditions are not the same on two subsequent days (Liu et al., 2006), the applicability of this method suffers from a lack of data and the random error is overestimated (Dragoni et al., 2007). The model residual approach (Hollinger and Richardson, 2005; Dragoni et al., 2007; Richardson et al., 2008) calculates CO_2 fluxes with a simple model and compares calculated values with measured values. The model residual is attributed to the random measurement error. The method is based on the assumption that the model error is negligible, which is however a very questionable assumption. Alternatively, if the high-frequency raw-data of an EC tower are available, uncertainty can be estimated directly from their statistical properties (Billesbach, 2011). Finkelstein and Sims (2001) introduced an operational quantification of the instrumental noise

and the stochastic error by calculating the auto- and cross-covariances of the measured fluxes. This method was implemented into a standard EC data processing scheme by Mauder et al. (2013). The advantage is that a second tower or the utilization of additional tools such as a simple model to estimate the EC measurement uncertainty is no longer required. However, many data users do not have access to the raw-data but to processed EC data only. Moreover, a large amount of solid metadata about the set-up of the EC measurement devices is required (but often not provided at second hand) to obtain reliable raw-data based uncertainty estimates adequately. Therefore, a two-tower based approach has still a large group of users. In particular with regard to pairs of nearby towers from local clusters, which play an increasing role in the monitoring strategies of e.g. ICOS and NEON, and have already been employed in case studies (e.g. Ammann et al., 2007). Important advantages of the two-tower approach are (1) its simplicity and user friendliness, (2) its usability for relatively short non gap-filled time series of several months, and (3) the independence of a model.

The classical two-tower approach (Hollinger et al., 2004; Hollinger and Richardson, 2005; Richardson et al., 2006) is based on the assumption that environmental conditions for both EC towers are identical and flux footprints should not overlap to guarantee statistical independence. Hollinger and Richardson (2005) use threshold values for three variables (photosynthetically active photon flux density PPFD, temperature & wind speed) to determine whether environmental conditions are equivalent. Independent of this definition, our understanding of "environmental conditions" includes both weather conditions and land surface properties such as soil properties (texture, density, moisture, etc.), plant characteristics (types, height, density, rooting depth, etc.), nutrient availability and fauna (microorganisms, etc.), which are irregularly distributed and affect respiration and/or photosynthesis. Strictly speaking, if footprints do not overlap 100%, the assumption of identical environmental conditions is already not fulfilled. When applying a two-tower based approach it is important to assure that systematic differences of the measured fluxes, which are partly caused by within site or among site heterogeneity, are not attributed to the random error estimate of the measured NEE. Our assumption that even within a site with apparently one uniformly distributed vegetation type (and for very short EC tower distances) land surface heterogeneity can cause significant spatial and temporal variability in measured NEE is e.g. supported by Oren et al. (2006). They found that the spatial variability of ecosystem activity (plants and decomposers) and LAI within a uniform pine plantation contributes to about half of the uncertainty in annual eddy covariance NEE measurements while the other half is attributed to micrometeorological and statistical sampling

errors. This elucidates the relevance of considering systematic flux differences caused by within site ecosystem heterogeneity when calculating a two-tower based uncertainty estimate.

Given the fact that site-specific, adequate uncertainty estimates for eddy covariance data are very important but still often neglected due to a lack of resources, the objective of this study is to advance the two-tower approach so that it can also be applied if environmental conditions at both eddy covariance towers are not very similar.

The main objectives of this study were (1) to analyze the effect of the EC tower distance on the two-tower based CO_2 flux measurement uncertainty estimate and (2) to extend the two-tower approach with a simple correction term that removes systematic differences in CO_2 fluxes measured at the two sites. This extension follows the idea of the extended two-tower approach for the uncertainty estimation of energy fluxes presented in Kessomkiat et al. (2013). The correction step is important for providing a more reliable random error estimate. In correspondence with these objectives, the following questions were analyzed: What is an appropriate EC tower distance to get a reliable two-tower based uncertainty estimate? Can the random error be quantified in reasonable manner with the extended two-tower approach, even though environmental conditions at both EC towers are clearly not identical? The total random error estimated with the raw-data based method (Mauder et al., 2013) was used as a reference to evaluate our extended two-tower approach based results.

3.2. TEST SITES AND EC TOWER SET-UP

The Rollesbroich test site is an extensively used grassland site, located in the Eifel region of western Germany (Figure 3.1). The mean temperature in Rollesbroich is ~ 7.7°C and the mean precipitation is ~ 1033mm per year (Korres et al., 2010). Predominating soil types at the site are Cambisols with a high clay and silt content (Arbeitsgruppe BK50, 2001). The grass species grown in Rollesbroich are mainly ryegrass, particularly perennial ryegrass (lolium perenne), and smooth meadow grass (poa pratensis) (Korres et al., 2010). A permanent eddy covariance tower (EC1) is installed at the Rollesbroich site since May 2011 at a fixed position. The measurement height of the sonic anemometer (CSAT3, Campbell Scientific, Logan, UT, U.S.A.) and the open-path gas analyzer (Li7500, Li-Cor, Lincoln, NE, U.S.A.) is 2.6 m above ground. The canopy height was measured every 1-2 weeks and varied between 0.03 m and 0.88 m during the measurement period. A second EC tower, the roving station (EC2), has been

installed at four different distances (8 m, 95 m, 173 m and 20.5 km) from EC1 for time periods ranging between 3 and 7.5 months (Table 3.1). The EC2 location "Kall-Sistig" 20.5 km north-east of Rollesbroich is another grassland site with similar environmental conditions as Rollesbroich. The vegetation in Kall-Sistig is extensively managed C3-grass, the same as for Rollesbroich. However, the average plant height measured between Aug. 14th and Oct. 30th 2012 was lower (~ 0.15 m) than the respective average for Rollesbroich (~ 0.2 m), which is also true for the plant height measured in May and June 2012 (Kall-Sistig: ~ 0.22 m; Rollesbroich: ~ 0.29 m). As in Rollesbroich, clayey-silty Cambisols are most widespread (Arbeitsgruppe BK50, 2001). The mean temperature for the entire measurement interval in Kall-Sistig (Table 3.1) measured at the EC station is 11.4 °C and the soil moisture 32% compared to 11.0 °C and 35% in Rollesbroich (same time interval for averaging). Additionally a third EC tower was located in Merzenhausen in ~ 34 km distance to EC1 (Figure 3.1). Merzenhausen (ME) is an agricultural site, where winter wheat was grown during the measurement period. Both the land use conditions and the average weather conditions differ from those in Rollesbroich and Kall-Sistig. The climate at the lowland site Merzenhausen is comparable to the one in Selhausen at a distance of 13 km from Merzenhausen, where the mean precipitation is ~ 690 mm/a and the yearly mean temperature ~9.8°C (Korres et al., 2010). The soils are mainly Luvisols with some patches of Kolluvisols (Arbeitsgruppe BK50, 2001). The measurement devices of EC2 and EC3 are the same as the EC1 devices and were installed 2.6 m above ground as well. Both, the sonic anemometers and the open-path gas analyzers were calibrated every 1-3 months thoroughly and consistently. Details on the EC data acquisition are summarized in Chapter 3.3.1.

Rollesbroich is part of the TERENO network (Zacharias et al., 2011). Information and additional data were collected showing that land surface properties are spatially heterogeneous distributed at the Rollesbroich site: (1) Single fields at the Rollesbroich site are managed by different farmers. Information the land owners provided, as well as periodic camera shots and grass height measurements around the EC towers indicated that the timing of fertilization and grass cutting as well as the amount of manure applied varied between the single fields during the measurement period; (2) Soil type distribution as displayed in the German soil map shows heterogeneity (Arbeitsgruppe BK50, 2001); (3) Soil carbon and nitrogen pools [g/kg] as well as bulk density [g/cm^3] and content of rock fragments [%] measured from April-May 2011 in three soils horizons at 94 locations across the Rollesbroich site are spatially highly variable (H. Schiedung 2013, personal communication); (4) During the eddy covariance measurement period, soil moisture and soil temperature data were collected in 10 min. resolution at three depths (5 cm, 20 cm and 50 cm) and 84 points by the wireless sensor network ("SoilNet";

Bogena et al., 2009), calibrated for the Rollesbroich site by Qu et al., (2013). SoilNet data shows that soil moisture is heterogeneously distributed within the Rollesbroich site (Qu et al., 2014).

Table 3.1: Measurement periods and locations of the permanent EC towers in Rollesbroich (EC1) and Merzenhausen (EC3) and the roving station (EC2).

	Coordinates	Sitename	Distance to EC1	Measurement period	alt. (m)
EC1	50.6219142°N / 6.3041256°E	Rollesbroich	–	13.05.2011 – 15.07.2013	514.7
EC2	50.6219012°N / 6.3040107°E	Rollesbroich	8m	29.07.2011 – 06.10.2011	514.8
	50.6219012°N / 6.3040107°E			05.03.2013 – 15.05.2013	
	50.6217990°N / 6.3027962°E	Rollesbroich	95m	07.10.2011 – 15.05.2012	516.3
	50.6210472°N / 6.3042120°E			01.07.2013 – 15.07.2013	517.3
	50.6217290°N / 6.3016925°E	Rollesbroich	173m	24.05.2012 – 14.08.2012	517.1
	50.5027500°N / 6.5254170°E	Kall-Sistig	20.5 km	14.08.2012 – 01.11.2012	498.0
				15.05.2013 – 01.07.2013	
EC3	50.9297879°N / 6.2969924°E	Merzenhausen	34 km	10.05.2011– 16.07.2013	93.3

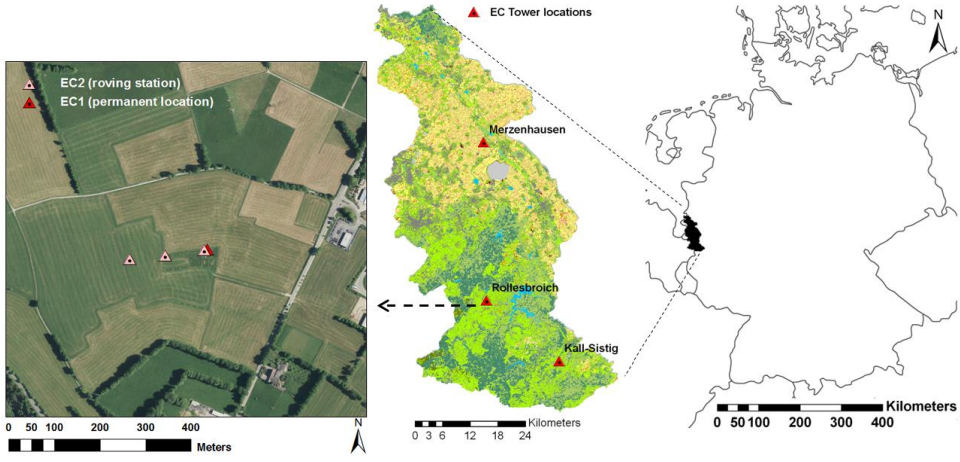

Figure 3.1: Eddy covariance (EC) tower locations in the Rur-Catchment (center) including the Rollesbroich test site (left).

3.3. DATA AND METHODS

3.3.1. EC data processing

The EC raw data were measured with a frequency of 20 Hz and fluxes were processed for flux intervals of 30 minutes. The complete processing of the data was performed with the TK3.1 software (Bayreuth, Department of Micrometeorology, Germany; Mauder and Foken, 2011), using the standardized strategy for EC data calculation and quality assurance presented in detail by Mauder et al., 2013. The strategy includes established EC conversions and corrections such as e.g. correction of spectral loss (Moore, 1986) and correction for density fluctuations (Webb et al., 1980). It includes tests on high frequency data (site-specific plausibility limits, statistical spike detection) as well as on processed half-hourly fluxes such as stationarity and integral turbulence tests (Foken and Wichura, 1996). The tests on half-hourly fluxes are the basis for a standardized quality flagging according to Mauder and Foken (2011) that classifies flux measurements as high (0), moderate (1) or low (2) quality data. For this analysis only flux measurements assigned to 0 or 1 were used, while low quality data were treated as missing values. Besides quality flags, TK3.1 also provides footprint estimates (Kormann and Meixner, 2001) and uncertainty estimates that were used for interpreting and analyzing flux data. To avoid introduction of additional uncertainty no gap filling of flux time series was performed.

3.3.2. Uncertainty estimation based on the two-tower approach

The two-tower approach (Hollinger et al., 2004; Hollinger and Richardson, 2005; Richardson et al., 2006) defines the random error of NEE eddy covariance measurements as the standard deviation $\sigma(\delta)$ of the difference between the CO_2 fluxes [µmol $m^{-2}s^{-1}$] simultaneously measured at two different EC towers (NEE_1, NEE_2):

$$\sigma(\delta) = \frac{\sigma(NEE_1 - NEE_2)}{\sqrt{2}} \tag{3.1}$$

Based on Equation 3.1 the two-tower based uncertainty estimates were calculated using the NEE_1 data measured at the permanent EC tower in Rollesbroich (EC1) and the NEE_2 data of a second tower, which was either the roving station (EC2) or – in case of the 34 km EC tower distance – another permanent EC tower (EC3, Table 3.1).

For comparison, the measurement uncertainty $\sigma(\delta)$ was calculated separately for each EC tower distance (Table 3.1) and independently for each of the following schemes:

1. The classical two-tower approach (Hollinger et al., 2004; Hollinger and Richardson, 2005; Richardson et al., 2006).
2. The classical two-tower approach including a filter for similar weather conditions (Chapter 3.3.4).
3. The extended two-tower approach with an added correction for systematic flux differences (sfd-correction; Chapter 3.3.3), without weather-filter.
4. The extended two-tower approach with sfd-correction and the previously applied weather-filter.

The uncertainty estimate of the two-tower approach is obtained by dividing the NEE data series into several groups ("bins") according to the flux magnitude and then using Equation 3.1 to calculate the standard deviation $\sigma(\delta)$ for each group (Richardson et al., 2006). Finally, a linear regression function between the flux magnitude and the standard deviation can be derived. The linear correlation of the uncertainty and the flux magnitude can be explained by the fact that the flux magnitude is a main driving factor for the random error and can explain about 63% of the variance in the CO_2 flux error as shown in a case study by Richardson et al. (2006). Accordingly, the standard deviation $\sigma(\delta)$ [µmol m^{-2} s^{-1}] was calculated based on 12 groups of the CO_2 flux magnitude; six groups for positive and six groups for negative fluxes. (NEE is positive if the amount of CO_2 released to the atmosphere via respiration is higher than the amount of CO_2 assimilated during photosynthesis. In contrast, negative NEE values denote a higher CO_2 uptake and a net flux from the atmosphere into the ecosystem.) Fixed class limits for the flux magnitude would have led to a different number of samples in each group. Now class limits were set such that all groups with positive NEE values had an equal amount of half-hourly data, the same holds for all groups with negative NEE values. For each single group the standard deviation $\sigma(\delta)$ was calculated using the single half-hourly flux differences of NEE_1 and NEE_2. The corresponding mean NEE magnitude for each group member was determined by averaging all half-hourly means of NEE_1 and NEE_2 in the respective group. Then, the linear regression equation was derived separately for negative and positive NEE values using the 6 calculated standard deviations $\sigma(\delta)$ and the 6 mean NEE values. This procedure was carried out for each dataset of the five EC tower distances and again for each of the four uncertainty estimation schemes so that altogether 20x2 linear regression equations were derived. The significance of the correlation between the NEE magnitudes and the standard deviations $\sigma(\delta)$ was tested with

the *p*- value determined with the Student's t-test based on Pearson's product moment correlation coefficient r. Moreover, the 95% confidence intervals of the slope and the intercept for each liner regression equation were determined. The linear regression equations were calculated imposing as constraint an intercept >= 0, because a negative standard deviation is not possible. With those linear regression equations, the uncertainty for the individual half-hourly NEE measurement values of the permanent EC tower in Rollesbroich (EC1) were estimated using the individual half-hourly NEE_1 values [µmol m^{-2} s^{-1}] as input (x) to calculate the corresponding uncertainty $\sigma(\delta)$ [µmol m^{-2} s^{-1}] (y).

The described calculation of the individual NEE uncertainty values was done for all half-hourly NEE data, including those data points that were discarded by the weather filter (Chapter 3.3.4) and/or the sfd-correction (Chapter 3.3.3). Hence, for each of the four two-tower based uncertainty estimation schemes the same amount of individual NEE uncertainty values was generated. These mean uncertainty estimates were used to evaluate the effect of the EC tower distance as well as the sfd-correction and the weather-filter on the two-tower based uncertainty estimation. Even though Hollinger et al. (2004) and Richardson and Hollinger (2005) already pointed out that the two-tower approach assumes similar environmental conditions and non-overlapping footprints, the classical approach was applied for all EC tower distances, even if these basic assumptions were not fulfilled, to allow for a comparison of the results before and after the usage of the weather-filter and the sfd-correction (extended two-tower approach).

3.3.3. Correction for systematic flux differences (sfd-correction)

Different environmental conditions and other factors such as instrumental calibration errors can cause systematic flux differences between two towers. Because these flux differences are not inherent to the actual random error of the measured NEE at one EC tower station they lead to an overestimation of the two-tower approach based uncertainty. Therefore, an extension of the classical two-tower approach is proposed here which includes a simple correction step for systematic flux differences (sfd-correction). The reason why systematic flux differences can statistically be separated quite easily from random differences of the EC flux measurements is their fundamentally different behavior in time: random differences fluctuate highly in time whereas systematic differences tend to be constant over time or vary slowly. The sfd-correction introduced is similar to the second correction step in Kessomkiat et al. (2013, Equation 6 therein), but adapted to the measured NEE instead of latent and sensible heat fluxes. An averaging time interval of 12 hours was used to calculate the running mean for the sfd-correction. For each moving average interval, the mean NEE_{12h} of one EC tower (separately for

EC1 and EC2) [µmol m^{-2} s^{-1}] and the mean CO_2 flux averaged over both EC towers NEE_{2T_12h} [µmol m^{-2} s^{-1}] were calculated to define the sfd-correction term which was used to calculate the corrected NEE_{corr} [µmol m^{-2} s^{-1}]:

$$NEE_{corr} = \frac{NEE_{2T\_12hr}}{NEE_{12h}} \cdot NEE \quad (3.2)$$

NEE is the single half-hourly, processed NEE value [µmol m^{-2} s^{-1}] of one EC tower. Only if both NEE data, NEE_{-EC1-} for the permanent EC1 tower and NEE_{-EC2-} for the second tower, were available at a particular half-hourly time step and if both values were either positive or negative, the respective data were included to calculate the correction term. The running averages were only calculated if at least 50% of the data for NEE_{-EC1-} and NEE_{-EC2} remained for averaging in that particular window. Due to the frequent occurrence of gaps in the data series the amount of available NEE_{corr} values considerably decreased by applying stricter criteria like 70% data availability (Table 3.2). We assume a 12 hour averaging period to be long enough to exclude most of the random error part but short enough to consider daily changes of systematic flux differences. For a six hour interval for instance the uncertainty of the mean NEE is usually higher. For larger window sizes (24 or 48 hours) further analysis was hampered by too many data gaps, i.e. the 50% criterion was hardly ever fulfilled and not enough averages remained to allow for the two-tower based uncertainty estimation (Table 3.2). The correction was done separately for positive and negative fluxes, due to the different sources, properties and magnitudes of the CO_2 flux measurements and different errors for daytime (negative) and night-time (positive) fluxes (e.g. Goulden et al., 1996; Oren et al., 2006; Wilson et al., 2002).

Table 3.2: R^2 for NEE uncertainty determined with the extended two-tower approach (including sfd-correction and weather-filter) as function of NEE_{corr} magnitude and for 20.5 km EC tower distance. Results are given for different moving average time intervals (6 hr, 12 hr, 24hr) and data coverage percentages (25%, 50%, 70%) for the calculation of the sfd-correction factor (Equation 3.2).

	6h	**12h**	**24h**
30%	0.73; 0.84; *(937)*	0.92; 0.72; *(904)*	0.84; 0.82; *(597)*
50%	0.58; 0.85; *(710)*	0.7; 0.43; *(463)*	-; -; *(32)*
70%	0.77; 0.78; *(408)*	0.66; 0.08; *(148)*	-; -; *(0)*

black: for negative NEE; grey: for positive NEE; *( )*: total number of half-hourly NEE left after sfd-correction and weather filter to build bins for NEE uncertainty versus NEE magnitude regressions

The final sfd-corrected $NEE1_{corr}$ values for EC1 and $NEE2_{corr}$ values for EC2 should not be understood as corrected NEE flux data. They were used only to enhance the two-tower based uncertainty estimation in a way that systematic flux differences, which cause an overestimation

of the uncertainty, are filtered out. Moreover, systematic flux differences at two EC towers are not to be confused with systematic errors, which are independent of the uncertainty estimation method and optimally corrected before the random error is estimated.

3.3.4. Filter for weather conditions

For larger distances of two EC towers, such as the 20.5 km and 34 km distance in this study, different weather conditions can cause differences of the measured fluxes in addition to the different land surface properties. Some weather variables (e.g. temperature) are following a clear diurnal and annual course and differences in e.g. temperature at two EC towers are therefore relatively constant. This is expected to cause rather systematic differences in the measured NEE, which can be captured with the sfd-correction. However, other variables such as wind speed or incoming short wave radiation are spatially and temporally much more variable, for example related to single wind gusts or cloud movement. Differences in the measured fluxes at two EC towers caused by those spatial-temporally highly variable weather variables cannot be captured well with the sfd-correction term due to this "random character". However, a weather filter can account for this because it compares the differences in weather variables at each single time step. Therefore, a filter for similar weather conditions was applied in addition to the sfd-correction following Hill et al. (2012) and Richardson et al. (2006) to only include half-hourly NEE data, if the weather conditions at the second EC tower are similar to those at the permanent EC1 tower location in Rollesbroich. Following the definition in Richardson et al. (2006), similar weather conditions were defined by a temperature difference < 3°C; wind speed difference < 1 m/s and difference in PPFD < 75 µmol m^{-2} s^{-1}. The weather-filter was applied before the (classical) uncertainty estimation and the sfd-correction. As shown e.g. in Tsubo and Walker (2005), the incoming short wave radiation (or solar irradiance SI) and the photosynthetically active radiation (PAR) are linearly correlated. Accordingly, SI and PPFD measured at the EC1 station in Rollesbroich were linearly correlated as well. Because direct PPFD measurements were not available for all measurement periods, a linear regression equation was derived on the basis of all SI and PPFD data for the permanent EC tower station (EC1). Using this equation, missing PPFD values were estimated if only SI but no PPFD data were available at a certain time step.

3.3.5. Footprint analysis

The footprint analysis was applied to quantify the percentage footprint overlap of the two EC-stations during the measurement periods. This information was not used to filter the data but to allow for a better understanding of the mean uncertainty estimates for the different scenarios.

Using the analytical model of Kormann and Meixner (2001) implemented in the TK3.1 software (Mauder and Foken, 2011), a grid of estimated source weights (resolution 2 m, extension 1 km by 1 km) was computed for each half-hour and station position. The overlap between the footprints of two simultaneously measuring towers was then quantified as:

$$O_{12}(t) = \sum_{x=1}^{N} \sum_{y=1}^{M} min(f_1(x,y,t), f_2(x,y,t)) \tag{3.3}$$

The indices 1 and 2 indicate the tower and *t* the time (in our case, half-hour). *N* and *M* are the number of pixels in east-west and north-south direction, *x* and *y* the respective running indices. The minimum function min() includes the source weight *f* computed for the respective tower, x and y location, and half-hour. *O* is 1 if both source weight grids are identical, and 0 in case of no overlap. During stable conditions, the footprint area of a tower increases and can result in considerable source weight contributions from outside the modeling domain. Assuming that two footprints, which overlap highly in the modeling domain, likely continue to overlap outside the modeling domain, *O* as defined above might be low-biased in such cases. We therefore additionally considered a normalized version $O/\min(\Sigma\Sigma f_1, \Sigma\Sigma f_1)$ as an upper limit estimate of the overlap. The overlap for the additional sites Kall and Merzenhausen more than 20 km away was assumed zero.

3.3.6. Comparison measures

To compare and evaluate the two-tower based uncertainty estimates, the random error estimates were calculated based on Mauder et al. (2013) as a reference. This reference method is independent of the two-tower based approach, because data of only one EC tower are used to quantify the random error of the measured fluxes and raw data instead of the processed fluxes are used. The raw-data based random error estimates – the instrumental noise σ_{cov}^{noise} and the stochastic error σ_{cov}^{stoch} – were calculated independently. Mauder et al. (2013) determine the instrumental noise based on signal autocorrelation. Following Finkelstein and Sims (2001) the stochastic error is calculated as the statistical variance of the covariance of the flux observations. Generally, σ_{cov}^{noise} was considerably lower than σ_{cov}^{stoch}. The total raw-data based random error σ_{cov} [µmol $m^{-2}s^{-1}$] was calculated by adding σ_{cov}^{noise} and σ_{cov}^{stoch} "in quadrature" ($\sigma_{cov} = \sqrt{{\sigma_{cov}^{stoch}}^2 + {\sigma_{cov}^{noise}}^2}$) according to Aubinet et al. (2011, p.176). The mean reference σ_{cov} used for the evaluation of the two-tower based random error estimates was calculated by averaging the single half-hourly σ_{cov} values for the permanent EC1 tower in Rollesbroich. In order to be

consistent with the two-tower based calculations, exactly the same half-hourly time steps of the EC1 data series used for the two-tower based uncertainty estimation were used to calculate the corresponding mean reference values σ_{cov}. As indicator for the performance of the two-tower based uncertainty estimation schemes applied for the five different EC tower distances, the relative difference $\Delta\sigma_{cov}$ [%] of a two-tower based uncertainty value [µmol m^{-2} s^{-1}] and σ_{cov} [µmol m^{-2} s^{-1}] was calculated:

$$\Delta\sigma_{cov}[\%] = \frac{\sigma(\delta) - \sigma_{cov}}{\sigma_{cov}} * 100 \quad (3.4)$$

Then, $\Delta\sigma_{cov}$ values were compared for the different EC tower separation distances and two-tower based uncertainty estimation schemes. The performance of the two-tower based uncertainty estimation was considered better if σ_{cov}[%] was closer to zero.

3.4. RESULTS

3.4.1. Classical two-tower based random error estimates

Figure 3.2 and Figure 3.3 show the linear regressions of the random error $\sigma(\delta)$ (also referred to as "standard error" or "uncertainty") as function of the NEE magnitude according to the classical two-tower approach for the different EC tower distances without weather-filter (Figure 3.2) and with weather-filter (Figure 3.3). The dashed linear regression lines denote that the linear correlation between $\sigma(\delta)$ and NEE is weak ($p > 0.1$), which is in particular true for the positive NEE values measured for 173 m and 20.5 km EC tower distances as well as for the negative NEE values for 20.5 km and 34 km distance. Uncertainty estimation with the classical two-tower approach is critical for those larger distances because measured flux differences caused by different environmental conditions at both EC towers can superimpose the random error signal, which e.g. originates from instrumental or turbulence sampling errors. This weakens the correlation of the random error and the flux magnitude. This is not surprising since Hollinger et al. (2004) and Richardson and Hollinger (2005) already pointed out that similar environmental conditions are a basic assumption of the two-tower approach. Therefore, statements on how the weather filter affects the mean uncertainty estimate $\sigma(\delta)$ for those large distances need to be treated with caution.

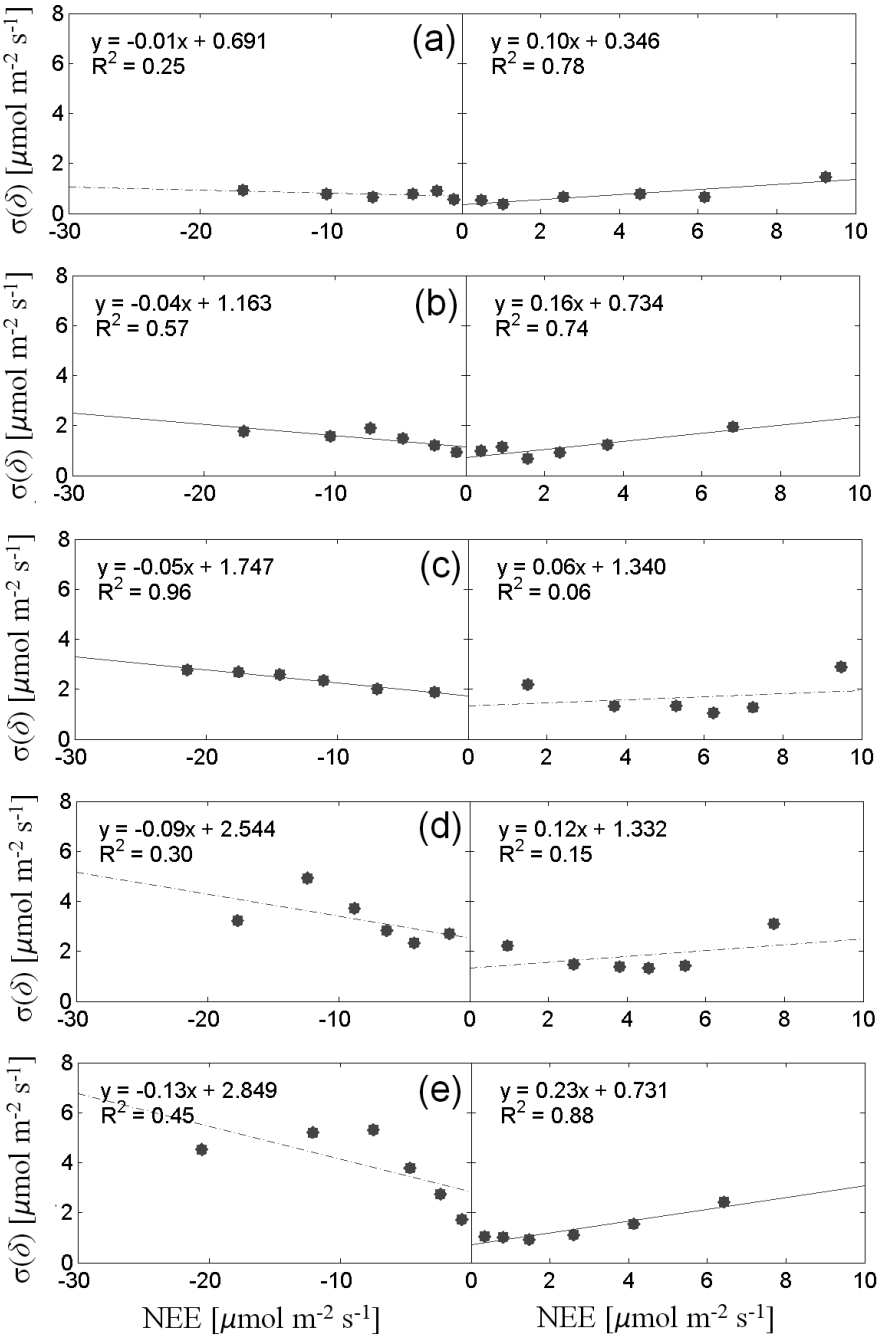

Figure 3.2: NEE uncertainty $\sigma(\delta)$ determined with the classical two-tower approach as function of the NEE flux magnitude for the EC tower distances 8m (a), 95m (b) , 173m (c), 20.5km (d) and 34 km (e). (Dashed line: regression slope not significantly different from zero ($p>0.1$)).

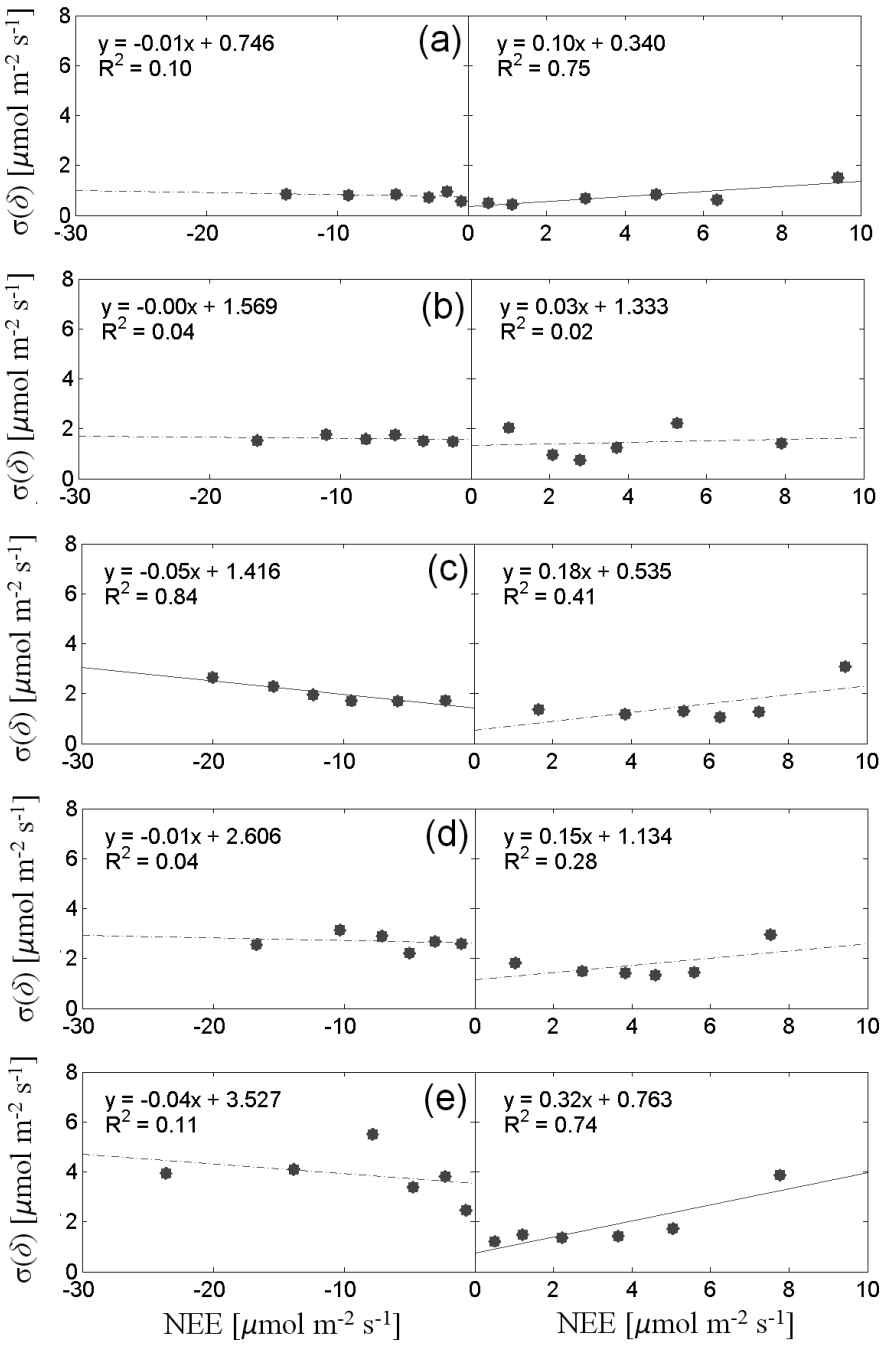

Figure 3.3: NEE uncertainty σ(δ) determined with the classical two-tower approach as function of the NEE flux magnitude including the application of the weather-filter for the EC tower distances 8m (a), 95m (b) , 173m (c), 20.5km (d) and 34km (e). (Dashed line: regression slope not significantly different from zero (p>0.1)).

The weather-filtering only increased the correlation between the flux magnitude and the random error $\sigma(\delta)$ for positive fluxes for separation distances of 173 m and 20 km whereas in most cases the linear correlation was weakened, mainly due to a decreased number of samples in each averaging group of the NEE flux magnitude. Therefore, testing stricter weather-filter criteria (e.g. wind speed < 0.5 m/s, PPFD < 50 µmol m^{-2} s^{-1}, Temp < 2 °C), which caused a decline of samples in each group from e.g. n > 1000 to 24 or less, resulted in little meaningful results.

As illustrated in Table 3.3, the mean NEE uncertainty estimate based on the classical two-tower approach increased as a function of EC tower distance. However, without applying the weather-filter, the mean uncertainty $\sigma(\delta)$ was nearly identical for the two largest distances (20.5 km and 34 km), although e.g. the land cover and management in Merzenhausen (EC3 tower at 34 km separation) were different from the Rollesbroich site. As a result of the weather-filtering, the mean uncertainty was less overestimated for the distances 173m and 20.5 km. However, for the 95 m and 34 km distance, the overestimation of the uncertainty estimate increased by the weather-filtering. This implies that for the classical two-tower approach (without sfd-correction) weather-filtering did not clearly reduce the overestimation of the uncertainty for largest EC tower distances (20.5 km and 34 km) where weather-filtering is expected to be particularly relevant.

Table 3.3: Mean NEE uncertainty [µmol m^{-2} s^{-1}] for five EC tower distances estimated with the classical two-tower approach, with and without including a weather-filter ($\sigma(\delta)$, $\sigma(\delta)_f$). and with the extended two-tower approach (sfd-correction), also with and without including a weather-filter ($\sigma(\delta)_{corr}$, $\sigma(\delta)_{corr,f}$). The table also provides the random error σ_{cov} [µmol m^{-2} s^{-1}] estimated with the raw-data based reference method (Mauder et al. 2013).

EC tower distance	***N***	$\boldsymbol{\sigma(\delta)}$ ($\Delta\sigma_{cov}$)	$\boldsymbol{\sigma(\delta)_f}$ ($\Delta\sigma_{cov}$)	$\boldsymbol{\sigma(\delta)_{corr}}$ ($\Delta\sigma_{cov}$)	$\boldsymbol{\sigma(\delta)_{corr,f}}$ ($\Delta\sigma_{cov}$)	$\boldsymbol{\sigma_{cov}}$
8m	*3167*	0.76 (18.8)	0.77 (20.5)	0.44 (-30.6)	0.44 (-30.8)	0.64
95m	*3620*	1.30 (116.7)	1.50 (149.4)	0.65 (8.2)	0.60 (0.2)	0.60
173m	*2410*	2.04 (98.5)	1.82 (77.0)	1.03 (-0.3)	1.00 (-2.5)	1.03
20.5 km	*2574*	2.72 (200.6)	2.35 (159.7)	1.52(67.8)	1.16 (28.7)	0.91
34 km	*15571*	2.73 (274.7)	2.86 (292.4)	1.18 (61.5)	1.14 (56.8)	0.73
mean		1.91	1.86	0.98	0.93	0.78

($\Delta\sigma_{cov}$): relative differences [%] between two-tower based uncertainty estimates and the references value σ_{cov} (Equation 3.4)

Comparing the mean uncertainty estimates of the classical two-tower approach with the reference random error estimates σ_{cov}, indicates that both with and without weather filter the uncertainties were overestimated (Table 3.3), for all EC tower differences. This could be expected for the large distances, because basic assumptions for the application of the classical two-tower approach are violated for these large distances. But results illustrate that even for short EC tower distances NEE uncertainty estimated with the classical two-tower approach is larger than the raw-data based estimates (Table 3.3).

3.4.2. Extended two-tower approach

The scatter plots in Figure 3.4 illustrate the effect the sfd-correction (Equation 3.2) had on the difference of the NEE data simultaneously measured at both EC towers. The sfd-correction reduced the bias and scattering, because systematic differences of the measured fluxes, e.g. induced by different environmental conditions, were removed. As expected, the effect of the sfd-correction was considerably higher for the larger EC tower distances because environmental conditions are also expected to differ more if the distance of two locations is larger. For the 8 m EC tower distance for instance, the effect of the sfd-correction is very minor because footprints are often nearly overlapping. However, for the EC tower distances >= 173 m, the bias and scattering of NEE_{-EC1-} and NEE_{-EC2-} was considerably reduced by the sfd-correction.

A comparison of Figure 3.2 and Figure 3.5 illustrates how the sfd-correction affected the linear regression of the NEE standard error as function of NEE flux magnitude: The sfd-correction considerably enhanced the correlation of NEE_{corr} and the standard error $\sigma(\delta)_{corr}$ for the EC tower distances 20.5 km and 34 km from R^2 >= 0.15 to R^2 >= 0.43.

Applying the sfd-correction (without weather-filter) reduced the mean uncertainty value by 41.6% to 56.9% for the EC tower distances from 8 m to 34 km. The relative differences $\Delta\sigma_{cov}$ indicate that the correction for systematic flux differences considerably improved the two-tower based uncertainty estimate for the distances > 8 m (Table 3.3): The difference $\Delta\sigma_{cov}$ was notably smaller (< 56.8%) for all distances except the 8 m distance compared to $\Delta\sigma_{cov}$ determined with the classical two-tower approach (< 274.7%). The most considerable improvement was achieved for the 95 m EC tower distance and the 173 m distance. Additional application of the weather-filter (Figure 3.6) on the sfd-corrected NEE_{corr} data reduced the mean uncertainty estimate $\sigma(\delta)_{corr}$ by 23.3% and 2.9% for the 20.5 km and the 34 km EC tower distance and reduced $\Delta\sigma_{cov}$ by 57.7% and 7.7%. The effect of the weather-filter on the uncertainty estimates of the shorter EC tower distances was very minor (Table 3.3). The

uncertainty estimates $\sigma(\delta)_{corr,f}$ determined with the extended two-tower approach agree best with the independent reference values σ_{cov} for the EC tower distances 95m and 173 m, suggesting that those distances were most suitable for the application of the extended two-tower approach.

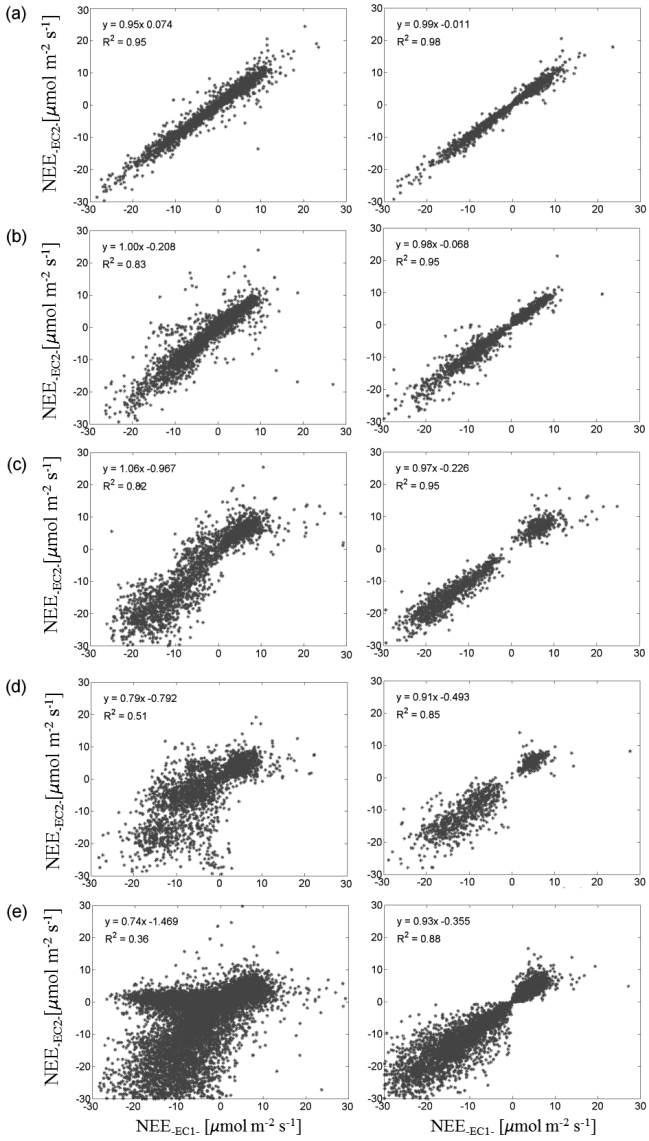

Figure 3.4: Scatter of the NEE measured at EC1 (NEE_{-EC1-}) and NEE measured at a second tower EC2/EC3 (NEE_{-EC2-}) for the uncorrected NEE (left) and the sfd-corrected NEE_{corr} (right) for the EC tower distances 8m (a), 95m (b) , 173m (c), 20.5km (d) and 34km.

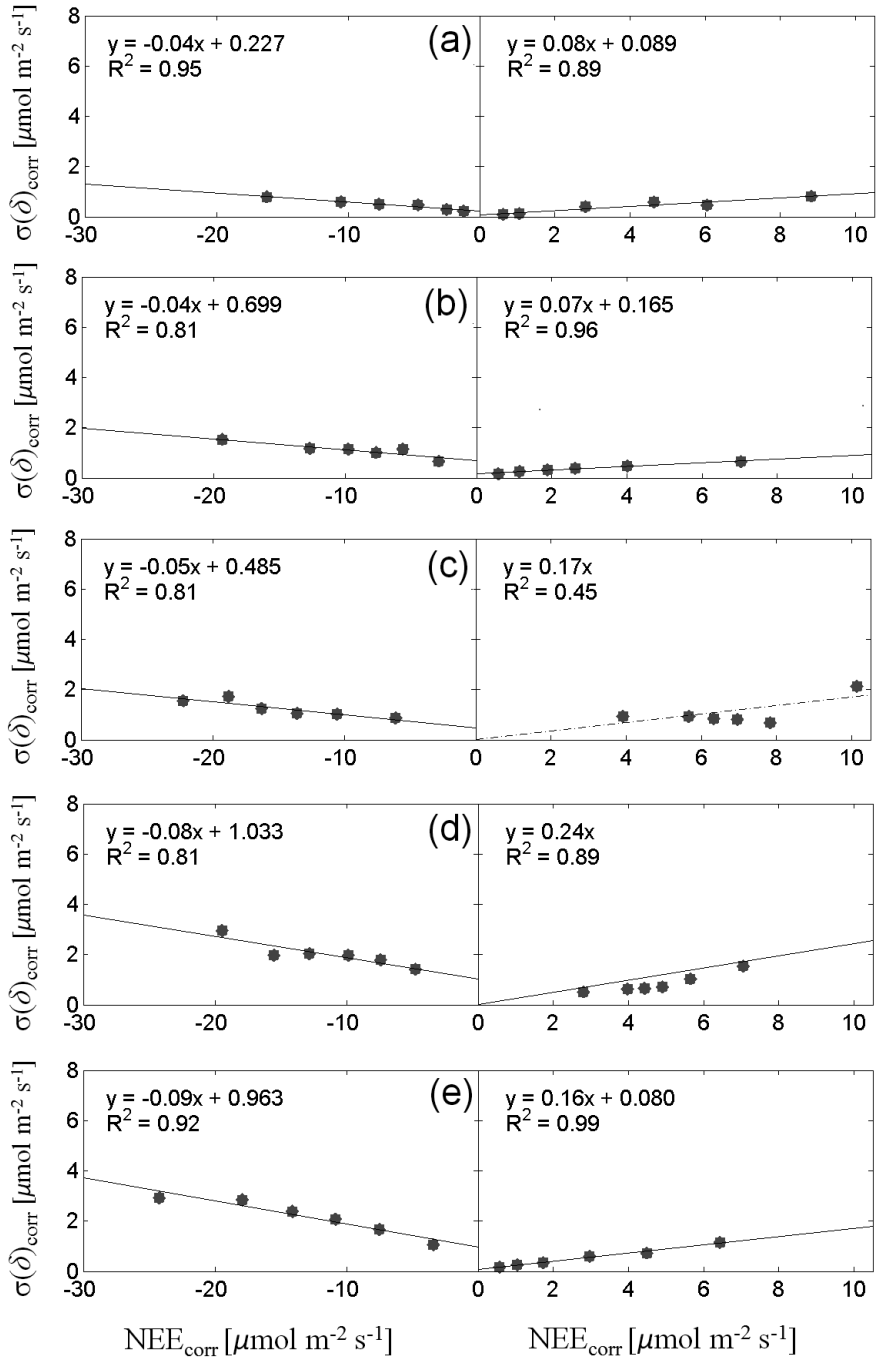

Figure 3.5: NEE uncertainty $\sigma(\delta)_{corr}$ determined with the extended two-tower approach as function of sfd-corrected NEE_{corr} magnitude (Equation 3.2) for the EC tower distances 8m (a), 95m (b), 173m (c), 20.5km (d) and 34 km (e) (Dashed line: regression slope not significantly different from zero ($p>0.1$)).

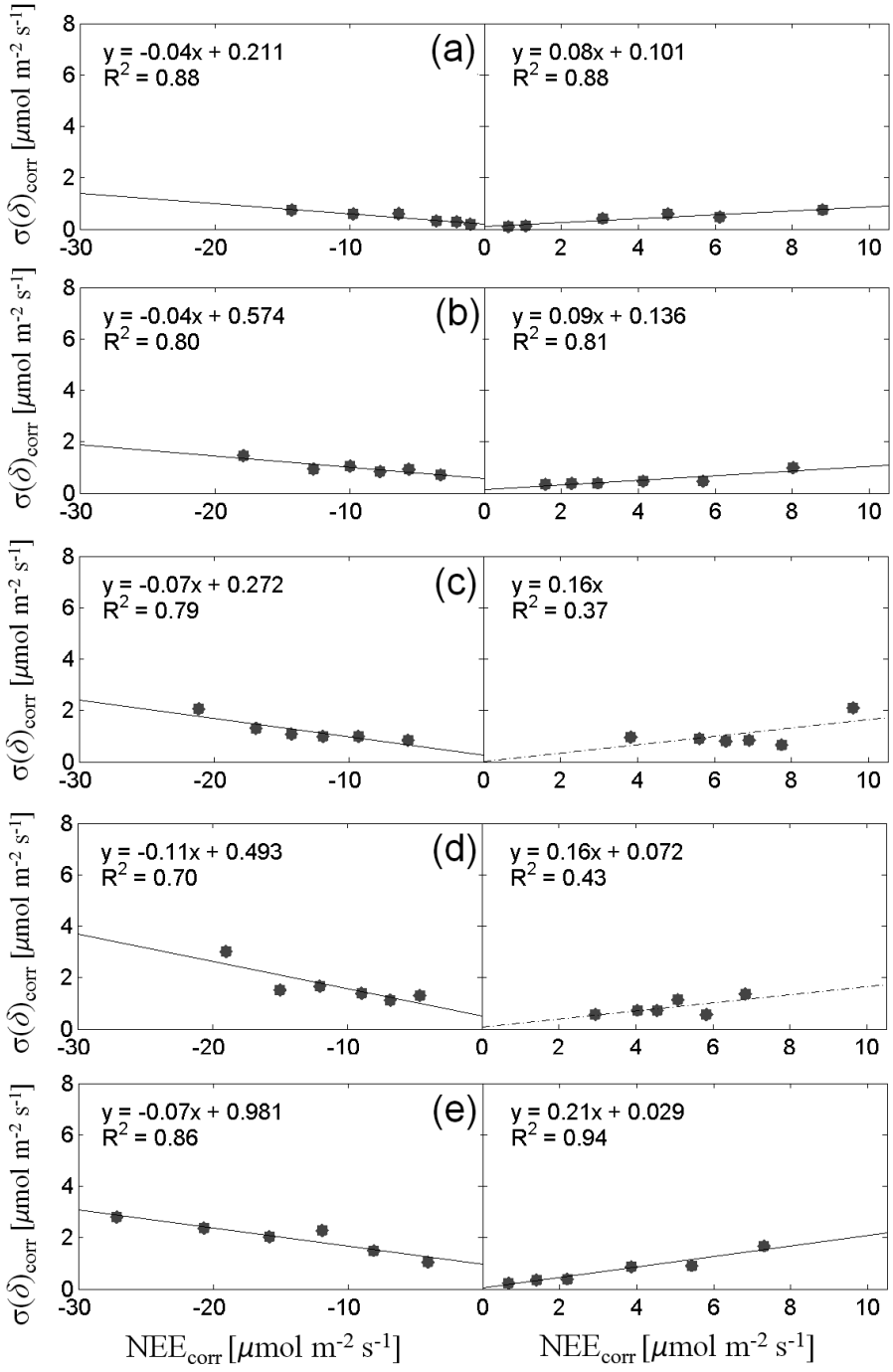

Figure 3.6: NEE uncertainty $\sigma(\delta)_{corr}$ determined with the extended two-tower approach as function of sfd-corrected NEE_{corr} magnitude (Equation 3.2) including application of the weather-filter for the EC tower distances 8m (a), 95m (b) , 173m (c), 20.5km (d) and 34km (e) (Dashed line: regression slope not significantly different from zero ($p>0.1$)).

3.5. DISCUSSION

The results show that the two-tower based uncertainty estimates (both classical and extended two-tower approach) were smallest for the 8 m distance. This can be explained with the results of the footprint analysis: While the average percentage footprint overlap is 13% (normalized 19%) for the 95 m EC tower distance and only 4% (7%) for the 173m EC tower distance, it is 68% (80%) for the 8 m EC tower distance. The stronger overlap of the 8 m distance footprint areas is associated with a more frequent sampling of the same eddies. As a consequence, part of the random error was not captured with the two-tower approach. If EC towers are located very close to each other (< 10 m) and the footprint overlap approaches 100%, only instrumental errors and stochasticity related to sampling of small eddies will be captured with the two-tower based uncertainty estimate. Because the EC measurements are statistically not independent if the footprints are overlapping, the classical EC tower method is not expected to give reliable uncertainty estimates for very short EC tower distances (Hollinger et al., 2004; Hollinger and Richardson, 2005). However, without applying the sfd-correction, the mean uncertainty estimate $\sigma(\delta)$ was higher than the raw-data based reference value $\sigma_{cov,}$ which includes both the instrumental noise $\sigma_{cov}^{noise}$and the stochastic error σ_{cov}^{stoch}. The raw-data based σ_{cov}^{noise} itself was only 0.04 µmol m^{-2} s^{-1} of 0.64 µmol $m^{-2}s^{-1}$ for the dataset of the 8 m EC tower distance. The mean uncertainty value derived with the extended two-tower approach $\sigma(\delta)_{corr,f}$ for the same dataset was lower than $\sigma(\delta)$ but still considerably higher than σ_{cov}^{noise}, suggesting that even at 8 m EC tower distance instrumentation errors were only a minor part of the two-tower based uncertainty estimate. For the larger separation distances 95 m or 173 m with notably less footprint overlap turbulence sampling errors are almost fully accounted for by a two-tower approach. (It should be noted that forest stations, with a typically larger aerodynamic measurement height and footprint size, will require larger separation distances). However, different land surface properties and management are more likely for the larger separation distances and can cause systematic flux differences that should not be attributed to the random error estimate. As outlined in Chapter 3.2, land surface properties related to management (e.g. nutrient availably due to fertilization), soil properties (bulk density, skeleton fraction), soil carbon-nitrogen pools, soil moisture and soil temperature are heterogeneously distributed at the Rollesbroich site. The effect of soil moisture, soil temperature and soil properties on CO_2 fluxes (respiration mainly) is well known (Lloyd and Taylor, 1994; Orchard and Cook, 1983; Xu et al., 2004; Flanagan and Johnson, 2005; Herbst et al., 2009) as well as the role of grassland management (e.g. Allard et al., 2007). Results indicate that an overestimation of the two-tower

based uncertainty caused by different land surface properties in the footprint area of both EC towers can be successfully filtered out by the extended approach. It should be noted that a shorter moving average interval of the sfd-correction term (e.g. 6 hours instead of the applied 12 hours window; Table 3.4), results in slightly lower uncertainty estimates compared to the reference. This can be explained by a possible "over-correction" of the NEE data related to a too short moving average interval for calculating the sfd-correction term. It needs to be emphasized that the estimated mean NEE values of the moving average intervals are associated with uncertainty. As mentioned, the moving average interval should be long enough to exclude random differences of the simultaneously measured fluxes but short enough to limit the impact of non-stationary conditions. However, the 12hr running mean NEE1 and NEE2 values (NEE_{12}) as well as the respective means of NEE1 and NEE2 (NEE_{2T_12}) used to calculate NEE_{corr} (Equation 3.2) are uncertain because they still contain the random error part, which cannot be corrected or filtered out. This uncertainty in the mean is expected to be higher for a shorter averaging interval such as 6 hours. Therefore, completely correcting the difference in mean NEE slightly overcorrects systematic differences in NEE. In general, results were not very sensitive to different moving average sizes of the sfd-correction term and data coverage percentages defined for this interval (Table 3.4).

Table 3.4: Relative difference [%] of mean uncertainty $\sigma(\delta)_{corr,f}$ estimated with the extended two-tower approach and the reference σ_{cov} for EC tower distances > 8m.

Diff	$\Delta\sigma_{cov}$ (6h)	$\Delta\sigma_{cov}$ (12h)	$\Delta\sigma_{cov}$ (24h)
30%	-0.8; 39.3	4.8; 55.5	10.9; 59.9
50%	-9.3; 32.5	-1.5; 41.2	-
70%	-10.5; 24.3	-5.2; 10.2	-

black: mean $\Delta\sigma_{cov}$ for 95m and 173m distance ; grey: mean $\Delta\sigma_{cov}$ for 20.5 km and 34 km distance

It is expected that systematic differences in measured NEE caused by spatially variable land surface properties are stronger during the night than during the day since they affect respiration more directly than photosynthesis (see e.g. Oren et al., 2006). Moreover, during night-time and/or winter (positive NEE), some conditions associated with lower EC data quality such as low turbulence, strong stability, and liquid water in the gas analyzer path prevail more often than in summer and/or daytime (negative NEE). The less severe cases of such conditions are not always completely eliminated by the quality control. In time series of eddy-covariance fluxes this typically shows up as implausible fluctuations of the flux during calm nights. This is reflected by plots of NEE flux magnitude versus uncertainty (Figure 3.2-3.3, Figure 3.5-3.6)

showing higher uncertainties for positive compared to negative NEE data which agrees with previous findings (e.g. Richardson et al., 2006).

At very large EC tower distances (20.5 km, 34 km) footprints were not overlapping and the environmental conditions were considerably different; in particular for the EC tower set-up Rollesbroich/Merzenhausen with different land use (grassland/crop) and climate conditions. For those distances, the relative difference $\Delta\sigma_{cov}$ between σ_{cov} and $\sigma(\delta)$ (classical two-tower approach) was much larger than $\Delta\sigma_{cov}$ between σ_{cov} and $\sigma(\delta)_{corr,f}$ (extended two-tower approach). $\Delta\sigma_{cov}$ was reduced by 85.7% for the 20.5 km distance and 79.3% for the 34 km if both sfd-correction and weather filter were used. However, after applying the sfd-correction and the weather-filtering, the mean uncertainty estimate was still higher than the raw-data based reference value (Table 3.3), suggesting that for these large EC tower distances the sfd-correction and the weather-filter do not fully capture systematic flux differences and uncertainty is still overestimated by the extended two-tower approach. This can have different reasons. We assume the major reason is that the weather-filter is supposed to capture all measured flux differences that can be attributed to different weather conditions at both EC towers, which cannot be captured with the sfd-correction. Applying stricter thresholds could increase the efficiency of the weather filter but in our case the reduced dataset was too small to allow further analysis. In general, the weather-filter did not improve the uncertainty estimates as much as the sfd-correction. However, this does not imply that differences in weather conditions are negligible when applying the extended two-tower approach for larger EC tower distances. In fact the systematic part of measured EC flux differences between both towers caused by (steady, systematic) among-site differences in weather conditions were already partly captured with the sfd-correction. In contrast, such systematic differences were difficult to capture with the weather-filter because much lower thresholds would have been required.

The absolute corrected and weather-filtered uncertainty value $\sigma(\delta)_{corr,f}$ [µmol m^{-2} s^{-1}] was slightly lower for the 34 km EC tower distance than for the 20.5 km EC tower distance (Table 3.3). The raw-data based reference σ_{cov} [µmol m^{-2} s^{-1}] however was also smaller for the 34 km dataset than for the 20.5 km dataset which can be related to the different lengths and timing (i.e., different seasons) of the measurement periods for each of the five EC tower distances: The roving station was moved from one distance to another within the entire measurement period of ~ 27 months. During this entire time period of data collection, the length and timing of the single measurement periods varied for the five EC tower separation distances (Table 3.1). This is not optimal because the random error is directly related to the flux magnitude and the flux

magnitude itself is directly related to the timing of the measurements. Because in spring and summer flux magnitudes are higher, the random error is generally higher as well (Richardson et al., 2006). To reduce this effect, spring/summer as well as autumn/winter months were captured in each measurement period. However, the timing of the measurements and the amount of data available were not the same for the five EC datasets. In particular the permanent EC tower in Merzenhausen was measuring considerably longer (> 2 years) than the roving station did for the other four EC tower distances. Therefore, differences of the mean uncertainty estimates for the five measurement periods were partly independent of the EC tower distance. This effect gets obvious when looking at the mean uncertainties σ_{cov} estimated with the reference method, which should be independent of the distance but were also found to be different for each dataset of the five EC tower distances. Against this background, statements about how EC tower distances affect the two-tower based uncertainty estimate need to be treated with caution.

The NEE uncertainty $\sigma(\delta)_{corr,f}$ estimated for the grassland site Rollesbroich agree well with the NEE uncertainty values for grassland sites by Richardson et al. (2006), and also the regression coefficients (Figure 3.2-3.3, Figure 3.5-3.6) do not show large differences. This can be expected since Richardson et al. (2006) applied their method for a very well-suited tower pair with low systematic differences, such that the classical approach and our extended approach should approximately converge. However, identical results are unlikely because even for two very similar neighboring sites some systematic differences occur. In addition, the random error is expected to vary between sites (see e.g. Mauder et al., 2013) which is in part related to instrumentation.

3.6. CONCLUSIONS

When estimating the uncertainty of eddy covariance net CO_2 flux (NEE) measurements with a two-tower based approach it is important to consider that the basic assumptions of identical environmental conditions (including weather conditions and land surface properties) on the one hand and non-overlapping footprints on the other hand are contradicting and impossible to fulfill. If the two EC towers are located in a distance large enough to ensure non overlapping footprints, different environmental conditions at both EC towers can cause systematic differences of the simultaneously measured fluxes that should not be included in the uncertainty

estimate. This study for the grassland site Rollesbroich in Germany showed that the extended two-tower approach, which includes a correction for systematic flux differences (sfd-correction) can be used to derive more reliable (less overestimated) uncertainty estimates compared to the classical two-tower approach. An advantage of this extended two-tower approach is its simplicity and the fact that there is no need to quantify the differences in environmental conditions (which is usually not possible due to a lack of data). Comparing the uncertainty estimates for five different EC tower distances showed that the mean uncertainty estimated with our extended two-tower approach for the 95 m and 173 m distances were nearly identical to the random error estimated with the raw-data based reference method. This suggests that these distances were most appropriate for the application of the extended two-tower approach in this study. Accordingly, the regressions in Figure 3.6(b,c) are considered to be most reliable. Also for the largest EC tower distances (20.5 km, 34 km) the sfd-correction significantly improved the correlations of the flux magnitude and the random error and significantly reduced the difference to the independent, raw-data based reference value. We therefore conclude that if no second EC tower is available at a closer distance (but available further away), a rough, probably overestimated NEE uncertainty estimate can be acquired with the extended two-tower approach although environmental conditions at the two sites are not identical.

A statement about the transferability of our experiment to other sites and EC tower distances requires further experiments. However, we assume transferability is given if both EC towers are located at sites of the same vegetation type (e.g. C3-grasses, C4-crops, deciduous forest, coniferous forest, etc.). Flux differences caused by a different phenology can be very hard to separate from the random error estimate, even though they are expected to be mainly systematic and could therefore be partly captured with the sfd-correction. Moreover, the EC raw data should be processed in the same way (as done here) and the measurement devices should be identical and installed at about the same measurement height. Important is also that the instruments are calibrated thoroughly and consistently. Because this was true for the three EC towers included in this study, we conclude that systematic flux differences that are corrected for with the sfd-correction arise mainly from different environmental conditions whereas calibration errors are assumed to have a very minor effect. Different weather conditions at both EC tower sites are a main drawback for applications of the two-tower approach. While systematic differences of the weather conditions are expected to be captured by the sfd-correction, less systematic weather fluctuations e.g. related to cloud movement, are difficult to be filtered of the two-tower based uncertainty estimate. Applying very strict thresholds can lead

to a too small dataset, especially if the measurement periods are short. If EC raw data is available, we recommend to use an uncertainty estimation scheme like the one presented in Mauder et al. (2013). Raw-data based NEE uncertainty estimation methods like the one suggested by Finkelstein and Sims (2001) and implemented by Mauder et al. (2013) have not been extensively applied yet and – to the best of our knowledge – never been compared to the ones derived with the more well-known two-tower approach. The fact that the two uncertainty estimates (extended two-tower approach and raw-data based reference) give very similar results therefore contributes to the confidence in both methods.

Chapter 4: Estimation of Community Land Model parameters for an improved assessment of NEE at European sites

*adapted from: Post, H., Vrugt, J.A., Fox, A., Vereecken, H., Hendricks Franssen, 2016. Estimation of Community Land Model parameters with DREAM$_{(zs)}$ for an improved assessment of net carbon fluxes at European sites (under review for the Journal of Geophysical Research - Biogeosciences).

4.1. INTRODUCTION

Land surface models (LSMs) such as the Community Land Model (CLM) (Oleson et al., 2013) simulate a myriad of highly interrelated water, energy, and nutrient fluxes and processes operating at or near the Earth's surface. LSMs are used widely to help analyze, understand, and predict the effects of environmental change on the hydrological and biogeochemical cycles of terrestrial ecosystems, and the impact of those changes (e.g., changes in carbon fluxes or albedo) on the atmosphere and the climate. In this context a major question to be answered is how the land carbon sink – including vegetation dynamics and soil carbon stocks – respond to climate and land use change (Quéré et al., 2012; Arora et al., 2013; Brovkin et al., 2013; Todd-Brown et al., 2014). The 5th Coupled Model Intercomparison Project (CMIP5) indicates that there are considerable uncertainties and model discrepancies related to carbon stock predictions (Piao et al., 2013). These discrepancies can be attributed to (1) model structural deficiencies (epistemic errors) due to inadequate and/or imperfect process knowledge and description, (2) wrong model parameter values, (3) uncertainty and biases in the initial values of the state variables, and (4) measurement uncertainty of the meteorological and land surface model input data (Piao et al., 2013; Todd-Brown et al., 2013).

Todd-Brown et al. (2013) found that model parameterization was a major source of diverging soil carbon predictions by different LSMs used in CMIP5. In most physical models, the parameters are often believed to be time-invariant (constant) and ascribed some fixed, or "universal" value. Various studies have questioned this conventional paradigm (Richardson et al., 2007; Mo et al., 2008; Williams et al., 2009; Kuppel et al., 2014) and demonstrate that certain LSM parameters vary dynamically in space and time, and possibly depend on environmental conditions. For example, consider the temperature sensitivity coefficient Q_{10}, which quantifies using a single value the fractional change of the respiration rate in response to

a 10°C temperature rise. This parameter exerts a strong control on the simulated carbon dynamics of land surface models such as CLM (Post et al., 2008; Hararuk et al., 2014). Various empirical and modeling studies have found the value of Q_{10} to vary dynamically in space and time, depending on the sites soil moisture conditions (Flanagan and Johnson, 2005; Kätterer et al., 1998; Reichstein et al., 2005), mean annual temperature (Kirschbaum, 2010, 1995) and quality of soil organic matter (Leifeld and Fuhrer, 2005; Rey et al., 2008). The maximum rate of carboxylation at 25°C, often referred to as V_{cmax25} is another key parameter, which affects strongly the predicted carbon fluxes of LSMs (Wang et al., 2007; Bonan et al., 2011; Göhler et al., 2013). This parameter is difficult to measure directly in the field, and CLM calibration of its value suffers heavily from model structural errors. As discussed in Bonan et al. (2011), this "may explain the lack of consensus in values for V_{cmax25} used in terrestrial biosphere models". Mo et al. (2008) found significant seasonal and inter-annual variations of V_{cmax25} and the (Ball-Berry) slope of the stomatal conductance-photosynthesis relationship using data assimilation of an ecosystem model. As a consequence, these authors have criticized LSM calibration methods that do not recognize properly the role of the initial states and temporal parameter variations.

Model calibration is a common approach to estimate parameters that cannot be measured directly in the field or laboratory. The word "calibration" usually involves searching for a single vector of parameter values that minimizes (or maximizes, if appropriate) some objective function of error residuals without recourse to investigating estimation of parameter and model predictive uncertainty. We therefore prefer the wording "parameter estimation" to coin a process of statistical inference using Bayesian analysis of modeling uncertainties. Yet, such approach is very challenging for LSMs as Todd-Brown et al. (2013) highlight that the CMIP5 models, including CLM, may suffer serious epistemic errors, in particular with respect to abiotic and biotic processes. These model structural deficits affect parameter estimation, as wrong process representations can often be compensated for by erroneous parameter values (Williams et al., 2009). Parameter estimation can only help maximize model performance, not fix structural errors (Braswell et al. 2005). Nevertheless, this approach can provide guidance on epistemic errors, thereby increasing our collective understanding of the processes and drivers that determine the magnitude size and spatiotemporal patterns of carbon fluxes (Verbeeck et al., 2011).

Historically, calibration approaches have been developed to estimate model parameters, whereas data assimilation methods such as the Ensemble Kalman Filter (EnKF) have focused on inference of state variables (Raupach et al., 2005). However, due to spatial-temporal variability of certain parameters and the close link between model states and parameters, the

conceptual distinction of model states and parameters is increasingly being considered arbitrary and with it methods to estimate them. Accordingly, sequential data assimilation methods such as the EnKF are increasingly being used to estimate ecosystem parameters for carbon flux predictions (Hill et al., 2012; Kuppel et al., 2012) and traditional Bayesian parameter estimation methods can serve for model state and parameter estimation (Braswell et al., 2005; Verbeeck et al., 2011; Hill et al., 2012; Kuppel et al., 2012). Different model-data fusion studies from point to global scale found that modeled land surface fluxes can be well constrained with eddy covariance data (Braswell et al., 2005; Knorr and Kattge, 2005; Xu et al., 2006; Mo et al., 2008; Verbeeck et al., 2011; Hill et al., 2012; Kuppel et al., 2012). However, studies highlight that only a few sensitive parameters (and states) can be well constrained to substantially improve NEE predictions (Wang et al., 2001; Santaren et al., 2007; Verbeeck et al., 2011).

Many previous model-data fusion studies for carbon flux estimation have focused on single forest ecosystems (Braswell et al., 2005; Williams et al., 2005; Santaren et al., 2007; Keenan et al., 2012; Mo et al., 2008; Verbeeck et al., 2011; Kato et al., 2012; Kuppel et al., 2012, 2013; Rosolem et al., 2013; Santaren et al., 2013) and have used simple ecosystem models instead of complex land surface models to simulate NEE. Notable exceptions are studies based on the CSIRO Biosphere Model (CBM) (Wang et al., 2001, 2007) or the ORCHIDEE model (Kuppel et al., 2014, 2012; Santaren et al., 2013, 2007; Verbeeck et al., 2011) that have used gradient-based algorithms for parameter estimation. These algorithms are not best suited to constrain highly dimensional, nonlinear LSMs, because they are prone to become stuck in a local minimum during the optimization process rather than finding the global minima (Williams et al., 2009). This is related to the challenge of equifinality (Beven and Freer, 2001; Mitchell et al., 2009; Laloy and Vrugt, 2012), i.e. multiple optimal parameter sets that generate equally good model outputs, which has been shown to be a major source of errors in simulated land surface fluxes including NEE (Schulz et al., 2001; Williams et al., 2009; Luo et al., 2009; Todd-Brown et al., 2013). Accordingly, Bayesian methods like Markov Chain Monte Carlo (MCMC) are considered more suited to estimate LSM parameters (Santaren et al., 2013). The main reason why MCMC approaches have not been generally applied to estimate LSM parameters is that computational demand is very high compared to other approaches.

For CLM, studies on calibration or estimation of ecosystem parameters in order to improve modeled carbon fluxes are very rare. Bilionis et al. (2015) estimated CLM parameters for soybean using a sequential MCMC approach and showed a significant improvement of predicted carbon pools and fluxes. Mao et al. (2016) showed that optimized CLM parameters reduced the misfit between modeled and measured soil respiration by 77% for a pine stand

forest. Several studies estimated ecosystem parameters of other models separately for different PFTs (He et al., 2013; Kuppel et al., 2014; Xiao et al., 2014). This has not been done yet in a comprehensive way for CLM.

As outlined above, ecosystem parameters and initial model states are highly uncertain and simultaneously important for carbon flux simulation in LSMs. The objective of this study was to obtain a better insight into CLM parameter and initial state uncertainty and the respective prospects and challenges to improve simulated NEE via parameter estimation, using measured NEE from EC sites in central and western Europe. We estimated key CLM4.5 parameters that regulate carbon flux predictions at sites in Germany and France for four different plant functional types: C3-grass, C3-crop, evergreen coniferous forest and broadleaf deciduous forest. Parameter estimation was done using the multi chain MCMC method DREAM$_{(zs)}$ (Ter Braak and Vrugt, 2008; Laloy and Vrugt, 2012; Vrugt, 2016). An advantage of the DiffeRential Evolution Adaptive Metropolis (DREAM) algorithm compared to other parameter estimation approaches is that (i) MCMC is not limited to Gaussianity, (ii) the full posterior probability distribution function (pdf) can be determined and (iii) the complete time series is considered at once in the parameter estimation (in contrast to e.g. sequential data assimilation methods). One hypothesis is that parameters estimated separately for single seasons instead of a complete year of NEE data would enhance model-data consistency more. The second hypothesis we tested is that carbon flux relevant model parameters and initial states are correlated and thus estimated parameter values differ if estimated jointly with the initial model states. Accordingly, a second objective is to estimate, evaluate and compare parameter estimates obtained with or without joint estimation of initial model states, under consideration of the respective uncertainty ranges. In this context we tested whether parameters estimated jointly with the initial model states would outperform the parameters estimated without initial states.

4.2. DATA AND METHODS

4.2.1. Eddy covariance sites and evaluation data

The half-hourly NEE data measured at four eddy covariance sites with different land cover types were used for CM parameter estimation (Figure 4.1). Three of the four sites are located in the Rur catchment and are part of the TERENO network (Zacharias et al., 2011). The extensively used C3-grassland site Rollesbroich (“RO”) [50.6219142°N; 6.3041256°E] is

located in the Eifel region of western Germany at 514.7 meters above sea level (MASL). The winter wheat site Merzenhausen ("ME") [50.92978°N / 6.2969924°E] is located 34 km northeast of RO in an agricultural lowland region. For further details see (Post et al., 2015). The EC raw data for both sites were processed with the TK3.1 software (Mauder and Foken, 2011), which includes a standardized quality assessment system and uncertainty estimation scheme as presented in Mauder et al. (2013). For RO, the statistically derived uncertainty estimates (Mauder et al., 2013) were verified with uncertainty estimates based on an extended two-tower approach (Post et al., 2015). The coniferous forest site Wüstebach ("WÜ") [50.5049024°N; 6.33138251°E] is located in the Eifel national park at 606.9 MASL and is covered by spruces. EC data for WÜ was processed with the software ECpack (Dijk et al., 2004) and with an additional post-processing according to Graf et al. (2014). NEE time series were available from June 2010 to May 2013 (WÜ) and from May 2011 to Dec. 2013 (RO, ME). Only non-gap filled, half-hourly data with quality flag 0 (high quality data) and 1 (moderate quality data) based on the quality assessment described in Mauder et al. (2013) were used in this study.

In addition to RO, ME and WÜ, we used FLUXNET data provided for the Fontainebleau deciduous forest site in France (FR-Fon) [48.4763°N, 2.7801°E] (from year 2005-2008) for parameter estimation. For this site no additional information such as site management was available.

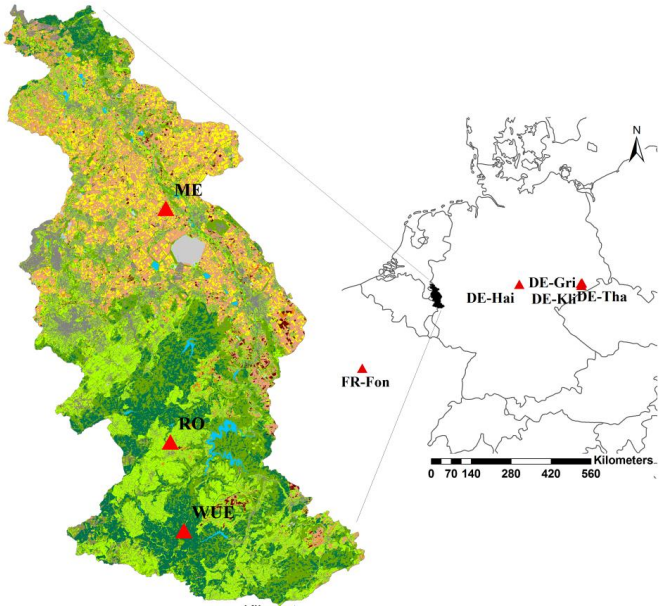

Figure 4.1: European eddy covariance sites used for parameter estimation (ME, RO, WÜ, FR-Fon), and model evaluation (all sites).

Four additional FLUXNET sites (Figure 4.1) served as evaluation sites: the grassland site Grillenburg (DE-Gri [50.9495°N, 13.5125°E]), the coniferous forest site Tharandt (DE-Tha [50.9636°N, 13.5669°E]), the agricultural site Klingenberg (DE-Kli, [50.8929°N, 13.5225°E]) and the deciduous forest site Hainich (DE-Hai, [51.0793°N, 10.4520°E]). Gap-filled Level 4 data for those FLUXNET sites were available for the years 2009-2012 (DE-Gri, DE-Tha, DE-Kli) and for the years 2005-2008 (DE-Hai). Again, only NEE data with quality 0 (original), 1 (most reliable) and 2 (medium reliable) were included in the analysis, while data with flag 3 (least reliable data) were not included. As uncertainty of FLUXNET NEE eddy covariance data was not provided, we estimated the NEE measurement uncertainty for the FLUXNET sites based on the linear regression functions obtained from the extended two-tower approach presented in Chapter 3.4.2, Figure 3.6(b).

4.2.2. CLM4.5 set-up and input data

For each site, CLM4.5BGC was set up using basic site specific input data. For each soil layer, the soil texture (percentage clay and sand) was defined. For the sites RO, WÜ and ME the German soil map (BK50) served as basis. For the FLUXNET sites no information on soil texture was available. Therefore, the soil texture for the forest sites was defined as for WÜ, and the soil

texture for DE-Kli and DE-Gri like ME and RO respectively. For all sites, the coverage by the site-specific PFT was set to 100%, which implies that smaller contributions of other PFTs within the EC-footprint were neglected. Winter wheat in CLM4.5 had not been parameterized or validated yet, so the winter wheat site ME was defined as C3-crop, which is treated like a non-managed C3-grass.

CLM was driven by the COSMO-DE reanalysis (Baldauf et al., 2009) provided by the German Weather Service (DWD) for the sites RO, WÜ and ME. The COSMO-DE data includes hourly time series of air temperature, incoming short wave radiation, incoming long wave radiation, precipitation, atmospheric pressure, specific humidity and wind speed. The meteorological input data (2008-2013) was provided in 2.8 km^2 resolution and downscaled to 1 km^2 grid resolution using nearest neighbor interpolation based on Delaunay triangulation. For the RO site gap-filled atmospheric input data measured at the EC tower were available. Half-hourly NEE was calculated for 2012 using either local site data or COSMO-DE reanalysis data as input. The differences between the simulations were very minor.

For each site CLM4.5 was spun-up for 1200 years in BGC ”spin-up mode”, i.e. accelerated carbon-nitrogen cycling, using atmospheric input of at least three years (2008-2010 in case of RO, WÜ and ME). The respective restart files with initial states were then used for a final 3 years spin-up in normal mode (“exit-spin-up”). We also tested longer exit-spin-up periods up to 100 years but found that results (both carbon pools and fluxes) were nearly identical after a 3-years and a 100-years exit-spin-up period.

The CLM set-up and procedure of the evaluation runs at the FLUXNET-sites was nearly identical to the parameter estimation runs. However, local meteorological data measured at the FLUXNET-sites were used for the CLM spin-up and forward runs.

4.2.3. Selection of parameters estimated with DREAM$_{(zs)}$

In this study, eight CLM4.5 parameters were estimated with DREAM$_{(zs)}$. The selection of these eight key parameters (Table 1) was based on a simple, local sensitivity study with 32 parameters. In the sensitivity study, linear correlation plots between each of the 32 parameters and the carbon fluxes (NEE, ER and GPP) were generated and compared, using monthly and annual means of different years.

Sensitivity analysis was carried out for the sites RO, ME and WÜ covering three different PFTs (C3-grass, C3-crop, coniferous forest). Sensitivity was tested for the year 2012 and for five individual months in 2012 (Mar., May, Jul., Sept., Dec.). For each site, each parameter and each

time period 100 different parameter values were sampled by Latin hypercube sampling (LHS). The sensitivity was tested by analyzing the average monthly or annual NEE as function of variation in the input parameter values.

Most of the eight sensitive parameters such as Q_{10}, b_s, fl_{NR} and sla_{top} were found to be critical key parameters in previous studies with CLM (Göhler et al., 2013; Foereid et al., 2014) or similar models (Post et al., 2008; Hararuk et al., 2014). fl_{NR} and sla_{top} are directly used to calculate V_{cmax25} (Eq.2.4). In addition, sla_{top} directly determines the prognostically calculated leaf area index (LAI) in CLM. Q_{10} is closely linked to mr_b because both parameters determine the degree of maintenance respiration. In addition, Q_{10} determines the heterotrophic respiration in the decomposition module. r_b and ψ_c go into the calculation of the effective root fraction which determines the root water uptake (Oleson et al., 2013). r_b determines the cumulative root faction for each soil layer (Zeng et al., 2011). The importance of r_b is also consistent with previous studies in the Amazonas region (Baker et al., 2008; Verbeeck et al., 2011) showing that the root profile parameter (describing the exponential root profile) is a particularly important parameter for improving NEE and LE simulated with LSMs.

The same is true for the Ball-Berry slope of stomatal conductance (b_s), which is an important key parameter for the calculation of LE and GPP in CLM 4.5, because it determines the water-use efficiency (WUE), i.e. ratio of CO_2 assimilation per unit water loss (Bonan et al., 2014). Since b_s is dependent on the effective water available for photosynthesis, b_s is also linked to r_b and ψ_c. Because not all carbon flux relevant CLM parameters were included in this sensitivity study and because sensitivity was tested only qualitatively with a local method that does not consider correlation among parameters (and states), it cannot be excluded that other critical CLM parameters exist and are not incorporated in this study. However, the intention of this study was not to perform an elaborated global parameter sensitivity study but to select only a small number of highly sensitive CLM parameters. Parameters showing a high sensitivity only at some sites and some months like the soil water potential at full stomatal closure (ψ_c) were also included.

4.2.4. Parameter (and initial state) estimation with DREAM$_{(zs)}$ –CLM

Parameter estimation experiments were conducted separately for four sites of different plant functional types (PFTs): RO (C3-grass), ME (C3-crop), WÜ (evergreen coniferous forest) and FR-Fon (broadleaf deciduous forest).

In order to test whether parameter estimates vary seasonally, DREAM$_{(zs)}$-CLM parameter estimation was carried out for four individual seasons as well as for the complete annual time series. Five of the eight CLM parameters are PFT-specific (Table 4.1). However, previous studies suggested that the parameters Q_{10}, mr_b, and b_s also could vary depending on the PFT (and season) (Mo et al., 2008; Post et al., 2008; Foereid et al., 2014). Therefore, the eight CLM parameters were estimated jointly for each site and time period.

Table 4.1: Parameters estimated with DREAM$_{(zs)}$ including lower bounds (Min) and upper bounds (Max) defined for the DREAM prior estimate and used as input to Latin Hypercube Sampling (LHS).

Short name	**Long name [unit]**	**CLM 4.5 default values** (Min/Max)			
PFT-parameters		**C3-grass**	**C3-crop**	**Coniferous forest**	**Deciduous forest**
fl_{NR}	Fraction of leaf N in Rubisco enzyme	0.1365 (0.05/0.35)	0.1758 (0.05/0.35)	0.0509 (0.02/0.15)	0.1007 (0.05/0.35)
sla_{top}	Specific Leaf Area (SLA) at top of canopy [m^2/gC]	0.03 (0.01/0.08)	0.03 (0.01/0.08)	0.01 (0.005/0.08)	0.03 (0.01/0.08)
g_R	Growth respiration factor	0.3 (0.1/0.4)	0.3 (0.1/0.4)	0.3 (0.1/0.4)	0.3 (0.1/0.4)
r_b	CLM rooting distribution parameter [1/m]	2.0 (0.5/4.0)	3.0 (0.5/4.0)	2.0 (0.5/4.0)	2.0 (0.5/4.0)
ψ_c	Soil water potential at full stomatal closure [mm]	-2.75*10^5 (-4.5*10^5/-1.5*10^5)	-2.75*10^5 (-4.5*10^5/-1.5*10^5)	-2.55*10^5 (-4.0*10^5/-1.5*10^5)	-2.55*10^5 (-4.0*10^5/-1.5*10^5)
hard-wired parameters (not PFT-specific)					
Q_{10}	temperature coefficient	1.5 (1.1/3.0)			
mr_b	base rate for maintenance respiration	2.53*10^{-6} (1.5*10^{-6}/4.5*10^{-6})			
b_s	Ball-Berry slope of conductance-photosynthesis relationship	9 (5.0/12.0)			

Additional experiments were conducted where two multiplication factors for initial CLM states were estimated together with the eight CLM key parameters (Table 4.2). Joint parameter and initial state estimation was carried out to determine the dependence of the eight parameters on the initial model states and because the initial model states are associated with a high uncertainty. Two multiplication factors were estimated for the following groups of initial CLM states:

- lCN: living carbon and nitrogen pools (leafc, leafc$_{storage}$, frootc, frootc$_{storage}$, livecrootc, livestemc, livestemc$_{storage}$, leafn, leafn$_{storage}$, frootn, frootn$_{storage}$, livecrootn, livestemn, livestemn$_{storage}$)
- dCN: dead carbon and nitrogen pools (litr1c, litr2c, litr3c, soil1c, soil2c, soil3c, litr1n, litr2n, litr3n, soil1n, soil2n, soil3n)

The factor dCN was applied to dead CN pools for each of the 15 CLM soil layers. The minimum and maximum bounds for LHS were set equal to 0.5 and 2.0 respectively for both multiplication factors. Joint parameter and initial state estimation was only conducted for the model runs that considered the complete year. The two initial state factors were estimated for the beginning of the parameter estimation period.

Table 4.2: CLM4.5 initial states estimated with DREAM$_{(zs)}$.

living CN pools		
leafc / leafn	leaf carbon / nitrogen content	[gC m^{-2}] / [gN m^{-2}]
leafc$_{storage}$ / leafn$_{storage}$	leaf carbon / nitrogen storage	[gC m^{-2}] / [gN m^{-2}]
frootc / frootn	fine root carbon / nitrogen content	[gC m^{-2}] / [gN m^{-2}]
frootc$_{storage}$/ frootn$_{storage}$	fine root carbon / nitrogen storage	[gC m^{-2}] / [gN m^{-2}]
livecrootc / livecrootn	living coarse root carbon / nitrogen content	[gC m^{-2}] / [gN m^{-2}]
livecrootc$_{storage}$/ livenrootc$_{storage}$	living coarse root carbon / nitrogen storage	[gC m^{-2}] / [gN m^{-2}]
livesteamc / livesteamn	live stem carbon / nitrogen content	[gC m^{-2}] / [gN m^{-2}]
livesteamc$_{storage}$/ livesteamn$_{storage}$	live stem carbon / nitrogen storage	[gC m^{-2}] / [gN m^{-2}]
dead CN pools		
lit1C / lit1N	litter carbon / nitrogen - fraction 1	[gC m^{-2}] / [gN m^{-2}]
lit2C / lit2N	litter carbon / nitrogen - fraction 2	[gC m^{-2}] / [gN m^{-2}]
lit3C / lit3N	litter carbon / nitrogen - fraction 3	[gC m^{-2}] / [gN m^{-2}]
soil1C / soil1N	soil carbon / nitrogen - fraction 1	[gC m^{-2}] / [gN m^{-2}]
soil2C / soil2N	soil carbon / nitrogen - fraction 2	[gC m^{-2}] / [gN m^{-2}]
soil3C / soil3N	soil carbon / nitrogen - fraction 3	[gC m^{-2}] / [gN m^{-2}]

The factors fdC and fdN were applied to dead carbon-nitrogen (CN) pools for each of the 15 CLM soil layers. Joint parameter and initial state estimation was only conducted for the model runs that considered the complete year. The four initial state factors were estimated for the beginning of the parameter estimation period.

Parameters were estimated with DREAM$_{(zs)}$ using half-hourly NEE time series [gC m^{-2} s^{-1}] excluding data with quality flags “low” (least reliable data). Prior parameter values were sampled by LHS using predefined upper and lower parameter bounds as constraints. We used three chains (default) for parameter estimation and four chains for the joint parameter and initial state estimation.

4.2.5. Evaluation of the DREAM$_{(zs)}$ derived MAP estimates

DREAM$_{(zs)}$ estimates for the eight CLM4.5 parameters were evaluated both in time and in space. Evaluation in time was carried out for CLM-simulation runs using estimated parameters over the year that followed the parameter estimation year (Table 4.3). These evaluation runs

were done for the same sites where parameters were estimated. The evaluation year started right after the end of the parameter estimation period (1 Dec. 2012 for RO and ME, 1 Jun. 2013 for WÜ, 1 Dec. 2006 for FR-Fon). Evaluation in space was carried out by using parameter estimates obtained for RO, ME, WÜ and FR-Fon for model simulations at the FLUXNET sites DE-Gri, DE-Kli, DE-Tha, and DE-Hai,that have corresponding PFTs to the estimation sites. The four FLUXNET evaluation sites were situated ~ 600 km away from the parameter estimation sites.

Table 4.3: DREAM$_{(zs)}$-CLM parameter estimation periods.

shortname	Season	time period	Sites
FR-Fon_w	Winter	01-12-2006 – 28-02-2007	FR-Fon
FR-Fon_sp	Spring	01-03-2007 – 31-05-2007	FR-Fon
FR-Fon_su	Summer	01-06-2007 – 31-08-2007	FR-Fon
FR-Fon_au	Autumn	01-09-2007 – 30-11-2007	FR-Fon
WÜ_su	Summer	01-06-2011 – 31-08-2011	WÜ
WÜ_au	Autumn	01-09-2011 – 30-11-2011	WÜ
site_w	Winter	01-12-2011 – 29-02-2012	WÜ,RO,ME
site_sp	Spring	01-03-2012 – 31-05-2012	WÜ,RO,ME
site_su	Summer	01-06-2012 – 31-08-2012	RO,ME
site_au	Autumn	01-09-2012 – 30-11-2012	RO,ME
WÜ_1y	whole year	01-06-2011 – 31-05-2012	WÜ
site_1y	whole year	01-12-2011 – 30-11-2012	RO,ME
FR-Fon_1y	whole year	01-12-2006 – 30-11-2007	FR-Fon

The evaluation was made for the one year (1y) and seasonal (s) -based parameter estimates. The 1y parameter estimates were applied to the whole evaluation run. The seasonal parameters were applied during the corresponding season over the course of the year-long evaluation run. In order to analyze the impact of the additional initial state estimation on the CLM performance, we also evaluated simulated NEE with parameters estimated jointly with the two initial state factors dCN and lCN ($1y^{IS}$) for RO, ME, WÜ and FR-Fon. The evaluation runs were compared with the outcome of one additional run with CLM default parameters, which served as a reference (Ref.).

To evaluate the performance of the parameters estimated with DREAM$_{(zs)}$-CLM, observed NEE time series (y) were compared to the modeled NEE time series (m). Chai and Draxler, (2014) highlight that any metric to quantify model errors only emphasizes a certain aspect of error characteristic. Therefore, it is beneficial to use a combination of different evaluation indices to assess model performance. In this study, we used the following evaluation indices:

(i) the relative difference of the simulated and measured NEE sum [%]:

$$\mathrm{RD}_{\sum \mathrm{NEE}} = \left| \frac{\sum_{i=1}^{n}(m_i) - \sum_{i=1}^{n}(y_i)}{\sum_{i=1}^{n}(y_i)} \times 100 \right| \tag{4.1}$$

with y = measured half-hourly NEE for a given year, m = modeled equivalent [µmol m^{-2} s^{-1}] and n = sum of all time steps where EC data were available during the evaluation year. We used the $RD_{\sum NEE}$ evaluation index, because the NEE sum (∑NEE) is in important indicator for the longer term carbon sink or source function of an ecosystem.

(ii) the root mean square error (RMSE) of half-hourly NEE [µmol m^{-2} s^{-1}], using the same time series as for $RD_{\sum NEE}$:

$$\mathrm{RMSE}_{\mathrm{m}} = \sqrt{\frac{1}{n}\sum_{i=1}^{n}(m_i - y_i)^2} \tag{4.2}$$

The RMSE is a commonly used metrics to evaluate model performance and was found to be sufficient index for comparing model errors in environmental studies (Chai and Draxler, 2014).

(iii) The mean absolute difference (MAD) of the mean diurnal NEE cycle:

$$\mathrm{MAD}_{\mathrm{diur\_1s}} = \frac{1}{48}\sum_{i=1}^{48}|m_i - y_i| \tag{4.3}$$

with m = average modeled NEE at a fixed time during the day and y = measured equivalent [µmol m^{-2} s^{-1}]. Compared are values at a 30 minutes interval for the daily cycle, giving 48 values per day. First, four MAD_{diur_1s} indices (one for each season) were calculated separately. Then, they were averaged to obtain one evaluation index MAD_{diur} for the complete evaluation year.

(iv) the MAD of the mean annual NEE cycle:

$$\mathrm{MAD}_{\mathrm{ann}} = \frac{1}{12}\sum_{i=1}^{12}|m_i - y_i| \tag{4.4}$$

with y = average measured NEE [µmol m^{-2} s^{-1}] for a given month and m = modeled equivalent.

We introduced MAD_{diur} and MAD_{ann} herein, because the reproduction of the diurnal or the annual NEE cycle is an important indicator on the physical plausibility of the simulated carbon fluxes. Since neither the RMSE nor $RD_{\sum NEE}$ provide this information, we decided that MAD_{diur} and MAD_{ann} should be evaluated in order to obtain a more comprehensive picture of model performance.

The relative improvement Δ_{MAP} [%] of simulations with estimated parameters compared to simulations with default parameters was evaluated as follows:

$$\Delta_{MAP} = \frac{I_{default} - I_{MAPs}}{I_{default}} \times 100. \quad (4.5)$$

With I_{MAPs} = evaluation index for NEE modeled with MAPs and $I_{default}$ =evaluation index for NEE modeled with CLM4.5 default parameters.

The 95% confidence intervals of the parameters were estimated from the posterior distribution.

The evaluation runs with estimated parameters were performed for the MAP estimates and for CLM ensembles with parameters sampled from the joint pfds (Ens_1y, Ens_1y^{IS}, and Ens_s). The indices MAD_{diur} and MAD_{ann} were determined for the evaluation runs with MAP estimates. The NEE sums and $RD_{\sum NEE}$ were also calculated for each of the 60 ensemble members in order to determine the respective 95% confidence intervals of the model output.

4.3. RESULTS

4.3.1. Evaluation of CLM forward runs with default parameters

Using default parameters, simulated NEE for the coniferous forest site WÜ and the deciduous forest site FR-Fon corresponded better with measured values than for the other sites. For the forest sites, summer daytime NEE was slightly underestimated between early spring and late autumn. Simulated NEE was slightly positive throughout winter. FLUXNET data for FR-Fon indicated slightly higher nighttime respiration magnitudes and also included days with net carbon uptake. This is probably a result of non-deciduous vegetation in the EC footprint area.

Systematic discrepancies between modeled and measured NEE at the grassland site RO were observed for the years 2011-2013. Modeled NEE was less negative than observed NEE data during summer daytime and considerably less negative in early spring (~March 2012) and late autumn (~November 2012), indicating an underestimation of carbon uptake. For ME, model-data discrepancies were more severe. Carbon uptake was underestimated during daytime and until mid-July. However, in mid-July, measured NEE abruptly increased due to the senescence of the winter wheat, which was recorded by the camera images that were regularly recorded at the site. Because the PFT C3-crop in CLM does not include the senescence of winter wheat, simulated NEE did not represent the sudden decrease in GPP and accordingly daytime carbon uptake was greatly overestimated from mid-July to mid-September. The model-data

discrepancy after the observed senescence of winter wheat was considerably higher than e.g. the model-data discrepancy after the harvest in August. As the ME site was managed the same way in the years 2011 to 2013, the abrupt shift from underestimation to overestimation of carbon uptake in mid-July was present in each of the three years.

A comparison of measured and modeled NEE at the RO and the ME site indicated that the simulated plant onset and offset (i.e. the time when simulated LAI jumps from zero to >0 and from >0 to zero respectively) was not represented correctly by CLM for these PFTs, which in case of ME is not surprising, since winter temperate cereal is not parameterized yet in CLM4.5. In the parameter estimation year 2012, onset was delayed about 2 weeks (observed: beginning of March; modeled: mid-March) at both sites. In the evaluation year 2013, onset was delayed about one month at the RO site (observed: beginning of April; modeled: beginning of May) and about 2 weeks early at the ME site (observed: ~10th of April, modeled: ~25th of March).

4.3.2. DREAM$_{(zs)}$ parameter (and initial state) estimation

The number of iterations required for a complete convergence of all parameters with DREAM$_{(zs)}$-CLM was 5000-8000 for seasonal parameter estimation (except ME_sp and FR-Fon_su where >10000 iterations were required). When parameters were estimated with NEE time series for a complete year, parameters generally converged after > 12,000 iterations, except for WÜ (~3000 iterations). For illustration, the courses of the convergence diagnostic R_{stat} for one year simulations of WÜ and for FR-Fon are shown in Figure 4.2.

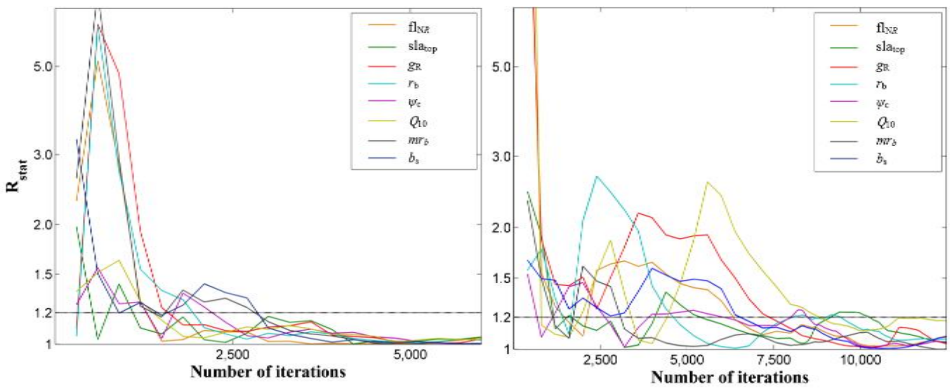

Figure 4.2: Convergence diagnostics (R_{stat}) of individual parameters estimated with DREAM$_{(zs)}$ for the coniferous forest site WÜ (left) and the deciduous forest site FR-Fon (right) using half-hourly NEE data of one year.

Table 4.4 summarizes the MAP estimates and the respective 95% confidence intervals (95%CI) of the eight CLM parameters for the four different plant functional types and the single seasons (s-MAPs). For most sites and parameter estimation periods, the CLM parameters could be well constrained with DREAM$_{(zs)}$ and the 95%CI were narrow and close to the MAP estimates. The uncertainty ranges of the season-based parameter estimates, i.e. the degree to which parameters were constrained, were comprehensible in most cases: The parameter ψ_c was most uncertain, i.e. the span of the 95%CI was large for most sites and time periods. This is probably related to the fact that longer dry phases in this region are very rare. Accordingly, for most sites and time periods, the simulated soil moisture is not a limiting factor for the simulated GPP or ER, such that NEE is not very sensitive to ψ_c. For all sites, b_s, which determines the rate of stomatal conductance, was most uncertain in winter. This is plausible, given that photosynthesis is limited in this period. For site ME, the spread of b_s was also high in autumn, which is plausible as well, because winter wheat was harvested end of July.

For all sites except RO, fl_{NR} and sla_{top} were also most uncertain in winter. This is reasonable, since fl_{NR} and sla_{top} determine GPP, which is lowest in winter. Thus, NEE is expected to be less sensitive to those parameters in winter. For the other seasons, these parameters could be well constrained. The base rate for maintenance respiration mr_b was not well constrained in winter for all sites except ME. For r_b, the uncertainty was particularly high in summer for all sites except FR-Fon, where the uncertainty of r_b was highest in winter and spring. This indicates that for those sites and seasons, simulated NEE was not strongly dependent on the rooting distribution.

Not only the uncertainty ranges, but also the variations of the parameter values estimated for the different seasons were plausible for most parameters and sites (Table 4.4). For all sites except WÜ, estimated parameter values varied notably among the different seasons and some parameters were significantly different for different seasons. Seasonal parameter variations were lowest at the evergreen coniferous forest site WÜ. For C3-grass and C3-crop (RO and ME), r_b was lowest in spring and summer. With lower r_b values, a higher percentage of water would be taken up by deeper roots. Against this background, both r_b and ψ_c are assumed to not only vary throughout the year, but also inter-annually considering drought years, which however was not tested here. Both for RO and ME, estimated values for b_s and thus stomata conductance were highest in spring. This is plausible, since photosynthetic capacity is high and stomatal opening less limited by high temperatures compared to summer.

Table 4.4: Season-based estimates for eight CLM parameters determined with DREAM$_{(zs)}$ for different time periods and the four sites with different plant functional types.

	year	fl_{NR}	sla_{top}	g_R	r_b	ψ_c	Q_{10}	mr_b	b_s
RO_w	11/' 12	0.12, 0.15, 0.14*	0.010, 0.010, 0.010*	0.16, 0.39, 0.36*	1.69, 3.62, 3.62*	-3.98*10^5, -1.61*10^5, -2.72*10^5*	2.13, 2.52, 2.39*	2.42*10^{-6}, 4.50*10^{-6}, 4.47*10^{-6}*	5.2, 10.8, 6.1*
RO_sp	2012	0.16, 0.25, 0.25*	0.025, 0.041, 0.041*	0.38, 0.40, 0.40*	1.01, 1.71, 1.01*	-3.94*10^5, -1.63*10^5, -2.24*10^5*	1.11, 1.19, 1.14*	4.33*10^{-6}, 4.50*10^{-6}, 4.50*10^{-6}*	8.2, 11.0, 9.4*
RO_su	2012	0.11, 0.16, 0.13*	0.010, 0.011, 0.010*	0.37, 0.40, 0.39*	0.50, 1.78, 0.51*	-4.48*10^5, -1.73*10^5, -2.35*10^5*	1.10, 1.57, 1.10*	4.38*10^{-6}, 4.50*10^{-6}, 4.50*10^{-6}*	5.6, 7.0, 6.1*
RO_au	2012	0.14, 0.16, 0.16*	0.010, 0.011, 0.011*	0.35, 0.40, 0.40*	1.04, 3.43, 2.01*	-3.80*10^5, -1.51*10^5, -2.77*10^5*	1.65, 1.84, 1.75*	4.23*10^{-6}, 4.50*10^{-6}, 4.47*10^{-6}*	5.8, 6.4, 5.9*
ME_w	11/'12	0.09, 0.13, 0.12*	0.050, 0.100, 0.100*	0.34, 0.40, 0.40*	2.62, 3.98, 3.70*	-4.49*10^5, -2.39*10^5, -4.34*10^5*	2.99, 3.00, 3.00*	1.50*10^{-6}, 1.56*10^{-6}, 1.50*10^{-6}*	5.2, 9.9, 5.2*
ME_sp	2012	0.08, 0.08, 0.08*	0.010, 0.010, 0.010*	0.10, 0.14, 0.10*	0.50, 0.76, 0.52*	-4.45*10^5, -1.69*10^5, -2.89*10^5*	1.10, 1.19, 1.10*	4.18*10^{-6}, 4.50*10^{-6}, 4.48*10^{-6}*	9.0, 10.0, 9.7*
ME_su	2012	0.05, 0.05, 0.05*	0.010, 0.011, 0.010*	0.26, 0.40, 0.31*	0.51, 1.35, 0.57*	-4.40*10^5, -1.58*10^5, -2.41*10^5*	2.57, 2.99, 2.95*	2.94*10^{-6}, 4.37*10^{-6}, 4.23*10^{-6}*	6.8, 7.6, 7.4*
ME_au	2012	0.07, 0.10, 0.08*	0.081, 0.100, 0.095*	0.10, 0.30, 0.10*	3.71, 4.00, 4.00*	-1.58*10^5, -1.50*10^5, -1.51*10^5*	2.85, 3.00, 2.98*	1.51*10^{-6}, 2.11*10^{-6}, 1.65*10^{-6}*	5.2, 10.0, 9.2*
WÜ_w	11/'12	0.03, 0.15, 0.14*	0.006, 0.073, 0.011*	0.11, 0.39, 0.37*	0.60, 3.92, 3.79*	-3.97*10^5, -2.07*10^5, -3.81*10^5*	1.40, 2.99, 2.89*	1.55*10^{-6}, 3.42*10^{-6}, 2.00*10^{-6}*	6.2, 11.9, 10.5*
WÜ_sp	2012	0.05, 0.06, 0.06*	0.005, 0.006, 0.005*	0.33, 0.40, 0.39*	1.16, 3.98, 3.69*	-3.90*10^5, -2.07*10^5, -3.51*10^5*	2.58, 3.00, 2.99*	2.30*10^{-6}, 3.49*10^{-6}, 3.45*10^{-6}*	5.0, 5.4, 5.0*
WÜ_su	2012	0.03, 0.06, 0.05*	0.005, 0.007, 0.005*	0.11, 0.39, 0.39*	0.76, 3.89, 3.58*	-3.96*10^5, -2.10*10^5, -3.05*10^5*	1.25, 2.79, 2.68*	2.29*10^{-6}, 3.48*10^{-6}, 3.32*10^{-6}*	6.0, 7.9, 6.7*
WÜ_au	2012	0.06, 0.13, 0.10*	0.005, 0.015, 0.005*	0.12, 0.50, 0.49*	0.63, 3.78, 3.39*	-3.97*10^5, -2.09*10^5, -2.08*10^5*	2.30, 2.99, 2.99*	1.57*10^{-6}, 3.45*10^{-6}, 2.50*10^{-6}*	5.0, 6.6, 5.0*
FR-Fon_w	06/'07	0.05, 0.25, 0.09*	0.012, 0.078, 0.064*	0.11, 0.39, 0.18*	1.10, 3.88, 3.00*	-3.95*10^5, -2.53*10^5, -2.55*10^5*	2.52, 2.85, 2.68*	1.59*10^{-6}, 3.46*10^{-6}, 3.34*10^{-6}*	5.2, 11.8, 11.0*
FR-Fon_sp	2007	0.07, 0.08, 0.08*	0.010, 0.010, 0.010*	0.10, 0.11, 0.10*	1.60, 3.99, 3.56*	-3.98*10^5, -2.59*10^5, -3.44*10^5*	1.17, 1.37, 1.27*	2.33*10^{-6}, 3.45*10^{-6}, 3.12*10^{-6}*	6.5, 7.0, 6.5*
FR-Fon_su	2007	0.19, 0.19, 0.19*	0.019, 0.021, 0.020*	0.39, 0.40, 0.40*	1.00, 1.27, 1.01*	-3.97*10^5, -2.58*10^5, -3.11*10^5*	1.10, 1.14, 1.10*	3.35*10^{-6}, 3.50*10^{-6}, 3.48*10^{-6}*	7.4, 9.1, 8.2*
FR-Fon_au	2007	0.17, 0.18, 0.17*	0.020, 0.023, 0.021*	0.38, 0.40, 0.40*	1.01, 1.84, 1.02*	-3.89*10^5, -2.57*10^5, -2.96*10^5*	2.91, 3.00, 2.99*	1.51*10^{-6}, 2.27*10^{-6}, 1.53*10^{-6}*	10.0, 12.0, 11.3*

MAP estimates (*), including lower bound (upper value) and upper bound (middle value) of the 95% confidence interval. RO: Rollesbroich site (C3-grass), ME: Merzenhausen site (C3-crop), WÜ: Wüstebach site (evergreen coniferous forest), FR-Fon: Fontainebleau site (broadleaf deciduous forest); w: winter (Dec.-Feb.); sp: spring (Mar.-May); su: summer (Jun.-Aug.); a: autumn (Sep.-Nov.)

In most cases, the estimated parameter values for Q_{10}, mr_b and g_R were higher than the CLM default, which would result in an increase of simulated ecosystem respiration with estimated parameters. Particularly estimated Q_{10} was higher than the CLM default (1.5) for most sites and time periods. In case of RO and FR-Fon, both fl_{NR} and sla_{top} were highest in spring or summer respectively. This is reasonable, given that photosynthetic capacity can be expected highest in this period.

For several parameters and sites, estimated parameters were estimated close to the predefined minimum or maximum bounds of the parameter values ("edge-hitting parameters"). One example is g_R, r_b and Q_{10} for ME (Table 4.4). In those cases, the degree of seasonal variations among parameters, jumping from one edge to the other, is not considered realistic. This is further discussed in Chapter 4.4.1.

Table 4.5 summarizes the estimates of the eight CLM parameters based on the whole year period with ($1y^{IS}$) and without (1y) joint estimation of the two initial state multiplication factors lCN and dCN. Not only the PFT-specific parameters, but also the non PFT-specific parameters mr_b, b_s and Q_{10} varied for the different sites or PFTs (Table 4.5). For the forest PFTs, estimated Q_{10} was higher (~ 1.9 - 3.0) compared to C3-grass and C3-crop, where Q_{10} was <= 2.0. For all sites except ME.

Along with Q_{10}, also estimated values for the Ball-Berry slope of stomatal conductance b_s clearly differed from the default throughout the different set-ups and sites (Table 4.5). The b_s parameter was estimated lower (~ 6) than the default (b_s = 9) for all PFTs except C3-crop, both with and without additional estimation of the two initial state factors. A lower b_s implies that the water-use efficiency is increased which results in higher CO_2 assimilation rates per unit water loss. The challenges and possible model development steps in terms of the Ball-Berry conductance model are thoroughly outlined in Bonan et al. (2014).

For all PFTs except coniferous forest, the relative difference between the size of the living and dead CN pools differed significantly from the initial states generated with CLM default parameters. dCN was >1.6, indicating that the initial amount of the dead plant material (litter and soil organic matter pools) was > 60% larger compared to the default set-up. In contrast, lCN was < 1.0 for those sites. Thus, the size of initial living CN pools was reduced, especially for deciduous forest (lCN=0.5).

Table 4.5: One-year based estimates for eight CLM parameters and two initial state multiplication factors, determined with DREAM$_{(zs)}$ for different time periods and the four sites (ME, RO, WÜ, FR-Fon) with different plant functional types.

	year	fl_{NR}	sla_{top}	g_R	r_b	ψ_c	Q_{10}	mr_b	b_s	lCN	dCN
C3-grass		*0.14*	*0.030*	*0.30*	*2.00*	*-2.75*10^5*	*1.50*	*2.53*10^{-6}*	*9.0*		
RO_1y	11/'12	0.13, 0.15, 0.14*	0.010, 0.010, 0.010*	0.39, 0.40, 0.40*	1.01, 1.27, 1.01*	-3.79*10^5, -1.65*10^5, -2.74*10^5*	1.39, 1.44, 1.41*	4.48*10^{-6}, 4.50*10^{-6}, 4.50*10^{-6}*	6.1, 6.9, 6.5*		
RO_1y^{IS}	11/'12	0.32, 0.35, 0.34*	0.064, 0.069, 0.068*	0.39, 0.40, 0.40*	1.01, 1.48, 1.15*	-3.77*10^5, -1.63*10^5, -2.39*10^5*	1.93, 1.99, 1.95*	4.41*10^{-6}, 4.50*10^{-6}, 4.49 *10^{-6}*	5.8, 6.4, 6.0*	0.9, 0.9, 0.9*	2.0, 2.0, 2.0*
C3-crop		*0.18*	*0.030*	*0.30*	*3.00*	*-2.75*10^5*	*1.50*	*2.53*10^{-6}*	*9.0*		
ME_1y	11/'12	0.25, 0.26, 0.25*	0.079, 0.080, 0.080*	0.20, 0.21, 0.21*	3.88, 4.00, 4.00*	-2.50*10^5, -2.02*10^5, -2.18*10^5*	1.10, 1.10, 1.10*	4.42*10^{-6}, 4.50*10^{-6}, 4.48*10^{-6}*	12.0, 12.0, 12.0*		
ME_1y^{IS}	11/'12	0.31, 0.35, 0.35*	0.057, 0.066, 0.064	0.38, 0.40, 0.39*	3.88, 4.00, 4.00*	-4.00*10^5, -3.72*10^5, -3.89*10^5*	1.28, 1.39, 1.34*	1.50*10^{-6}, 1.59*10^{-6}, 1.53*10^{-6}*	11.5, 12.0, 12.0*	0.7, 0.8, 0.7*	2.0, 2.0, 2.0*
coniferous forest		*0.05*	*0.010*	*0.30*	*2.00*	*-2.55*10^5*	*1.50*	*2.53*10^{-6}*	*9.0*		
WÜ_1y	11/'12	0.05, 0.07, 0.06*	0.005, 0.006, 0.005*	0.29, 0.40, 0.40*	0.75, 3.95, 3.88*	-3.91*10^5, -2.07*10^5, -3.91*10^5*	2.50, 2.99, 2.96*	2.13*10^{-6}, 3.48*10^{-6}, 3.42*10^{-6}*	5.0, 6.2, 5.2*		
WÜ_1y^{IS}	11/'12	0.04, 0.07, 0.06*	0.005, 0.006, 0.005*	0.28, 0.40, 0.40*	0.84, 3.92, 3.95*	-3.96*10^5, -2.12*10^5, -3.01*10^5*	2.72, 3.00, 2.93*	1.51*10^{-6}, 3.78*10^{-6}, 1.54*10^{-6}*	5.0, 6.0, 5.0*	1.0, 1.8, 1.4*	0.9, 1.6, 1.4*
deciduous forest		*0.05*	*0.010*	*0.30*	*2.00*	*-2.55*10^5*	*1.50*	*2.53*10^{-6}*	*9.0*		
FR-Fon_1y	06/'07	0.12, 0.12, 0.12*	0.010, 0.010, 0.010*	0.39, 0.40, 0.40*	1.00, 1.17, 1.00*	-3.89*10^5, -2.57*10^5, -3.81*10^5*	1.87, 1.97, 1.94*	3.47*10^{-6}, 3.50*10^{-6}, 3.48*10^{-6}*	5.7, 6.0, 5.8*		
FR-Fon_1y^{IS}	06/'07	0.24, 0.27, 0.26*	0.018, 0.021, 0.020*	0.23, 0.32, 0.29*	1.91, 3.92, 2.59*	-3.97*10^5, -2.55*10^5, -2.59*10^5*	2.77, 2.99, 2.96*	1.50*10^{-6}, 1.75*10^{-6}, 1.75*10^{-6}*	6.0, 6.2, 6.0*	0.5, 0.5, 0.5*	1.6, 1.7, 1.7*

MAP estimates (*), including lower bound (upper value) and upper bound (middle value) of the 95% confidence interval. 1y: one year of half hourly NEE time series. grey: CLM default parameters, ^{IS}: with joint estimation with the multiplication factors lCN and dCN for the initial living and dead carbon-nitrogen pools

For the coniferous forest site WÜ, MAPs for both dCN and lCN were 1.4. Thus, the size of the living and dead CN pools was increased but the ratio remained unchanged. The finding that dCN and fCN were closer to 1 compared to the other sites may be related to the fact that spruces at the WÜ site were planted in the 1940s and since then the site, which is now part of Eifel National Park, has not been managed such that the steady state assumption may be more correct compared to the other sites. Besides, WÜ was the only site where the uncertainty of lN and dCN was relatively large as indicated by the upper and lower 95%CI. Thus, for coniferous forest, simulated NEE was less sensitive to the size of the initial carbon-nitrogen pools.

Some of the estimated parameter values differed significantly depending on whether or not they were estimated jointly with lCN and dCN (Table 4.5). For RO and ME for example, Q_{10} was

higher for $1y^{IS}$ than for 1y. In case of ME and FR-Fon, mr_b was significantly lower for $1y^{IS}$ compared to 1y. For FR-Fon, fl_{NR}, sla_{top} and r_b were significantly higher for $1y^{IS}$ compared to 1y. This shows that estimated parameter values are strongly dependent on the amount of initial carbon and nitrogen [gC m^{-2}, gN m^{-2}]. Due to this dependency, parameter sets can be considered tailored to a specific range of initial states and thus may not be valid if the initial states differ notably from the ones parameters were originally estimated for.

Figure 4.3 and Figure 4.4 highlight that estimated parameters correlate with each other and with initial states. For example, Q_{10} strongly correlates with fl_{NR} in case of RO and FR-Fon, and fl_{NR} correlates strongly with b_s. Those among-parameter correlations changed depending on whether or not they were estimated jointly with dCN and lCN. For all sites, the correlation between fl_{NR} and sla_{top} substantially increased when parameters were estimated together with lCN and dCN. At the same time, lCN and/or dCN correlated strongly with some of the estimated parameters. The direction and the degree of the correlation between parameters (and initial state factors) varied among the four sites. This highlights the difficulty in treating processes, initial states and parameters separately when examining their contribution to the uncertainty of modeled NEE.

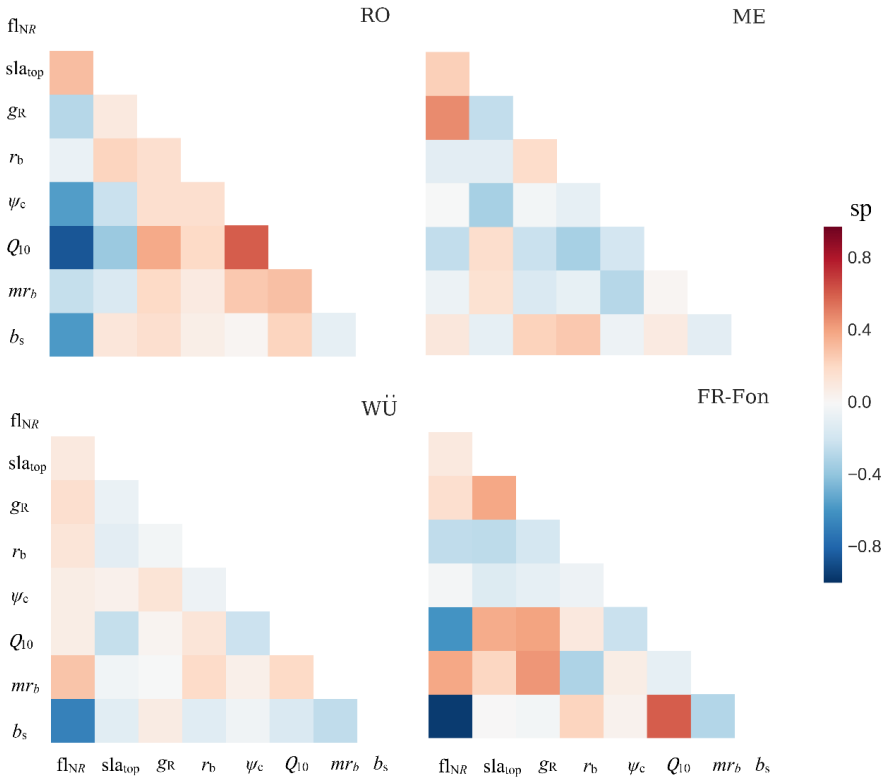

Figure 4.3: Spearman correlation coefficients (sp) for the two-dimensional correlations of the posterior samples determined with DREAM$_{(zs)}$-CLM for four sites with a one year time series of eddy covariance NEE data.

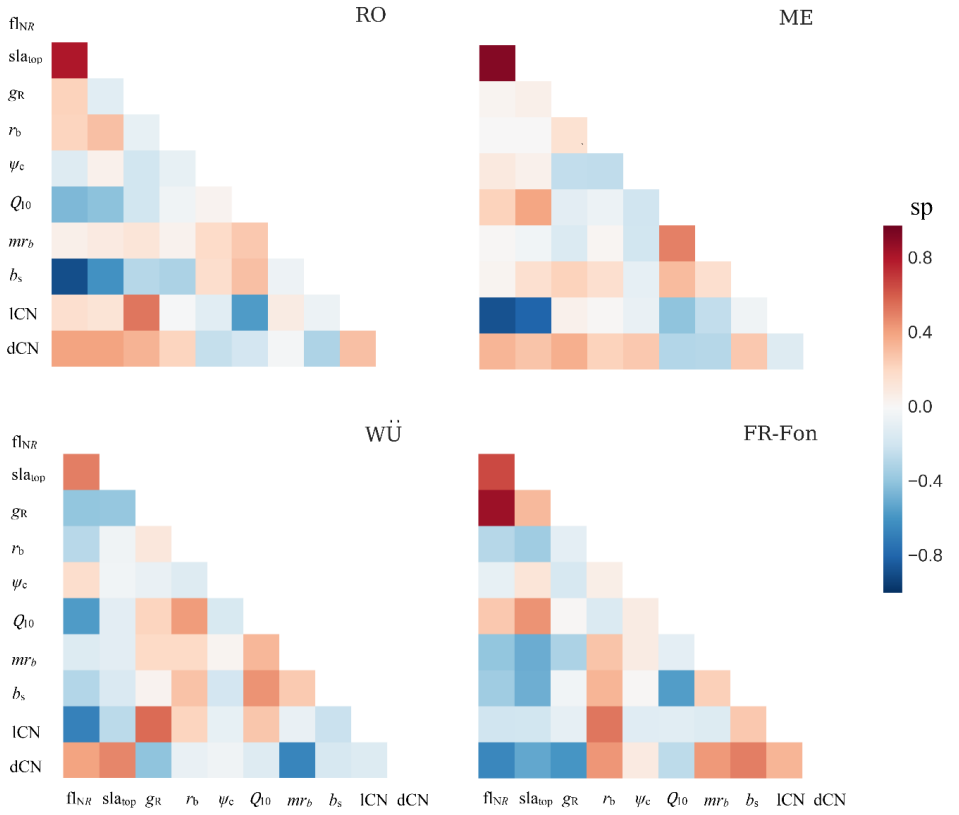

Figure 4.4: Spearman correlation coefficients (sp) for the two-dimensional correlations of the posterior samples determined with DREAM$_{(zs)}$-CLM for four sites with a one year time series of eddy covariance NEE data, with estimation of the initial state multiplication factors dCN and lCN for the in dead and living CN pools.

4.3.3. Evaluation of the parameter estimates in terms of model performance and uncertainty in simulated NEE

The CLM parameter sets estimated for RO, WÜ, ME and FR-Fon were evaluated in time for the evaluation year and in space for the FLUXNET sites DE-Gri, DE-Tha, DE-Kli and DE-Hai with corresponding PFTs.

The mean diurnal NEE cycles for the four seasons in the evaluation year are shown for the parameter estimation sites RO (Figure 4.5), ME (Figure 4.6), WÜ (Figure 4.7) and FR-Fon (Figure 4.8). The mean diurnal NEE cycles for the four seasons are shown Figure 4.9 (DE-Gri), Figure 4.10 (DE-Kli), Figure 4.11 (DE-Tha) and Figure 4.12 (DE-Hai).

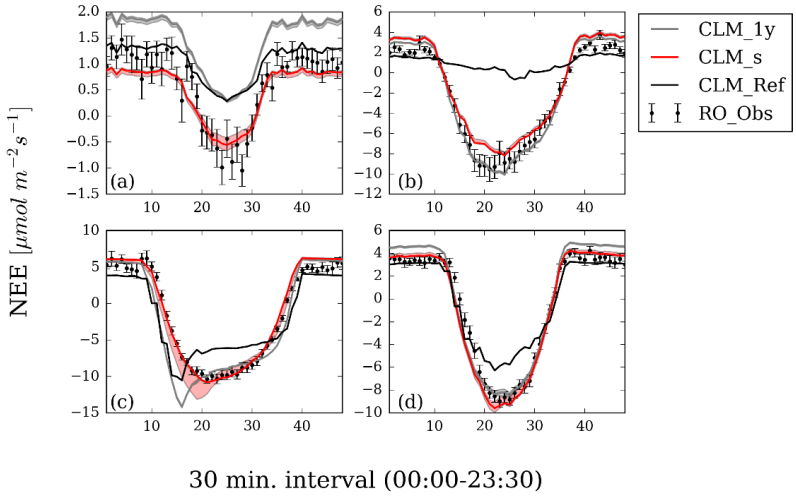

Figure 4.5: Daily course of (mean) NEE for winter '12/ '13 (a), spring 2013 (b), summer 2013 (c) and autumn 2013 (d) for the Rollesbroich site. Individual lines indicate observed NEE (RO_Obs), NEE simulated with CLM default parameters (CLM_Ref) and NEE simulated with MAPs determined for the one year parameter estimation period (CLM_1y) and for single seasons (CLM_s). The 95% confidence intervals are also plotted and were determined by sampling from DREAM posterior distributions.

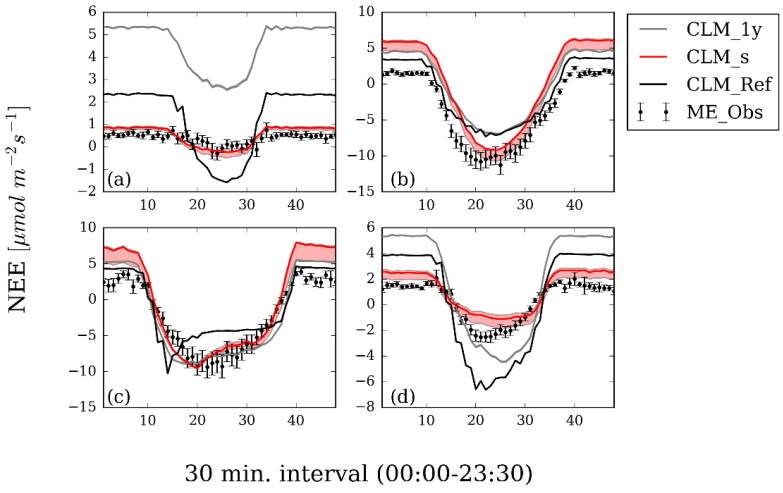

Figure 4.6: Daily course of (mean) NEE for winter '12/'13 (a), spring 2013 (b), summer 2013 (c) and autumn 2013 (d) for the Merzenhausen site. Shown are observed NEE with the EC method (ME_Obs), NEE simulated with CLM default parameters (CLM_Ref) and NEE simulated with MAPs determined for the one year parameter estimation period (CLM_1y) and for single seasons (CLM_s). The 95% confidence intervals are also plotted and were determined by sampling from DREAM posterior distributions.

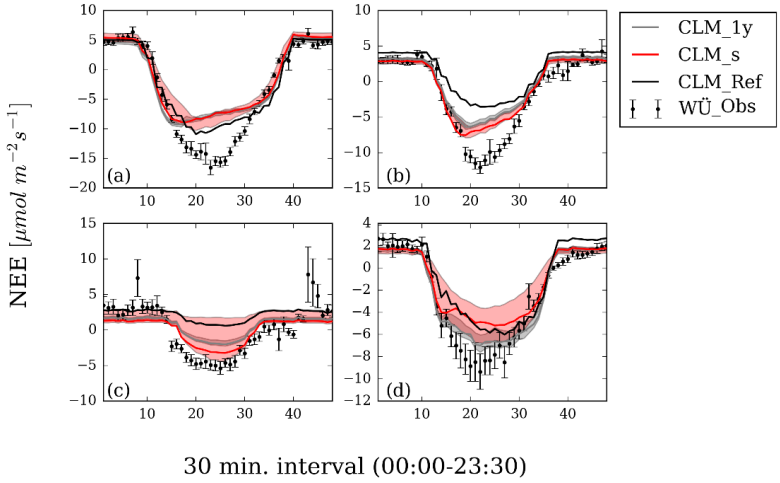

Figure 4.7: Daily course of (mean) NEE for summer 2012 (a), autumn 2012 (b), winter 2012/2013 (c) and spring 2013 (d). Individual lines indicate observed NEE for the Wüstebach site (WÜ_Obs), NEE simulated with CLM default parameters (CLM_Ref), NEE simulated with MAPs determined for the one year parameter estimation period (CLM_1y) and for single seasons (CLM_s). The 95% confidence intervals are also plotted and were determined by sampling from DREAM posterior distributions.

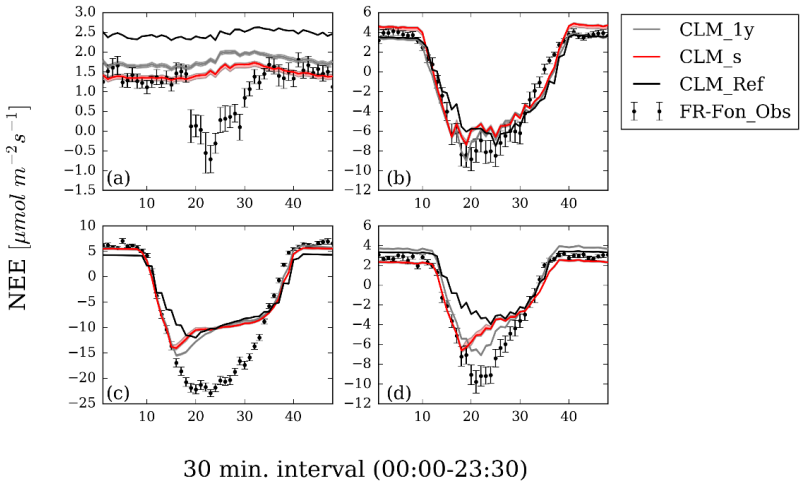

Figure 4.8: Daily course of (mean) NEE for winter ‘07/ ‘08 (a), spring 2008 (b), summer 2008 (c) and autumn 2008 (d) for the FR-Fon site. Individual lines indicate observed NEE (FR-Fon_Obs), NEE simulated with CLM default parameters (CLM_Ref) and NEE simulated with MAPs determined for the one year parameter estimation period (CLM_1y) and for single seasons (CLM_s). The 95% confidence intervals are also plotted and were determined by sampling from DREAM posterior distributions.

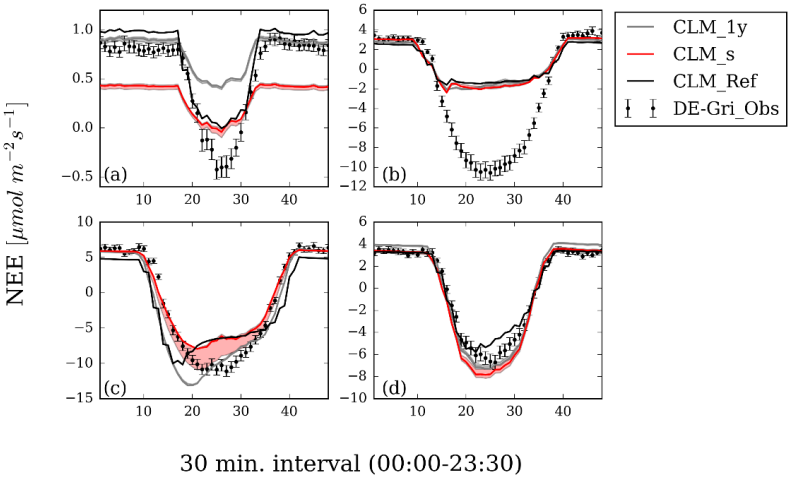

Figure 4.9: Daily course of (mean) NEE for winter '11/' 12 (a), spring 2012 (b), summer 2012 (c) and autumn 2012 (d) for the FLUXNET site DE-Gri. Shown are measurements with the EC method (DE-Gri_Obs), NEE simulated with CLM default parameters (CLM_Ref), NEE simulated with MAPs determined for the RO site (same PFT: C3-grass) for the one year parameter estimation period (CLM_1y) and for the single seasons (CLM_s). The 95% confidence intervals are also plotted and were determined by sampling from DREAM posterior distributions.

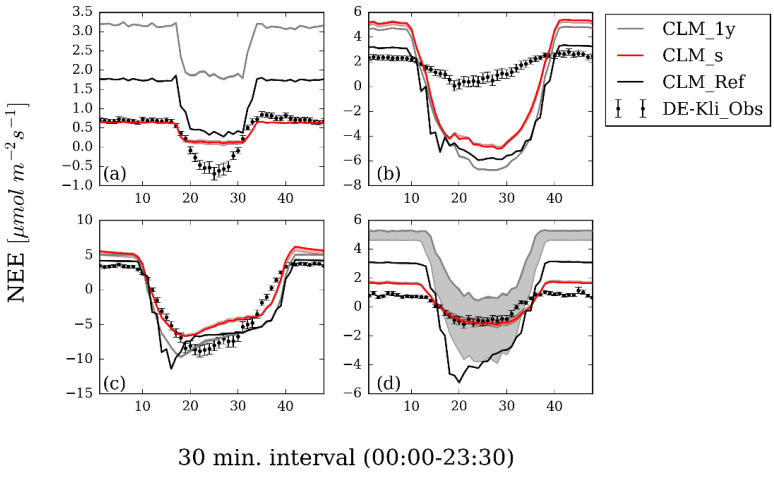

Figure 4.10: Daily course of (mean) NEE for winter '11/'12 (a), spring 2012 (b), summer 2012 (c) and autumn 2012 (d) for the FLUXNET site DE-Kli. Shown are observed NEE with the EC method (DE-Kli_Obs), NEE simulated with CLM default parameters (CLM_Ref), NEE simulated with MAPs determined for the ME site (same PFT: C3-crop) for the one year parameter estimation period (CLM_1y) and for the single seasons (CLM_s). The 95% confidence intervals are also plotted and were determined by sampling from DREAM posterior distributions.

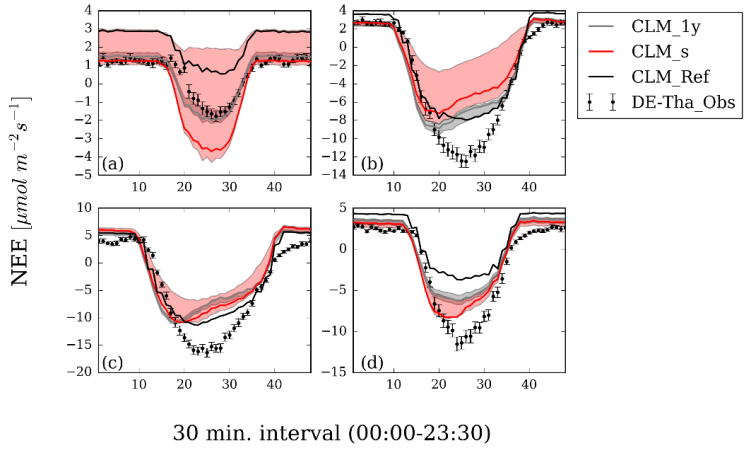

Figure 4.11: Daily course of (mean) NEE for winter '11/' 12 (a), spring 2012 (b), summer 2012 (c) and autumn 2012 (d) for the FLUXNET site DE-Tha. Shown are observed values with the EC method (DE-Tha_Obs), NEE simulated with CLM evaluation runs using default parameters (CLM_Ref), NEE simulated with MAPs determined for the WÜ site (same PFT: coniferous forest) for the one year parameter estimation period (CLM_1y) and for the single seasons (CLM_s). The 95% confidence intervals are also plotted and were determined by sampling from DREAM posterior distributions.

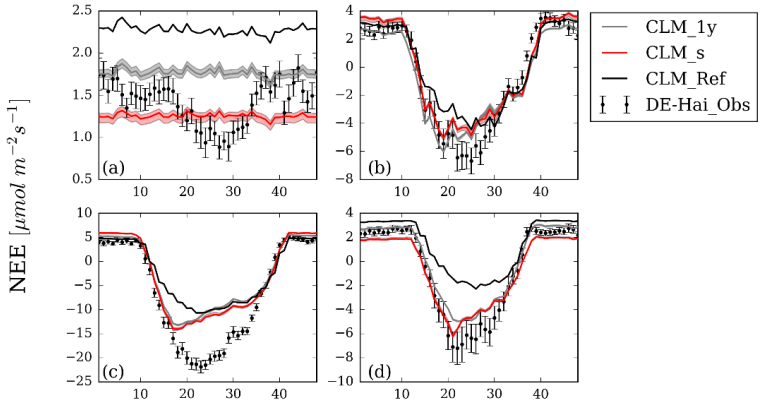

Figure 4.12: Daily course of (mean) NEE for winter '06/' 07 (a), spring 2007 (b), summer 2007 (c) and autumn 2007 (d) for the FLUXNET site DE-Hai. The lines shown are observed NEE the EC method (DE-Hai_Obs), NEE simulated with CLM evaluation runs using default parameters(CLM_Ref), NEE simulated with MAPs determined for the FR-Fon site (same PFT: deciduous forest) for the one year parameter estimation period (CLM_1y) and for the single seasons (CLM_s). The 95% confidence intervals are also plotted and were determined by sampling from DREAM posterior distributions.

As indicated by those plots, seasonal- and/or one-year based parameter estimates reduced the model-data mismatch in winter and at night for at least two of the four seasons. Thus, respiration is probably better represented with estimated parameter values than with CLM default parameter values, since the contribution of GPP to the total NEE signal at that time is low. Besides, estimated parameters reduced the overestimation of daytime NEE in spring (RO, ME, WÜ, FR-Fon, DE-Hai), summer (RO, ME, WÜ, DE-Gri, DE-Hai) and autumn (RO,WÜ, FR-Fon DE-Gri, DE-Tha, DE-Hai). At that time, the relative contribution of GPP to the total NEE signal is higher than the relative contribution of ER. Thus, the reduced NEE model-data mismatch in those cases mainly attribute to a reduced underestimation of carbon uptake, i.e. a higher GPP simulated with estimated parameters.

The mean diurnal NEE cycles were evaluated using MAD_{diur}. As shown in Table 4.6, seasonally determined MAP parameter sets (s-MAPs) improved the representation of the mean diurnal NEE course compared to the reference with CLM default parameters for all evaluation sites, and most of them substantially. In terms of the evaluation in time, the relative reduction of MAD_{diur} with s-MAPs, i.e. the improvement Δ_{MAP} in comparison to MAD_{diur}_Ref, was 16% for C3-crop to 66% for C3-grass. In terms of the evaluation in space, MAD_{diur} was reduced by 19% (C3-grass) to 35% (deciduous forest). For most sites, the diurnal cycles of the evaluation periods were better represented with s-MAPs than with 1y-MAPs. With 1y-MAPs, MAD_{diur} were reduced by 12% (DE-Tha) to 45% (RO) for all PFTs except C3-crop, indicating that the diurnal NEE cycles for those sites were in better correspondence with observations compared to default parameters.

Table 4.6: Mean absolute difference MAD_{diur} [µmol m^{-2} s^{-1}] for eight evaluation sites, averaged over all four seasons of the evaluation year.

PFT	site	val. years	MAD_{diur}_1y	MAD_{diur}_1y^{IS}	MAD_{diur}_s	MAD_{diur}_Ref
C3-grass	RO	'12/'13	1.05	1.56	0.64	1.91
	DE-Gri	'11/'12	1.46	-	1.36	1.67
C3-crop	ME	'12/'13	2.98	2.48	1.81	2.15
	DE-Kli	'11/'12	2.87	-	1.47	2.08
coniferous forest	WÜ	'12/'13	1.82	1.7	1.74	2.32
	DE-Tha	'11/'12	1.95	-	1.92	2.21
deciduous forest	FR-Fon	'07/'08	1.59	1.58	1.67	2.32
	DE-Hai	'06/'07	1.38	-	1.32	2.02

1y: CLM-evaluation runs for annual (1y)-MAPs; ^{IS}: with joint estimation of initial state factors; s: CLM-evaluation runs with seasonal (s)-MAPs; ref: calculated NEE with default parameters (reference).

As indicated by MAD_{ann}, also the annual NEE cycles were best represented by s-MAPs (Table 4.7). However, the differences between MAD_{ann}_1y and MAD_{ann}_s were minor for the sites

DE-Gri, DE-Tha, FR-Fon and DE-Hai. s-MAPs reduced MAD_{ann} by 6% (DE-Gri) to 49% (WÜ) compared to the reference run with default parameters. The improvement of the mean annual NEE cycle with 1y-MAPs was 21% (RO) to 40% (WÜ). For DE-Gri, ME and DE-Kli, MAD_{ann} was only reduced with s-MAPs, not with 1y-MAPs.

Table 4.7: Mean absolute NEE difference MAD_{ann} [µmol m^{-2} s^{-1}] for eight evaluation sites and the evaluation year.

PFT	site	val. years	MAD_{ann}_1y	MAD_{ann}_1y^{IS}	MAD_{ann}_s	MAD_{ann}_Ref
C3-grass	RO	'12/'13	1.04	1.61	0.77	1.31
	DE-Gri	'11/'12	1.17	-	1.10	1.17
C3-crop	ME	'12/'13	3.31	2.49	1.88	2.36
	DE-Kli	'11/'12	2.67	-	1.37	1.59
coniferous forest	WÜ	'12/'13	1.37	1.28	1.16	2.27
	DE-Tha	'11/'12	1.51	-	1.51	2.05
deciduous forest	FR-Fon	'07/'08	1.27	0.88	1.24	1.71
	DE-Hai	'06/'07	1.50	-	1.49	1.97

1y: CLM-evaluation runs for annual (1y)-MAPs; ^{IS}: with joint estimation of initial state factors; s: CLM-evaluation runs for seasonal (s)-MAPs; ref: calculated NEE with default parameters (reference).

Table 4.8 summarizes $RMSE_m$ and $RD_{\sum NEE}$ including the upper and lower 95% confidence intervals obtained from the posterior pdfs. $RD_{\sum NEE}$ was most substantially reduced for DE-Kli with s-MAPs. The observed ∑NEE for DE-Kli was ~82 gC m^{-2} y^{-1}. The modeled ∑NEE were -104 gC m^{-2} y^{-1} for CLM-Ref and 78-130 gC m^{-2} y^{-1} with season-based parameter estimates. For RO, $RD_{\sum NEE}$ was significantly reduced with 1y-MAPs and s-MAPs from 66% (CLM-Ref) to 5% and 17%. Also for DE-Gri, $RD_{\sum NEE}$ was significantly reduced with the one-year based estimates (by 19-25%), but not with the season-based estimates. For the forest PFTs, the indices differed only minor between 1y- and s-MAPs. The reduction of $RD_{\sum NEE}$ was 22% (WÜ) – 49% (DE-Hai) with s-MAPs and 23% (FR-Fon) – 38% (DE-Hai) with 1y-MAPs. However, for coniferous forest, the improved representation of ∑NEE was only significant with 1y-estimates due to the high uncertainty of the simulated NEE sum with season-based parameter estimates. This is also indicated by the simulated annual NEE sums (Figure 4.13) and the diurnal NEE cycles, which exhibit a higher spread with season-based parameter estimates, especially for WÜ and DE-Tha in winter and spring. In contrast to ∑NEE calculated for the model evaluation, the NEE time series used to calculate the annual NEE sums in Figure 4.13 were not filtered according to available observations.

Figure 4.13 illustrates the effect of the jointly estimated parameter values on the annual NEE sum of the evaluation period. For all forest evaluation sites, parameter estimates would result

in a strong increase of the carbon sink function. For forest, the ∑NEE calculated with estimated parameters was significantly more in correspondence with observations than ∑NEE calculated with global default parameters. This highlights the strong impact parameter estimates can have on predictions of climate-ecosystem feedbacks and simulated carbon pools.

Table 4.8: $RMSE_m$ and $RD_{\sum NEE}$ [%] for the evaluation year and on the basis of half hourly NEE data. Results are given for the evaluation sites RO, WÜ, ME and FR-Fon (left), and DE-Gri, DE-Tha, DE-Gri and DE-Hai (right)

		$RMSE_m$	$RD_{\sum NEE}$	$RD_{\sum NEElow}$	$RD_{\sum NEEup}$	$RMSE_m$	$RD_{\sum NEE}$	$RD_{\sum NEElow}$	$RD_{\sum NEEup}$
RO, DE-Gri	CLM-1y	4.7	5	4	40	4.7	80	79	86
	CLM-1y^{IS}	5.8	96	99	170	-	-	-	-
	CLM-s	4.5	17	24	52	4.6	121	69	133
	CLM-Ref	5.8	66	-	-	4.8	104	-	-
ME, DE-Kli	CLM-1y	6.0	122	122	122	5	320	124	320
	CLM-1y^{IS}	5.6	119	118	124	-	-	-	-
	CLM-s	5.7	99	58	101	3.9	39	4	59
	CLM-Ref	6.4	67	-	-	4.2	227	-	-
WÜ, DE-Tha	CLM-1y	6.1	51	49	54	5	61	53	67
	CLM-1y^{IS}	5.9	45	37	67	-	-	-	-
	CLM-s	6.1	53	44	91	4.9	54	39	128
	CLM-Ref	6.2	76	-	-	4.7	89	-	-
FR-Fon, DE-Hai	CLM-1y	5.0	70	69	70	4.1	56	55	57
	CLM-1y^{IS}	5.0	17	14	20	-	-	-	-
	CLM-s	5.2	66	62	71	4.0	45	42	51
	CLM-Ref	5.4	93	-	-	4.8	94	-	-

1y-MAPs, s-MAPs: Maximum a posteriori estimates determined based on the whole year time series (1y) and separately for the single seasons (s); ^{IS}: with joint estimation of initial state factors; ref.: reference run with CLM4.5 default parameters; $RD_{\sum NEElow}$, $RD_{\sum NEEup}$: upper and lower boundary of 95% confidence interval for Δsum

In terms of the jointly estimated parameters and initial state multiplication factors dCN and lCN, we found that 1y^{IS} estimates significantly improved the representation of simulated NEE ($RD_{\sum NEE}$, MAD_{ann}) for FR-Fon in comparison to the reference. For this site, CLM-1y^{IS} clearly outperformed the equivalent simulations without initial state estimates (CLM-1y) as well as the season-based estimates. Also for ME and WÜ, the model performance was slightly better for CLM-1y^{IS} in comparison to CLM-1y, but not significantly. For WÜ, the uncertainty of the predicted NEE sum increased considerably if initial states were jointly estimated with the eight parameters (Figure 4.13). 1y^{IS} estimates did not outperform the CLM default parameters for ME. For RO, CLM-1y clearly outperformed CLM-1y^{IS}.

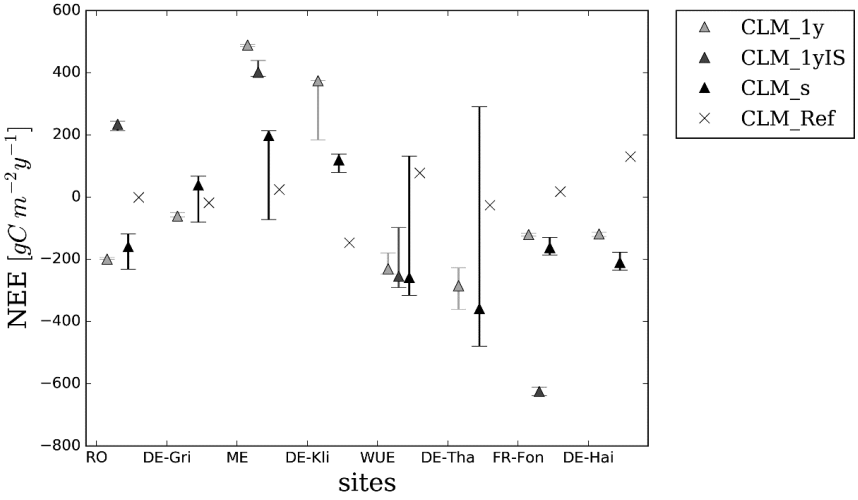

Figure 4.13: Annual NEE sum in the evaluation year simulated with CLM and parameters estimated for the one year period without and with two initial state factors (CLM_1y, CLM_1yIS) and separately for four different seasons (CLM_s), in comparison to the reference run with default parameters (CLM_Ref).

Overall, evaluation results indicate that parameter estimates for the forest PFTs were best transferable both in time and in space. 1y-based and seasonal parameter estimates performed similarly well for forest and also $1y^{IS}$ estimates considerably reduced the model-data mismatch in comparison to the reference. In this respect, parameters for the forest PFTs were found suitable to be estimated jointly with the initial CN pools, whereas this was not the case for C3-grass and C3-crop. For C3-crop, only season-based parameters provided NEE outputs that corresponded notably better with the observed data than the reference. For C3-grass, MAD_{diur}, MAD_{ann} and $RMSE_m$ were lower with s-MAPs than with 1y-MAPs, but ∑NEE was best represented with the 1y-based parameter estimates. For all PFTs, the uncertainty of the estimated parameters and the corresponding NEE model output was very low (and probably underestimated) for the 1y-based estimates and notably higher for the season-based parameter estimates.

4.4. DISCUSSION

4.4.1. Plausibility of estimated parameter values and possible impact on predicted climate-ecosystem feedbacks

Previous studies showed that ecological parameters like V_{cmax25}, mr_b and Q_{10} vary in time, which can be related to variations in environmental conditions such as mean annual temperature or soil moisture (Kätterer et al., 1998; Flanagan and Johnson, 2005; Mo et al., 2008; Reichstein et al., 2005). Our results support those findings. For all sites except WÜ, estimates of the eight CLM4.5 parameters varied notably among the four different seasons. For example, sla_{top} was highest in autumn and winter and lowest in spring and summer in case of ME. The specific leaf area varies with the development stage of the plant and decreases linear with life span, along with leaf nitrogen (e.g. Chapin III et al., 2002, p.111). In CLM, sla_{top} determines both V_{cmax25} (Eq.2.4) and LAI. Since winter wheat is seeded in early autumn and usually starts growing in this season, the direction of seasonal course of sla_{top} for ME is plausible. Our results are also in correspondence with Curiel Yuste et al., (2004), who found that Q_{10} is strongly influenced by the deciduousness of the vegetation and thus varies seasonally for mixed temperate forest.

Nevertheless, we do not assume that the actual estimated parameter values mimic "real" measurable parameter variations in all cases. For example, despite that fact that the rooting distribution (r_b) may change slightly throughout the year, the high degree of change as for C3-grass and C3-crop (RO and ME), is not considered reasonable. The strong seasonal variations of estimated r_b may be related to the fact that r_b is used to calculate the effective root fraction which determines the root water uptake (Oleson et al., 2013). The effective root fraction is not only dependent on the degree of stomata conductance, but also dependent on the matrix potential, the soil porosity and the water content in each soil layer. Thus, these parameters are closely linked to soil hydrology and differences in the uncertainty of r_b and ψ_c may be related to differences in soil moisture (e.g. higher sensitivity during dry conditions). We assume that in case of CLM4.5BGC, the seasonal variations of the estimated parameters were strongly related to (i) a dependency of the parameters on meteorological variables like temperature and model states such as soil moisture, and (ii) a dependency of those parameters on the initial model states as discussed below.

Since NEE includes GPP and ER, and ER is composed of heterotrophic and autotrophic respiration, compensation effects in terms of the estimated parameter values are likely. Therefore, the single carbon fluxes that contribute to NEE were not necessarily improved by

itself in all cases, even if the model-data mismatch for NEE was reduced. This is also linked to the finding that seasonal estimates outperformed 1y-based estimates. For example, during winter, the relative contribution of heterotrophic respiration to the NEE signal is higher than in summer, when NEE is much more determined by GPP. Therefore, parameters determining heterotrophic respiration like Q_{10} were better constrained in winter than parameters like sla_{top}, which mainly determine GPP and thus were better constrained in spring and summer.

We found that estimated parameters like Q_{10} were often close to the predefined minimum or maximum bounds of the parameter values ("edge-hitting parameters"). The finding is in correspondence with results by Braswell et al. (2005) who estimated SIPNET parameters with a MCMC method based on NEE data for the Harvard forest site. Also *Santaren et al.* (2007) revealed "edge-hitting" parameters when using a gradient-based model-data fusion approach to constrain ORCHIDEE parameters for a pine forest with EC data and state that this is an indicator for model-structural deficits. In correspondence with that, we assume the tendency of CLM parameters to be estimated towards their upper or lower bounds indicates that estimated parameters compensated for model errors such as missing key processes (e.g. senescence and management in case of winter wheat) or erroneous magnitudes of the initial carbon-nitrogen pools. Moreover, we emphasize that the estimated CLM parameters are not purely physical. Instead, they were e.g. developed based on empirical data obtained under specific conditions, like a temperature range of 20°C to 35°C in case of b_s (Ball et al., 1987), using e.g. (multi)linear regression analysis. Therefore, they underlay simplified concepts to represent plant physiology.

Despite the fact that the seasonal variations of parameter values are probably overestimated for most of the parameters, we found that estimated parameter values are often plausible and more in correspondence with literature values than the CLM default values. For example, different field studies provide common average Q_{10} values: Flanagan and Johnson (2005) e.g. showed that Q_{10} takes values of ~2 ± 0.8 for northern temperate grassland sites. Kätterer et al. (1998) summarized in a review Q_{10} values of ~2 ± 0.5 for different agricultural sites. Rey et al. (2008) found Q_{10} values between 2.5 and 3.3 for most of the investigated European broadleaf and deciduous forest sites, including DE-THA (~2.9) and DE-HAI (~2.6). They also highlight that Q_{10} also varies for different soil layers and respective soil properties. Season-based parameter estimates (autumn and winter only) and 1y-based parameter values are more in correspondence with these field-based estimates than the CLM default value of 1.5.

But how would an increased Q_{10} affect predicted carbon stocks and fluxes and climate-ecosystem feedbacks? CLM4.5 defines a reference temperature of 20°C for maintenance

respiration and 25°C for decomposition and heterotrophic respiration. If low Q_{10} values are applied and the actual temperature is below the reference temperature, respiration rates are higher and less sensitive towards temperature compared to high Q_{10} values. Above the reference temperature, respiration is more sensitive to temperature and overall higher with higher Q_{10} values (illustrated in Figure 4.14). In most parts of central Europe, temperatures below 20°C predominate throughout the year. This implies that respiration rates are mostly higher for lower Q_{10} values and less sensitive to temperature. The suggested increase of Q_{10} would thus have two major effects on the LSM carbon cycle: (i) Nutrients would be slower released and available to plants. Thus, along with decreased respiration rates, simulated GPP decreases, which was also indicated in a sensitivity analysis for Q_{10} (Figure 4.15). This has a compensating effect on the relative change of NEE. (ii) The predicted increase of land carbon stocks is considerably higher. This would have a particularly large impact if the higher Q_{10} is already applied in the model spin-up and may strongly affect predicted climate-ecosystem feedbacks.

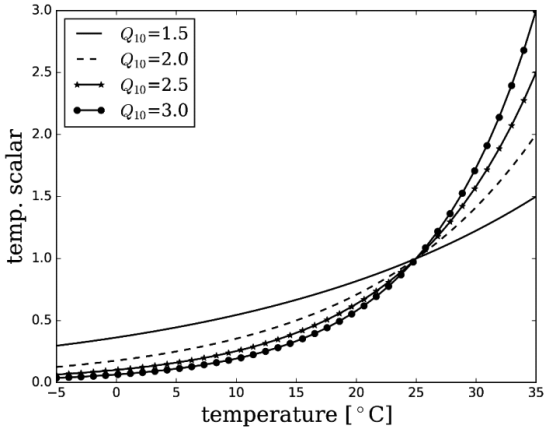

Figure 4.14: Temperature scalar for the calculation of heterotrophic respiration in CLM, for a reference Temperature of 25°C and different Q_{10} values.

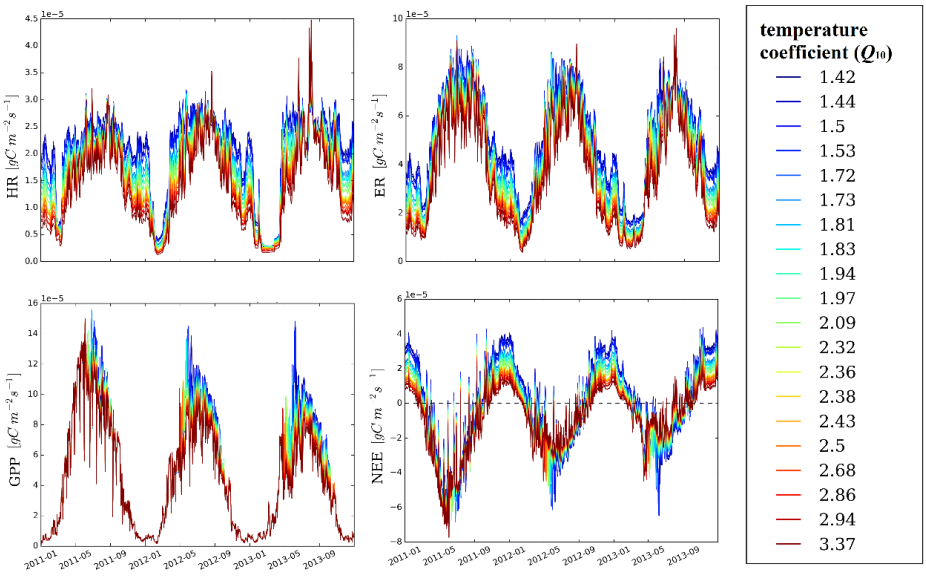

Figure 4.15: Sensitivity of CLM4.5BGC carbon flux simulation to the Q_{10} parameter for the coniferous forest site Wüstebach.

Among-parameter correlations changed when parameters were estimated jointly with the two initial state multiplication factors lCN and dCN (Figure 4.3 and Figure 4.4). This is related to the finding that some of the estimated parameter values differed significantly, depending on whether or not they were estimated jointly with lCN and dCN. For FR-Fon, the correlation of lCN and fl_{NR} (or sla_{top}) was low, but high for dCN. GPP is expected to be directly determined by the size of the living CN pools rather than the size of the dead CN pools. However, living and dead CN pools are strongly linked in CLM. For example, the biogeochemical cycling includes competition for nitrogen between plants and decomposers. Accordingly, an increase of the CN content in the dead pools results in a larger amount of nitrogen released during decomposition, which is then present to fulfill the nutrient demands of the plants. This is linked to the finding that not only ER but also GPP was highly sensitive to Q_{10} (Figure 4.15). In this regard, also Q_{10} correlated strongly with b_s, which mainly determines GPP. In case of ME, Q_{10} correlated with sla_{top} which again correlated very strongly with fl_{NR}. Both fl_{NR} and sla_{top} correlated very strongly with lCN. This highlights complex interactions among the estimated parameters and initial CN pools. The parameters fl_{NR} and sla_{top} determine V_{cmax25}. In CLM, V_{cmax25} is directly related to the LAI-based upscaling of leaf scale photosynthesis to ecosystem

scale GPP. This explains the correlation of fl_{NR}, sla_{top} and lCN. Thus, probably compensation effects occur between parameters and between parameters and the initial state factors.

The strong dependency of the estimated parameters on the initial carbon- and nitrogen pools highlights how critical the model spin-up is for the prediction of carbon fluxes. This is linked to the results by Carvalhais et al.(2008) showing that CASA model parameters such as radiation-use efficiency are strongly affected by model initial states and that relaxing the carbon cycle steady state assumption can improve parameter inversion and model performance. In general, the steady state assumption is very critical, particularly for crop sites such as ME that have been managed extensively for many centuries. Therefore, the initial states generated via the model spin-up do not represent the true state of the ecosystem, which is a well-known problem. More realistic initial states may be obtained from transient simulations, which considers the historical land cover change. However, often it is not possible to obtain the respective information and input data required to perform this kind of simulation adequately.

4.4.2. CLM performance with estimated parameters

By tendency, season-based parameter estimates outperformed one-year based parameter estimates. Mo et al., (2008) showed that considering seasonal variations of parameters such as b_s and V_{cmax25} during model-data fusion and modeling instead of assuming static parameters can enhance the final results. However, the number of degrees of freedom is multiplied by four in case of the seasonal parameter estimation and thus the comparability of performance of seasonal and one-year based parameters is somewhat limited. Nevertheless, since both seasonal and yearly parameter estimates were evaluated for an independent period, the evaluation approach used herein is considered appropriate. A more formal evaluation could be made on the basis of for example the Akaike information criterion (AIC).

The uncertainty of the estimated parameters and the corresponding spread of simulated NEE were higher for the season-based estimates compared to the 1y-based estimates. The latter probably underestimated parameter and model uncertainty. An underestimation may partly be related to the likelihood function used herein (Equation 2.11), which does not consider heteroscedastic measurement error and may have underestimated the measurement uncertainty. As shown in various studies (e.g. Post et al., 2015; Richardson et al., 2006), the measurement uncertainty of eddy covariance NEE data increases with the flux magnitude. In terms of the model uncertainty, a realistic estimate can only be obtained if additional sources of model uncertainty are taken into account, including initial states and atmospheric forcings.

For C3-crop, one-year based parameter estimates were not well transferable in time and in space. We think this is related to the fact that simulated NEE was already strongly flawed in the reference run for this PFT, particularly with respect to errors in the timing of simulated plant onset and offset. The deficits of various LSMs in representing plant phenology and inter-annual variations in carbon cycling have been highlighted in previous studies (Braswell et al., 2005; Keenan et al., 2012a; Richardson et al., 2012; Melaas et al., 2013) and can significantly alter the simulated annual net productivity (e.g. Hollinger et al., 2004; Richardson et al., 2009). We assume the major reasons for the deviations of simulated and measured NEE for C3-crop are (i) missing or poorly represented key processes including management and senescence, and (ii) initial conditions that do not represent the true state of the ecosystem for those sites. Senescence as observed at the ME site end of July was related to an abrupt shift from NEE overestimation to a strong NEE underestimation. Such a model-data discrepancy is impossible to correct or compensate with one-year based parameter estimates, but was obviously partly compensated by the season-based parameter estimates. On the other hand, the ME site is subject to management (seeding, fertilization, harvest, etc.), which in CLM4.5 was not implemented and validated yet for the PFT "winter wheat" or "winter temperate cereals". Accordingly, major drivers of the carbon cycle are missing. Besides, initial carbon-nitrogen pools are probably highly flawed, since the site has been managed since many centuries. Thus, the steady state is not true. A better process representation including site management is important before being able to successfully estimate robust parameters for C3-crops. This seems obvious, is however highlighted here, given that LSMs like CLM are commonly applied to simulate land surface fluxes on continental to global scales, using global default parameters defined for those very broad PFT-groups. However, crops are highly divers in terms of both species grown and management practices applied. Accordingly, previous studies showed that crop parameters are critical to transfer to other sites (Sus et al., 2013) or different resolutions (Iizumi et al., 2014).

Different studies outlined an intra-PFT variability of parameters, which can hinder parameter transferability to other sites (Groenendijk et al., 2011; Xiao et al., 2011; Kuppel et al., 2012). Parameters estimated for a single EC site cannot generally be transferred to other sites of the same group of PFTs, as the estimated parameters are sometimes overly tuned to site-specific conditions (Kuppel et al., 2012). Nevertheless, we showed that in most cases, parameter estimates significantly improved modeled NEE at the evaluation sites in more than 600 km distance to the parameter estimation sites. This indicates that transferability was given, although environmental conditions and plant-characteristics were presumably different at those sites. Also for the C3-crop evaluation site DE-Kli, season-based parameter estimates significantly

reduced the model-data mismatch. This is probably related to the fact that here also winter temperate cereals were grown. Accordingly, we assume that the transferability of LSM parameters strongly depends on the representativeness of one particular site, e.g. in terms of site management or plant species. Generalized statements in this respect are difficult. Results showed that also for C3-grass, parameter estimates did improve simulated NEE at evaluation site DE-Gri, but not as strongly and clearly as for the forest PFTs. Thus, the RO site is probably not representative for DE-Gri, which may be related to different environmental conditions and plant properties at both sites. The finding that parameter estimation was more successful for the forest sites compared to C3-crop and C3-grass is in correspondence with findings by Kuppel et al. (2014), who applied ORCHIDEE and a gradient-based data assimilation approach.

In case of RO, the notably better performance with both s-MAPs and 1y-MAPs compared to the reference was mainly related to the fact that simulated plant onset in spring was shifted ahead, and thus daytime NEE (GPP), was much less underestimated in this period. The finding that estimated parameters had an impact on the simulated plant onset is probably due to model internal links with variables or parameters in the stress-deciduous phenology scheme of CLM4.5, which determines the active growing season for C3-grasses and C3-crops. Estimated parameters affect not only the simulated carbon-nitrogen pools but also other states like soil moisture. This again can affect the simulated onset and/or offset.

4.5. CONCLUSIONS

In this work, eight sensitive parameters and two multiplication factors for the initial carbon- and nitrogen- pools of the Community Land Model v. 4.5 were estimated for four sites in Germany and France. Parameters were constrained with measured NEE-data using the Markov Chain Monte Carlo method DREAM$_{(zs)}$. Parameter estimates were evaluated for a subsequent year at the same sites, as well as for evaluation sites with corresponding PFTs, separated ~ 600 km from the estimation sites.

DREAM$_{(zs)}$-CLM parameter estimates successfully reduced NEE model-data discrepancies, e.g. in terms of obtaining more reliably estimates of annual NEE sums. By tendency, season-based parameter estimates outperformed parameters that were estimated based on the complete one-year set of NEE data. This suggests that taking into account seasonal variations of the estimated parameters can improve the representation of simulated NEE in CLM.

The validation of the estimated parameters was most successful for the forest PFTs, because the NEE model-data mismatch was substantially reduced for all sites, both with one-year and season-based estimates. We also showed that for coniferous forest, differences of the parameter values estimated with or without initial states were considerably lower compared to the other sites. We therefore conclude that CLM4.5 parameter estimates for evergreen needleleaf forest and broadleaf deciduous forest were best transferable and most reliable.

For C3-crop, parameter estimation was least successful. This is probably related to missing key processes and drivers like senescence and management, which caused major systematic model-data discrepancies. Nevertheless, we showed these discrepancies were partly compensated by season-based parameter estimates, which significantly improved simulated NEE also for the evaluation site. Accordingly, we assume that the evaluation sites were affected by similar errors in model structure and initial conditions as the parameter estimation sites.

This study revealed strong correlations between some of the estimated CLM4.5 parameters and the initial carbon-nitrogen pools. This elucidates a high level of model complexity and the challenge to estimate or optimize CLM parameters, which depend on the initial model states. This has major drawbacks in terms of transferring site-based parameter estimates to other sites or larger scales. Because complex land surface models like CLM include hundreds of parameters in order to simulate the coupled carbon-, nitrogen-, water- and energy- cycles, over-parameterization is a common problem in those models. In order to better constrain LSMs and eventually reduce among-parameter correlations, we consider an extension of measurements at EC-sites, including e.g. rooting depths and densities, leaf area indices and leaf C:N ratios at EC sites important.

Moreover, we conclude that goodness-of-fit indices like the RMSE by itself are not sufficient to evaluate the representation of modeled NEE. The model reproduction of the diurnal and annual NEE cycles deserves a critical evaluation as well.

Chapter 5: Upscaling of net carbon fluxes from the plot scale to the catchment scale: evaluation with NEE and LAI data

*adapted from: Post, H., Hendricks Franssen, H.-J., Han, X., Hoar, T., Baatz, R., Montzka, C., Schmidt, M., Vereecken, H., 2016. Upscaling of net carbon fluxes from the plot scale to the catchment scale: evaluation with NEE and LAI data (under review for Biogeosciences).

5.1. INTRODUCTION

Eddy covariance measurements of net ecosystem exchange (NEE) fluxes are limited to a relatively small area. Chen et al. (2012) showed that the 90% cumulative annual footprint area of 12 eddy covariance (EC) towers located at Canadian sites (with different land cover including grassland and forest) varied from about 1.1 km^2 to 5.0 km^2, and that the spatial representativeness of the EC flux measurements depends on the degree of the land surface heterogeneity (Chen et al., 2012). Due to the spatial heterogeneity of soil properties, vegetation, and fauna, and the temporal variability of the environmental drivers (e.g. meteorological conditions), biogeochemical fluxes are spatially and temporally highly variable and nonlinear (Chen et al., 2009; Stoy et al., 2009). Therefore, conventional interpolation methods are not suited to upscale EC carbon flux measurements to larger areas. The understanding of factors controlling this spatial and temporal variability of carbon fluxes like respiration is still very limited (Reichstein and Beer, 2008). Hence, obtaining spatial patterns of carbon stocks and fluxes is highly desired.

The two central approaches to obtain spatially distributed carbon flux estimates for larger areas are either (i) inverse atmospheric modeling approaches (Deng et al., 2007; Peters et al., 2007; Peylin et al., 2013; Chevallier et al., 2014), or (ii) the application of terrestrial ecosystem models or land surface models (LSMs) such as the Community Land Model CLM (Oleson et al., 2013). In case of inverse atmospheric modeling, atmospheric transport models are combined with observed atmospheric CO_2 concentrations, using data assimilation methods such as the Ensemble Kalman Filter (e.g. Peters et al., 2007; Tolk et al., 2011). Inverse atmospheric modeling mainly provides carbon flux estimates at continental or global scales and coarse spatial resolutions (Deng et al., 2007), as flux estimates at regional scales are highly biased

(Tolk et al., 2011; Chevallier et al., 2014). As highlighted in Turner et al., (2011) such "top-down" approaches are not suited to estimate small scale patterns of terrestrial carbon fluxes.

Commonly, LSMs are applied at global or continental scales (e.g. Stöckli et al., 2008; Bonan et al., 2011; Lawrence et al., 2012) with grid sizes of ~ 0.25°- 1.5°. With such a high degree of spatial aggregation, the error of both the model input and output can be very high. Moreover, a reliable calibration and validation of global LSMs is difficult, because observed data including soil carbon stocks and EC fluxes are only available for single locations. When applying a LSM for a small region or catchment with a high spatial resolution (e.g. 1 km^2, as in this study) the error of simulated fluxes is expected to be smaller due to the lower degree of spatial aggregation (Anderson et al., 2003). Besides, the land cover within a 1 km^2 grid cell more likely matches with the land cover at the eddy covariance site, which enables a grid-based evaluation of modeled NEE. A high spatial resolution can better represent the land surface heterogeneity and regional weather variability than a coarse spatial resolution. Thus, regional or catchment scale applications of LSMs allow for investigating spatial patterns of model states, biogeochemical fluxes and interactions with the regional climate and catchment hydrology. Accordingly, quantification of carbon fluxes at regional scales can enhance the understanding of CO_2 dynamics and their drivers (Desai et al., 2008). This has been shown in various studies e.g. for West Africa (Bonan et al., 2002; Li et al., 2007) and the Alaskan Arctic (Fisher et al., 2014). However, to our knowledge, studies like Xiao et al. (2011) who optimized a simple ecosystem model to upscale measured EC carbon fluxes to the regional scale do not exist yet for more complex LSMs like CLM. This is because (i) high resolution input data is often not available, (ii) the implementation of a new model set-up to a specific region is relatively time consuming, and (iii) careful parameter estimation is required to allow for meaningful predictions.

The Rur catchment in western Germany, subject of study in this paper, is expected to experience increased mean annual temperatures with a decrease of the number of freezing days in the future. Associated with climate change, vegetation periods are expected to start earlier and to prolong longer (Regionaler Klimaatlas Deutschland, 2015). In order to support the development of climate change mitigation and adaptation strategies and the decision making in land and water management, reliable carbon flux predictions with accurate uncertainty estimates are essential. However, LSM predictions of carbon, water and energy fluxes are still subject to a high degree of uncertainty due to (i) model structural deficits related to an imperfect and incomplete model representation of the biogeochemical processes (Todd-Brown et al., 2012; Foereid et al., 2014), (ii) poorly constrained model parameters (Abramowitz et al., 2008; Beven and Freer, 2001; Todd-Brown et al., 2013), (iii) errors in the representation of initial model

conditions generated via a spin-up (Carvalhais et al., 2010; Kuppel et al., 2012), as well as (iv) errors in both atmospheric and land surface input data. Some studies estimate the uncertainty of terrestrial carbon flux predictions based on an ensemble or comparisons of many different LSMs (e.g. Huntzinger et al., 2012; Piao et al., 2013; Fisher et al., 2014). Those studies highlight that (i) carbon flux predictions are generally highly uncertain, which also contributes to the uncertainty in climate change predictions, (ii) interactions of the different processes and drivers is not understood satisfactorily, and (iii) models require structural improvement to produce more consistent predictions. In order to improve LSM model structure and thus model-data and inter-model consistency, a more comprehensive understanding of model functionality and the contribution and link of the different model error sources is required. However, as highlighted by Xiao et al. (2014), the uncertainty of carbon fluxes obtained by ecosystem models has largely been overlooked, particularly in regional scale studies. The same is true for land surface models. To our knowledge, no study has been published yet, where the uncertainty of CLM carbon flux predictions has been comprehensively studied and estimated.

In this study, CLM version 4.5 in the biogeochemistry (BGC) mode (CLM4.5BGC) was used, which simulates the coupled terrestrial carbon, nitrogen, water and energy cycles, and prognostically predicts the leaf area index (LAI). The LAI determines photosynthesis and transpiration and is a key state variable for land surface-atmosphere exchange fluxes of water and carbon. It is also a major indicator for the model representation of plant phenology. A flawed representation of plant phenology in LSMs can cause large errors in carbon flux and carbon stock estimates (Baldocchi and Wilson, 2001; Richardson et al., 2012). Thus, a correct representation of the simulated LAI in terms of magnitude and timing is highly desirable.

Against this background, the first objective of this study was to test whether plant functional type (PFT)-specific parameters, estimated with the DiffeRential Evolution Adaptive Metropolis DREAM (Laloy and Vrugt, 2012; Ter Braak and Vrugt, 2008; Vrugt, 2016) can improve regional scale CLM4.5BGC predictions of both NEE and LAI. Therefore, five PFT-specific parameters were estimated separately for each of the four main PFTs in the Rur catchment, using single site eddy covariance NEE data, according to Chapter 4. The four PFTs were C3-grass, C3-crop, temperate evergreen needleleaf forest (short: coniferous forest) and temperate broadleaf deciduous forest (short: deciduous forest). We evaluated model performance using LAI data derived from remotely sensed RapidEye data and NEE data from seven grid cells of the catchment domain where EC towers were located. We assumed a positive evaluation indicates that parameter estimates improve NEE predictions for most grid cells in the Rur catchment that are dominated by those PFTs. The second main objective was to

comprehensively estimate the uncertainty of the simulated LAI and NEE, considering the uncertainty in initial model states and atmospheric forcings in addition to the parameter uncertainty.

5.2. MATERIALS AND METHODS

5.2.1. The Rur catchment

The Rur catchment (Figure 5.1) is located in the Belgian-Dutch-German border region and covers an area of 2354 km^2. It is characterized by two distinctly different areas of land use and climate. In the northern lowland part, precipitation amounts are lower (650-850 mm/a), and potential evapotranspiration is higher (580-600 mm/a) compared to the mountainous Eifel region in the south where annual precipitation is 850-1300 mm/a and potential evapotranspiration is 450-550 mm/a (Montzka et al., 2008a, 2008b). The annual mean temperature in the catchment ranges from about 7.5°C in the south of the catchment to about 10.3°C in the north (Baatz et al., 2014). The northern part is dominated by fertile loess soils and is intensely used for agriculture. Sugar beet and cereals (winter wheat, barley) are the most cultivated crops in the catchment (Figure 5.1). In the mountainous southern part shallow, less fertile soils predominate. It is mainly covered by meadows and forests. The Rur catchment is one of four central research regions of the TERENO project (Zacharias et al., 2011; Hohlfeld et al., 2012), which has the main goal to determine global change impacts across different terrestrial compartments at the regional level. Therefore, comprehensive input and evaluation data is available for the catchment, including information on land use (Lussem and Waldhoff, 2013), leaf area indices (Ali et al., 2015) and eddy covariance data (Schmidt et al., 2012; Graf et al., 2014; Post et al., 2015).

Eddy covariance (EC) data in the Rur catchment were measured at seven sites of different land use. Rollesbroich (RO) and Kall Sistig (KA) are extensively used grassland sites (Chapter 3.2) Perennial ryegrass (lolium perenne) and smooth meadow grass (poa pratensis) are main grass species grown in Rollesbroich (Korres et al., 2010). Wüstebach (Graf et al., 2014) is located in the Eifel national park and is largely covered by evergreen coniferous forest, particularly spruces. The crop sites Merzenhausen (ME), Niederzier (NZ), Selhausen (SEL), and Engelskirchen (EN) are located in the northern lowland region of the catchment.

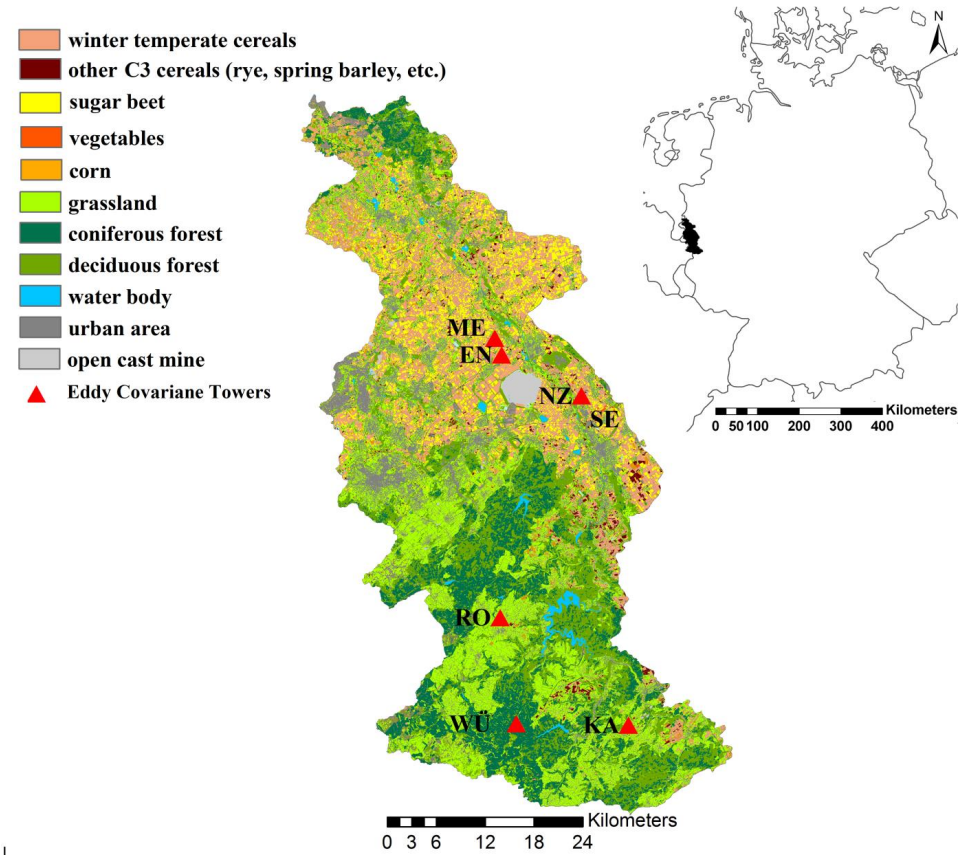

Figure 5.1: Land cover (Waldhoff, 2010) and eddy covariance tower sites in the Rur catchment.

5.2.1.1. Eddy covariance data

In ME and SE winter wheat was grown during the measurement period, in EN and NZ sugar beet. Four of the seven EC towers (RO, ME, SE and WÜ) were permanently installed. For those sites EC data were available for more than one year. EC data at the other sites (KA, EN and NZ) were measured by a roving station, which was installed two to three months at each of the three sites (Table 5.1).

The WÜ eddy covariance data were processed with the software ECpack (Dijk et al., 2004) using additional post-processing according to Graf et al. (2014). For the other sites, the complete processing of the raw data was performed with the TK3.1 software (Mauder and Foken, 2011), also using the quality flagging and uncertainty estimation scheme by Mauder et al., 2013 as outlined in Chapter 3.3.1 and Chapter 3.3.6 respectively. Accordingly, the instrumental noise σ_{cov}^{noise} and the stochastic error σ_{cov}^{stoch} determined according to Mauder et al. (2013) were added (in quadrature) to determine the uncertainty or random error of the NEE data. Only non-gap

filled data with quality flag 0 (high quality data) and 1 (moderate quality data) were included in this study.

Table 5.1: Eddy covariance tower sites in the Rur catchment.

EC site name	Latitude [°N]	Longitude [°E]	Altitude [m]	Land use	NEE time series for: Parameter estimation & *model evaluation	+tower
Rollesbroich (RO)	50.6219142	6.3041256	514.7	grassland	01.12.2011-30.11.2012 *01.12.2012-30.11.2013	Per.t
Kall-Sistig (KA)	50.5027500	6.5254170	498	grassland	*15.8.2012 - 14.10.2012	Rov.st.
Merzenhausen (ME)	50.9297879	6.2969924	93.3	agriculture	01.12.2011-30.11.2012 *01.12.2012-30.11.2013	Per.t
Selhausen (SE)	50.8658339	6.4473888	103.0	agriculture	*01.12.2012-30.11.2013	Per.t
Niederzier (NZ)	50.8795149	6.4498871	102.9	agriculture	*05.04.2013 - 10.07.2013	Rov.st.
Engelskirchen (EN)	50.9115426	6.3088546	108.9	agriculture	*18.8.2012 - 24.10.2012	Rov.st.
Wüstebach (WÜ)	50.5049024	6.3313825	606.9	oniferous forest	01.06.2011-31.05.2013 *01.06.2012-31.05.2013	Per.t

+ Per.t.: Permanent EC tower; Rov.st.: roving station

5.2.1.2. RapidEye-based leaf area index

RapidEye is a commercial satellite mission initiated by the RapidEye AG (Tyc et al., 2005) and consists of five identical satellites, which were launched in August 2008. RapidEye provides multi-spectral images of five spectral bands (blue, green, red, red edge and near infra-red). The nominal temporal resolution is daily. The ground sampling distance is 6.5 m and the pixel size is 5m for the orthorectified Level 3A data used here. The LAI data derived from satellite images are determined based on the NDVI (Normalized Difference Vegetation Index), which is related to the chlorophyll content in leaves. The NDVI is calculated based on the reflectances at near infra-red (NIR) and (RED). NDVI-based LAI data (LAI_{NDVI}) are affected by various error sources, which can result in a high uncertainty of the LAI estimate. The major error sources are summarized in Garrigues et al. (2008), such as (i) uncertainties in surface reflectance measurements resulting e.g. from calibration errors or cloud contamination, or (ii) deficiencies in the representation of canopy architecture in the algorithms applied for the LAI retrieval, e.g. the negligence of foliage clumping. This can lead to a high underestimation of actual LAI, especially for needleleaf forests (Chen et al., 1997). Clumping effects on landscape scale are also related to the fact that LAI algorithms have been calibrated at the plot scale, but are applied over larger heterogeneous pixels, which can induce substantial scaling biases on the LAI estimates (Garrigues et al., 2006). The latter error source is assumed relatively small for the LAI retrieval from RapidEye due to the high spatial resolution (5m) of the images. Studies on verification or uncertainty quantification of LAI data derived from satellite images are very rare

(Garrigues et al., 2008), but very important for land surface model applications. Ali et al. (2015) used orthorectified and radiometrically corrected Level 3A data (Blackbridge, 2015) to generate 5 m resolution LAI data for the Rur catchment, with the same methodology previously applied to MODIS data (e.g. Propastin and Erasmi, 2010). Those LAI data were validated for two crop sites (Merzenhausen and Selhausen) in the Rur catchment using in situ data measured with a destructive, ground-based method (Bréda, 2003) at several equally distributed points within the fields at six and eleven days during the growing season. The results indicate a high consistency between in situ measured LAI and LAI_{NDVI} derived from RapidEye (Ali et al., 2015). Because only the two crop sites were included in this evaluation approach, the LAI data for crop sites (winter wheat) are considered most reliable.

For this study, the LAI_{NDVI} data for the Rur catchment obtained according to Ali et al. (2015) were aggregated from the $5m^2$ to the $1km^2$ grid of the CLM Rur catchment domain by arithmetically averaging ($LAI_{RapidEye}$).

5.2.2. Community Land Model set-up

In this study, the Community Land Model (CLM) version 4.5 (Oleson et al., 2013) with the active biogeochemistry model (CLM4.5BGC) was used, which is described in Chapter 2.2. Accordingly, in the following CLM refers to CLM4.5BGC. To apply CLM for the Rur catchment domain, a land surface input dataset was generated with a spatial resolution of $1km^2$. The land unit for each grid cell and the PFT distribution of each vegetated land unit were defined based on the land use classification derived from supervised, multi-temporal remote sensing data analysis using RapidEye and ASTER data (Waldhoff et al., 2012; Lussem and Waldhoff, 2013). The percentage PFT coverage of the vegetated land in Rur catchment was ~34% C3-crops, ~32% grassland, ~17% broadleaf deciduous forest and ~14% coniferous forest. In addition to the land use coverage, CLM requires information on the percentage clay and sand content for each of the 15 soil columns of the vegetated area per grid cell. For each soil layer, the soil texture was defined based on the German soil map (BK50) provided by the Geological Survey NRW. Mean topographic slope, mean elevation and maximum fractional saturated area were determined for the 1 km^2 grid from a 10 m resolution digital elevation model (scilands GmbH, 2010). Additional land surface data required to run CLM4.5 such as soil color was adopted from the default CLM4.5 0.9° x 1.25° resolution global land surface data file of year 2000 (surfdata_0.9x1.25_simyr2000_c110921.nc).

The atmospheric forcing data used to run CLM consists of hourly time series of precipitation (mm/s), incoming short wave radiation (W m^{-2}), incoming long wave radiation (W m^{-2}),

atmospheric pressure (Pa), air temperature (K), specific humidity (kg/kg) and wind speed (mm/s) at the lowest atmospheric level. The data were obtained for the years 2008-2013 from the reanalysis COSMO_DE dataset provided by the German Weather Service (DWD) in 2.8 km^2 resolution (Baldauf et al., 2009). The COSMO_DE data were downscaled to 1 km^2 using natural neighbor interpolation based on Delaunay triangulation.

To generate the initial state variables such as the carbon and nitrogen pools, CLM was spun up over a period of 1200 years, using COSMO_DE data of the years 2008-2010. The model states obtained after the 1200-year spin-up were then used as input for a second three years "exit spin-up" (in normal, non spin-up mode) also using the meteorological data for the years 2008-2010.

5.2.3. Parameter estimation with DREAM for single sites of Rur catchment domain

In Chapter 4, eight CLM4.5BGC key ecological parameters were estimated with half-hourly NEE time series for four EC sites of different plant functional types. As shown in Figure 4.1, three of the four sites were located in the Rur catchment (RO: C_3-grass, ME: C_3-crop, WÜ: coniferous forest). The fourth temperate deciduous forest site Fontainebleau was located in France (FR-Fon) [48.4763 N, 2.7801 E]. The estimated parameters were validated with FLUXNET data from four other sites (DE-Hai, DE-Tha, DE-Kli, DE-Gri), which were located about 600 km away from the original parameter estimation sites. This evaluation indicated that parameter estimates are transferable to other years and sites.

Following this study, we used the adaptive Markov Chain Monte Carlo (MCMC) method $DREAM_{(zs)}$ (Chapter 2.3) to estimate five key PFT-specific parameters: (1) the fraction of leaf N in Rubisco enzyme (fl_{NR}), (2) the growth respiration factor (g_R), (3) the rooting distribution parameter [1 m^{-1}] (r_b), (4) the specific Leaf Area at top of canopy [m^2/gC] (sla_{top}), and (5) the soil water potential at full stomatal closure [mm] (ψ_c). All parameters converged completely after about 3000 iterations (WÜ) to 6000 iterations (RO). We used the same $DREAM_{(zs)}$ set-up and the same data as applied by in Chapter 4 for parameter estimation, but included only the five PFT-specific parameters, and not the three hard-wired parameters. The three hard-wired parameters Q_{10} (temperature coefficient), mr_b (base rate for maintenance respiration) and b_s (Ball-Berry slope of conductance-photosynthesis relationship) are also important key parameters in terms of NEE. However, they cannot be defined separately for each PFT without changes of the CLM source code structure. A PFT-specific definition of those parameters is possible for single site simulations with one PFT only, but not for a regional application with different PFTs in the model domain. Given correlations among the eight parameters estimated (Chapter 4), adopting only the subset of the five PFT-specific parameters from the previous

study was no option. Thus, new sets of parameters were estimated in this study. The three hard-wired parameters were set to Q_{10} = 2.5, mr_b = 3.5*10^{-6}, and b_s = 6.0, which was in better correspondence to the maximum a posteriori (MAP)-estimates determined in Chapter 4 for the one year period (Table 4.5), than the CLM default values (Q_{10} = 1.5, mr_b = 2.53*10^{-6}, and b_s = 9.0).

The one year NEE time series used for parameter estimation comprised twelve months between June 2011 and Nov. 2012, depending on the site and the respective data available (Table 5.1).

5.2.4. Perturbation of atmospheric input data

In order to take the uncertainty of the meteorological input data into account, a 60 member ensemble of perturbed meteorological forcings was generated for the years 2008-2012 using hourly COSMO-DE data. The approach used to generate the perturbation fields has previously been applied for studies on soil moisture data assimilation (Reichle et al., 2007, 2010; Kumar et al., 2012; Han et al., 2012, 2013, 2014). Perturbation fields were applied to air temperature [K], incoming long wave radiation [W/m^2], incoming short wave radiation [W/m^2] and precipitation [mm/s]. Normally distributed additive perturbations were applied to longwave radiation (LW) and air temperature (Temp). Log-normally distributed multiplicative perturbations were applied to precipitation (Prec) and shortwave radiation (SW). The parameters used for the perturbations were adapted from Han et al. (2014) and are listed in Table 5.2.

Table 5.2: Parameters applied for the perturbation of the meteorological input data, adapted from Han et al. (2014).

Variables [unit]	additive (A) or multiplicative (M)	Std. dev.	Cross correlation coefficients		
			T	SW	LW
Air temperature (T) [K]	A	1	-	0.4	0.4
Incoming shortwave radiation (SW) [W m^{-2}]	M	0.3	0.4	-	-0.5
Incoming longwave radiation (LW) [W m^{-2}]	A	20	0.4	-0.5	-
Precipitation (P) [mm/s]	M	0.5	0	-0.8	0.5

The perturbations for the different atmospheric variables (incoming short wave radiation, incoming long wave radiation, air temperature and precipitation) are cross-correlated in order to generate physically plausible perturbations of the atmospheric forcings. We considered spatial cross-correlation in addition to temporal correlation of the meteorological variables. The multiplicative perturbations are truncated by a defined maximum standard deviation of 2.5 (standard normal distribution), to remove outliers from the generated perturbation fields

(Reichle et al., 2007). The spatially-correlated noise is calculated first using the Fast Fourier Transform approach (Park and Xu, 2013) with a 10 km spatial correlation scale. Next, the temporally-correlated noise is added to the spatially-correlated noise. The temporal correlation for all perturbed variables is imposed using a first-order AR(1) autoregressive model (Reichle et al., 2007). The AR(1) temporal correlation coefficient for a time lag of one day was 0.368 for all variables.

5.2.5. Generation of perturbed initial state input files and the perturbed forward run for the Rur catchment

As shown in various studies, carbon fluxes predicted by land surface models strongly depend on the carbon-nitrogen pools generated during the model spin-up (Carvalhais et al., 2010; Kuppel et al., 2012). In order to take the uncertainty of initial states into account, a 60 member ensemble of perturbed initial states was generated. This was done via a 15 year spin-up using the perturbed atmospheric forcings for the years 2008-2010 and parameter values sampled randomly from the joint DREAM posterior pdfs. The initial conditions used at the beginning of the 15 year perturbed spin-up were the ones generated with the main spin-up (1200 years in spin-up mode, plus 3 years in normal mode) as described in Chapter 5.2.2.

5.2.6. Performance evaluation measures and uncertainty estimation

Three CLM cases were defined to evaluate the effect of the updated ecosystem parameters and to estimate the uncertainty of the model predictions: (i) The reference run (CLM-Ref): a single instance forward run for the years 2011-2013 with default parameters and the atmospheric input data and initial conditions as described in Chapter 5.2.2; (ii) a 60 instance forward run for the same time period and with the same initial conditions and atmospheric input data as CLM-Ref, but with parameters sampled randomly from the joint DREAM posterior pdfs (CLM-Ens$_P$); (iii) a 60 instance forward run for the same period with parameters sampled according to CLM-Ens$_P$, but applying both perturbed atmospheric forcings and perturbed initial states (CLM-Ens$_{PAI}$). The case CLM-Ens$_{PAI}$ was set up to estimate the overall uncertainty of simulated NEE and LAI given that the parameters as well as the atmospheric input data and the initial model states are uncertain. The case CLM-Ens$_P$ was defined to allow for a direct evaluation of the updated parameters in comparison to CLM-Ref with global default parameters.

5.2.6.1. Evaluation of NEE-based on eddy covariance data

The evaluation of NEE was conducted with time series of half-hourly NEE data measured at seven EC tower sites within the catchment (Table 5.1). First, it was verified that the PFT

coverage of one CLM grid cell coincided with the dominant PFT at the respective EC tower site. Each of the seven grid cells were covered more than 80% by the PFT of the respective EC tower site. This was considered sufficient to allow for a grid-based model evaluation. In the following, the subscript "gc" is used to refer to the grid cell, in which one of the EC towers is located, e.g. "RO_{gc}" to the respective grid cell of the RO site.

The length of the available NEE time series differed among the seven EC sites, ranging from two to twelve months (including data gaps). See Table 5.1. Accordingly, only the model output that coincides with the observed NEE data were used.

The calculated NEE output was evaluated based on the following indices:

(i) The root mean square error ($RMSE_m$):

$$\mathrm{RMSE_m} = \sqrt{\frac{1}{n}\sum_{i=1}^{n}(y_i - m_i)^2}, \tag{5.1}$$

with y = measured half-hourly NEE [µmol m^{-2} s^{-1}] at time step i for the given time series of length n, and m = modeled equivalent.

(ii) The mean absolute difference of the mean diurnal NEE cycle:

$$\mathrm{MAD_{diur}} = \frac{1}{48}\sum_{i=1}^{48}|y_i - m_i|, \tag{5.2}$$

with y = average measured NEE at a given time i during the day [µmol m^{-2} s^{-1}] and m= modeled equivalent. This performance measure is evaluated half-hourly and therefore 48 times per day.

(iii) The relative difference [%] of the NEE sum calculated for all half-hourly data available in the respective evaluation period:

$$\mathrm{RD_{\sum NEE}} = \left|\frac{\sum_{i=1}^{n}(m_i) - \sum_{i=1}^{n}(y_i)}{\sum_{i=1}^{n}(y_i)} \times 100\right|, \tag{5.3}$$

with y = measured NEE (non-gap filled), and m = modeled equivalent.

For the sites RO, ME, WÜ and SE, where a complete year of NEE data was available, the mean diurnal NEE cycle and the index $\mathrm{MAD_{diur}}$ were calculated separately for each of the four seasons within the evaluation year (winter: Dec.-Feb.; spring: Mar.-May; summer: Jun.-Aug.; autumn: Sept.-Nov.). The four seasonal indices were averaged to obtain the respective $\mathrm{MAD_{diur}}$ index for the entire evaluation year. For the other sites where only NEE data for ~ 2-3 months were available, the indices including $\mathrm{MAD_{diur}}$ were calculated for this shorter time series. All evaluation indices were determined both for CLM-Ref and for the ensemble mean of CLM-Ens_P.

In order to compare the ensemble spread of CLM-Ens$_P$ and CLM-Ens$_{PAI}$, the annual NEE sum NEE$_{sum}$ [gC m^{-2} y^{-1}] was calculated for each of the 60 ensemble members, both for CLM-Ens$_P$ and CLM-Ens$_{PAI}$. The complete half-hourly time series (without gaps) of modeled NEE data between the 1st of Dec. 2012 and the 30th of Nov. 2013 was used to calculate NEE$_{sum}$. Then, the standard deviation (STD) as well as the absolute difference (Diff$_{CI90}$) between the upper and the lower boundary of the 90% confidence interval (CI90$_{up}$, CI90$_{low}$) for the ensemble of NEE$_{sum}$ was calculated:

$$\mathrm{Diff}_{\mathrm{CI90}} = |\mathrm{CI90}_{\mathrm{up}} - \mathrm{CI90}_{\mathrm{low}}|. \tag{5.4}$$

5.2.6.2. Evaluation of LAI predictions

The effect of the parameter estimates on LAI was evaluated for the 1 km^2 grid of the Rur catchment domain. LAI data from RapidEye (LAI$_{RapidEye}$) of about 18 days (depending on the location) between the 1st of November 2011 and the 16th of September 2012 were used for the LAI evaluation. As LAI$_{RapidEye}$ data were available only for several days and not for all grid cells at all days, the simulated leaf area indices (both for CLM-Ens$_P$ and CLM-Ref) were subsetted according to the days and grid cells where RapidEye data were available. The LAI was evaluated (1) for the whole set of RapidEye data available for the Rur catchment domain (independent of the land cover in each grid cell), separately for the winter half year (1st Nov. 2011 – 30th Apr.2012) and the summer half year (1st May – 31st Oct. 2012), and (2) individually for each of the four main PFTs in the catchment, also separately for the winter and summer half year. To evaluate and compare modeled LAI for CLM-Ens$_P$ and CLM-Ref, the mean absolute difference between simulated LAI and measured LAI (MAD$_{LAI}$) was calculated:

$$\mathrm{MAD}_{\mathrm{LAI}} = \frac{1}{n_{\mathrm{days}} \cdot n_{\mathrm{gc}}} \sum_{i=1}^{n_{\mathrm{days}} \cdot n_{\mathrm{gc}}} |m_i - y_i| \tag{5.5}$$

with m = modeled daily LAI [m^2 m^{-2} day^{-1}] and y = measured equivalent, n_{days}= number of days, and n_{gc}= number of grid cells for which LAI$_{RapidEye}$ data were available at a particular day.

For the PFT-specific evaluation, MAD$_{LAI(PFT)}$ was calculated according to Equation 5.5, but this time including a substantially smaller number of grid cells (n_{pftgc}) that were covered by >80 % with one of the four main PFTs (coniferous forest, deciduous forest, C_3-grass or C_3-crop):

$$\mathrm{MAD}_{\mathrm{LAI(PFT)}} = \frac{1}{n_{\mathrm{days}} \cdot n_{\mathrm{pftgc}}} \sum_{i=1}^{n_{\mathrm{days}} \cdot n_{\mathrm{pftgc}}} |m_i - y_i|. \tag{5.6}$$

The MAD$_{LAI(PFT)}$was calculated separately for each of the four main PFTs in the Rur catchment.

For the respective data used in Equation 5.6, the mean LAI for each PFT was calculated by:

$$\mathrm{LAI_{PFT}} = \frac{1}{n_{\mathrm{days}} \cdot n_{\mathrm{pftgc}}} \sum_{i=1}^{n_{\mathrm{days}} \cdot n_{\mathrm{pftgc}}} \mathrm{LAI}_i \quad (5.7)$$

with n_{days}= number of days RapidEye data for a given PFT were available, and LAI_i= LAI observed or modeled at a particular day [$m^2\ m^{-2}\ day^{-1}$].

Each of the indices $\mathrm{MAD_{LAI}}$, $\mathrm{MAD_{LAI(PFT)}}$ and $\mathrm{LAI_{PFT}}$ were calculated for both, CLM-Ref, in the following indicated with the abbreviation "(Ref)", and the ensemble mean of CLM-Ens$_P$, in the following indicated with the abbreviation "(Ens)".

5.3. Results and Discussion

5.3.1. Parameter estimates

In this section, estimates of the five PFT-specific CLM parameters (Table 5.3) are summarized and compared to the corresponding parameter values estimated jointly with Q_{10}, mr_b and b_s in the previous study (Chapter 4, Table 4.5). The "new" parameter estimates for the C3-crop site ME (all parameters) differ significantly from the one-year based estimates of the previous study. For C3-grass (RO), only fl_{NR} and g_R differ significantly, sla_{top} is the same, and r_b and ψ_c have overlapping 95% confidence intervals. For deciduous forest (FR-Fon), fl_{NR}, sla_{top} and r_b differ significantly, whereas g_R values are identical. For coniferous forest (WÜ), the estimated parameter values are the same or very similar and did not differ significantly from the ones in Table 4.5.

Overall, differences of the herein estimated parameter values between RO and ME (Table 5.3) are considerably smaller than the differences shown in Table 4.5. For each of the five parameters, estimated values for RO were nearly identical to the corresponding MAP estimates for ME. We assume this is because (i) C3-grass and C3-crop calculations in CLM are governed by the same stress deciduous phenology scheme, and (ii) the grass species and crops grown at the sites RO and ME have similar PFT-specific properties e.g. in terms of plant height, LAI or rooting depth.

Table 5.3: Maximum a posteriori (MAP)-estimates of five plant functional type specific CLM parameters estimated with DREAM for the sites ME, RO, WÜ and FR-Fon.

case	year	fl_{NR}	sla_{top}	g_R	r_b	ψ_c
CLM default (C3-grass)		*0.18*	*0.030*	*0.30*	*3.00*	*-2.75E+05*
RO	11/'12	0.11	0.010	0.39	1.00	-3.93E+05
		0.11	0.010	0.40	1.15	-1.54E+05
		0.11*	0.010*	0.40*	1.10*	-3.47E+05*
CLM default (C3-crop)		*0.14*	*0.030*	*0.30*	*2.00*	*-2.76E+05*
ME	11/'12	0.09	0.010	0.40	1.01	-3.94E+05
		0.10	0.010	0.40	1.04	-2.62E+05
		0.10*	0.010*	0.40*	1.01	-3.89E+05*
CLM default (coniferous forest)		*0.05*	*0.010*	*0.30*	*2.00*	*-2.55E+05*
WÜ	11/'12	0.04	0.005	0.32	0.90	-2.02E+05
		0.05	0.007	0.40	3.90	-3.94E+05
		0.05*	0.005*	0.39*	3.50*	-2.04E+05*
CLM default (deciduous forest)		*0.10*	*0.030*	*0.30*	*2.00*	*-2.24E+05*
FR-Fon	06/'07	0.20	0.026	0.39	1.44	-3.48E+05
		0.22	0.030	0.40	3.00	-2.50E+05
		0.21*	0.027*	0.40*	2.30*	-2.51E+05*

*: MAP estimates, including lower bound (upper value) and upper bound (middle value) of the 95% confidence interval.

5.3.2. NEE - evaluation of parameter estimates and uncertainty

For most sites, estimated parameters improved the consistency between modeled and measured data in comparison with the CLM reference run with global default parameters (Table 5.4). For five of seven sites (RO, ME, SE, NZ and WÜ), at least two of the three evaluation indices (MAD_{diur}, RMSEm, $RD_{\sum NEE}$) were improved for CLM-Ens_P compared with CLM-Ref. In case of NZ, EN and KA, the different evaluation indices were contradictory. For all sites, either MAD_{diur} or $RMSE_m$ or both were lower for CLM-Ens_P than for CLM-Ref. For ME_{gc} and SE_{gc}, MAD_{diur} and $RMSE_m$ were between 7.7% and 36.6% lower for the ensemble mean of CLM-Ens_P than for CLM-Ref. In case of $WÜ_{gc}$, MAD_{diur} was 17.7% lower and $RMSE_m$ 2.9% lower for CLM-Ens_P compared to CLM-Ref. For RO_{gc}, MAD_{diur} improved by 7.9 % and $RMSE_m$ by 0.6%, again comparing the same model runs. For EN_{gc} and KA_{gc}, $RMSE_m$ was reduced by 0.4% and 3.8% with parameter estimates, but MAD_{diur} was 7.4% and 12.3% higher. For the NZ_{gc}, MAD_{diur} was 28.7% lower with updated parameters, but $RMSE_m$ was 14% higher.

The measured NEE sum over the whole evaluation period was negative for each of the seven EC sites and for all of the respective model outputs. This would indicate that all sites were net carbon sinks during the evaluation period. However, because data gaps were included in the NEE time series and because more EC data were available for summer and daytime than for winter and nighttime, those values do not represent the true NEE sum of the evaluation period.

The measured NEE sums were -806 gC m^{-2} (SE) to -87 gC m^{-2} (KA). The corresponding NEE sums for CLM-Ref were -85 gC m^{-2} (WÜ) to -3 gC m^{-2} (NZ), indicating that overall CLM-Ref underestimated GPP and/or overestimated ER for all PFTs. For the ensemble mean of CLM-Ens$_P$, the corresponding NEE sums were -362 gC m^{-2} for ME to -26 gC m^{-2} for RO, indicating that by tendency GPP was less underestimated and/or ER less overestimated compared to CLM-Ref.

Table 5.4: Root mean square error $RMSE_m$ [µmol m^{-2} s^{-1}], mean absolute difference for the mean diurnal NEE cycle MAD_{diur} [µmol m^{-2} s^{-1}], and relative difference of the NEE sum over the evaluation period $RD_{\sum NEE}$ [%] for the CLM ensemble with estimated parameters (Ens$_P$) in comparison to the reference run (Ref) with default parameters.

grid cells	*n*	MAD_{diur} [µmol m^{-2} s^{-1}]		$RMSE_m$ [µmol m^{-2} s^{-1}]		$RD_{\sum NEE}$ [%]	
		Ens$_P$	Ref	Ens$_P$	Ref	Ens$_P$	Ref
RO	*9687*	1.65	1.80	5.72	5.75	92	92
KA	*1728*	1.28	1.14	5.15	5.36	19	12
ME	*10157*	1.46	2.30	6.02	6.74	5	79
SE	*9597*	3.19	3.45	8.27	9.41	80	94
NZ	*2772*	2.58	3.61	10.68	9.37	34	99
EN	*2272*	4.87	4.53	8.89	8.93	87	82
WÜ	*7621*	2.30	2.79	6.73	6.93	60	82

The relative difference of the observed and modeled NEE sum ($RD_{\sum NEE}$, Equation 3.5) was very high (>79%) in case of CLM-Ref for each of the seven sites except KA (Table 5.4). With estimated parameters, i.e. for the ensemble mean of CLM-Ens$_P$, $RD_{\sum NEE}$ was reduced by 14% (SE) to 73% (ME). For the sites NZ and KA on the contrary, $RD_{\sum NEE}$ was slightly (5-7%) lower for CLM-Ref than for CLM-Ens$_P$. On average, $RD_{\sum NEE}$ reduced by 23% with estimated parameters. Accordingly, the estimated parameters are assumed to provide more reliable estimates of the annual NEE sum for the Rur catchment han CLM-Ref with default parameters. Parameters estimated for FR-Fon could not be explicitly evaluated for NEE in this study, because no broadleaf deciduous forest EC tower site was available within the catchment. However, Table 4.8 in Chapter 4.3.3 showed that with DREAM-CLM parameters estimated for FR-Fon, $RD_{\sum NEE}$ decreased by 38% for the evaluation site DE-Hai in 630 km distance to FR-Fon, indicating that transferability of those parameters over larger distances are given. Thus, the new parameter estimates for FR-Fon are assumed to provide more reliable estimates of the annual NEE sum for broadleaf deciduous forests in the catchment than global default parameters. Figure 5.2 illustrates the effect the estimated parameters had on the annual NEE sum [gC m^{-2} y^{-1}] (Dec.2012 – Nov.2013) determined with CLM for the Rur catchment, in this

case for complete time series without data gaps. With global default parameters, NEE was positive for most of the grid cells, particular in the northern part of the catchment, which is predominated by agriculture. In terms of NEE, the catchment would then be a clear net CO_2 source during this period. With estimated parameters, NEE sum [gC m^{-2} y^{-1}] became negative for most grid cells in the catchment, including a large part of the northern lowland area. In terms of NEE, the catchment would then be a net CO_2 sink, disregarding CO_2 fluxes due to harvesting, land use change and anthropogenic CO_2 emissions like fossil fuel combustion. As shown in Figure 5.2, both GPP and ER increased with estimated parameters. GPP increased more than ER such that the NEE sum was lower for CLM-Ens$_P$ than for CLM-Ref.Overall, the evaluation indices suggested that modeled NEE was clearly improved with estimated parameters for RO_{gc}, ME_{gc}, $WÜ_{gc}$ and SE_{gc}. However, for KA_{gc}, NZ_{gc} and EN_{gc} the improvement of modeled NEE was less distinct. For the roving station sites NZ, KA and EN, NEE time series of only 2-3 months were available for evaluation in contrast to the other sites, where time series of a whole year were available. Accordingly, evaluation results are not directly comparable between those sites. Chapter 4.3.3 showed that the evaluation runs with parameter estimates had a strongly varying performance over the year. Thus, if a complete year of NEE data had been available for evaluation of the roving station sites, evaluation indices for those sites would be informative.

Results indicate that the RO site might not be very representative for other grassland sites. Besides, the transfer of parameters estimated for the winter wheat site ME to C3-crop sites where very different crop types are grown is critical. At the SE site, also winter wheat was grown during the evaluation period like in ME. Here, parameter estimates clearly improved the model performance in terms of NEE. In EN and in NZ, sugar beet was cultivated during the evaluation period. For those sites, the evaluation was less successful. Sugar beets have considerably different plant characteristics and are managed differently than winter wheat, and therefore a limited transferability of PFT-specific parameter estimates is likely. Several studies emphasized already that LSM parameters can vary within one group of PFT such that the transfer from single site estimates to other sites with the same PFT is not trivial (Groenendijk et al., 2011; Xiao et al., 2011).

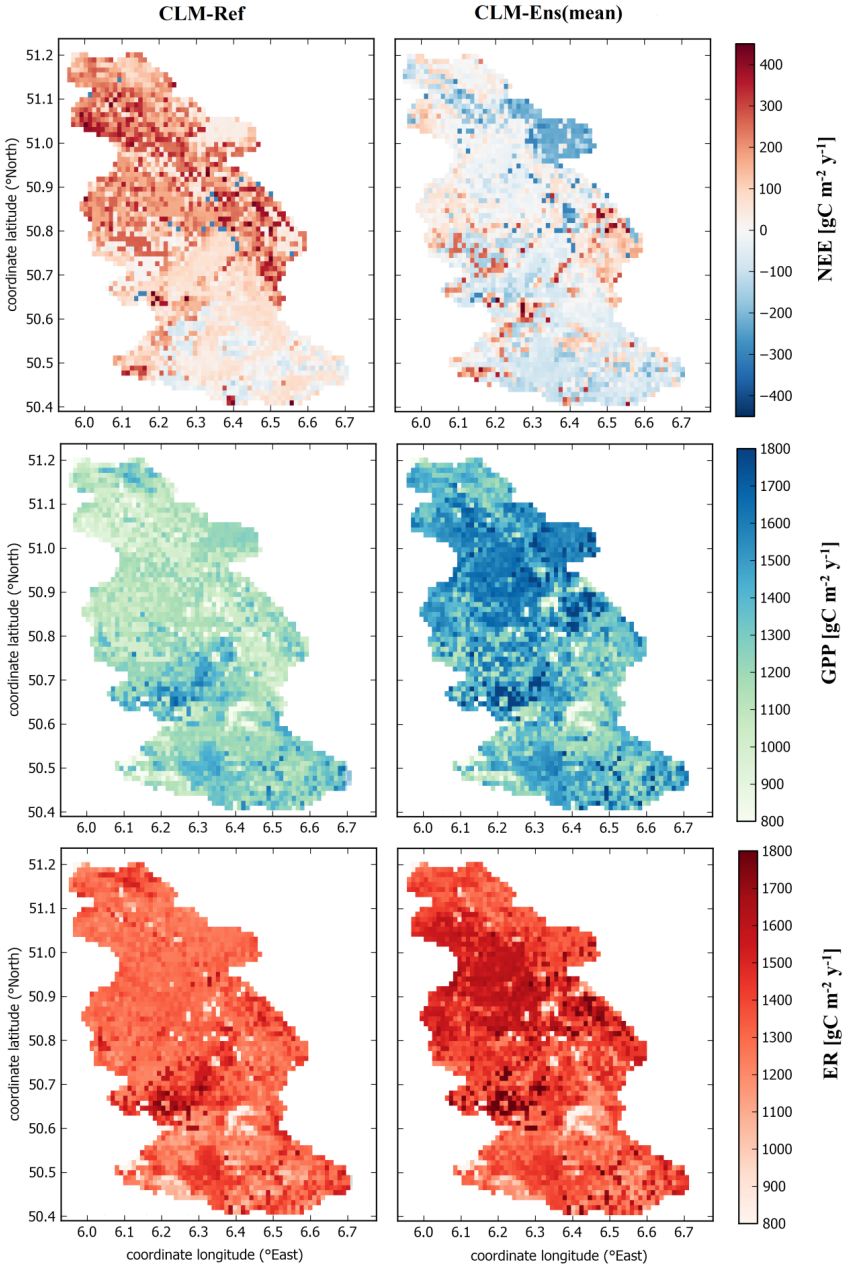

Figure 5.2: Annual sum of net ecosystem exchange (NEE), gross primary production (GPP) and ecosystem respiration (ER) determined with CLM4.5BGC for the Rur catchment (Dec.2012-Nov.2013) with default parameters (CLM-Ref.) and with estimated parameters (CLM-Ens).

5.3.3. LAI - evaluation of parameter estimates and uncertainty

The evaluation indices MAD_{LAI} (Equation 5.5) calculated for the complete set of RapidEye data (independent of the land cover within each grid cell) indicated that $LAI_{RapidEye}$ was considerably more in correspondence with LAI(Ens) than with LAI(Ref). In the winter half year MAD_{LAI}(Ref) was 1.76 and MAD_{LAI}(Ens) was 0.88. In the summer half year MAD_{LAI}(Ref) was 2.12 and MAD_{LAI}(Ens) was 1.42. This highlights that the parameter estimates obtained from DREAM based on eddy covariance NEE data reduced the mean absolute difference of LAI data (observed versus modeled) by 50% in winter and by 33% in summer.

Table 5.5 summarizes the PFT-specific $MAD_{LAI(PFT)}$ indices (Equation 5.6) and the corresponding mean LAI values LAI_{PFT} (Equation 5.7) obtained from CLM or RapidEye, indicating that the reliability of modeled LAI data differed strongly among the different PFTs and depending on the time of year (winter half year or summer half year). CLM-Ref overestimated the LAI for all PFTs and both half year periods by 30%-76% compared to $LAI_{RapidEye}$, except for deciduous forest in winter, where LAI_{PFT}(Obs) was 30% higher than LAI_{PFT}(Ref).

Table 5.5: Mean leaf area indices (LAI_{PFT}), determined for the RapidEye data (Obs), the CLM ensemble with estimated parameters (Ens) and the CLM reference run (Ref) with default parameters, and the mean absolute difference ($MAD_{LAI(PFT)}$), for the respective grid cells and days.

Plant functional types (PFTs)		LAI_{PFT}(Obs)	LAI_{PFT}(Ens)	LAI_{PFT}(Ref)	MAD_{LAI}(Ens)	MAD_{LAI}(Ref)
C3-grass	w	1.5	1.1	2.9	1.0	2.4
C3-grass	S	3.6	2.2	5.4	1.7	2.1
C3-crop	w	1.3	0.9	3.3	0.7	2.2
C3-crop	S	2.6	1.7	5.5	1.1	2.9
coniferous forest	w	1.3	4.0	5.3	2.7	4.0
coniferous forest	S	2.8	4.8	6.2	2.0	3.4
deciduous forest	w	1.1	0.5	0.8	0.6	0.5
deciduous forest	S	4.3	6.5	6.4	2.6	2.5
average over all PFTs and time					1.1	2.4

*w: winter half year (Nov.-Apr.), s: summer half year (May-Oct.)

The parameter estimates notably improved the consistency of modeled and observed LAI data for all PFTs except broadleaf deciduous trees. For C3-crop and C3-grass, $MAD_{LAI(PFT)}$(Ens) was more than 60% lower compared to $MAD_{LAI(PFT)}$(Ref) for the winter half year. In summer, $MAD_{LAI(PFT)}$ was reduced by 67% for C3-crop and by 17% for C3-grass with estimated parameters. The LAI for C3-grass and C3-crop were underestimated by Ens, compared to the measurements, by 24-39%, both in winter and in summer. For coniferous forest, $MAD_{LAI(PFT)}$ was reduced by a factor of 1.5 in winter and by a factor of 1.7 in summer with estimated

parameters. In case of deciduous forest, $MAD_{LAI(PFT)}$(Ens) was slightly (0.1) higher than $MAD_{LAI(PFT)}$(Ref), both in the winter half year and the summer half year.

$LAI_{RapidEye}$ was very low for the forest sites, and most probably underestimated the true LAI in summer, and, in case of coniferous forest, probably also in winter. Usually coniferous forests like those in the Rur catchment dominated by spruces have LAI values of about 5.5 (Asner et al., 2003). It is well known that LAI derived from remotely sensed images such as MODIS or RapidEye data is often highly underestimated for forest (e.g. Chen et al., 1997). Therefore, the LAI values and the evaluation indices in Table 5.5 are suspect for the forest PFTs. The observed $LAI_{RapidEye}$ data for C3-crop and C3-grass (summer half year) were lower than expected for the main growing season of those PFTs. This supports findings by Ali et al. (2015) showing that LAI from RapidEye underestimates the in situ measured LAI in the growing season. However, Ali et al. (2015) compared the LAI data on a daily basis. Here $LAI_{RapidEye}$ was averaged over the complete summer half year. Between beginning of Mai 2011 and end of October 2012 for example, the in situ measured LAI in Selhausen varied between 0 and ~4.5 (Ali et al., 2015) indicating that the half year average LAI_{PFT}(Obs) values in Table 5.5 are reasonable for C3-crop. Because C3-grass is usually not (completely) harvested in this region, it is also reasonable that observed LAI_{PFT} in the summer is higher than for C3-crop.

The close link between simulated LAI and NEE has already been reported in previous studies (e.g. Keenan et al., 2012). Chapter 4.3.2 showed that in CLM the parameters fl_{NR} and sla_{top} correlate with the carbon-nitrogen pools and LAI, particularly for C3-grass and C3-crop. This is related to the fact that in CLM both LAI and NEE are strongly determined by the maximum rate of carboxylation at 25 °C, V_{cmax25} [µmol m^{-2} s^{-1}] (Equation 2.4), which is calculated based on sla_{top} and fl_{NR}. This explains why the DREAM-estimates of the five PFT-specific parameters strongly affected and improved the predicted LAI.

5.3.4. Uncertainty of simulated NEE and LAI

In this section, the uncertainties of NEE and LAI simulated by CLM-Ens_P or CLM-Ens_{PAI} are discussed and compared. An indicator for this uncertainty is the ensemble spread, which in case of NEE was quantified with the standard deviation (STD) and $Diff_{CI90}$ (Equation 5.4) of the annual NEE sum (NEE_{sum}) of the 60 ensemble members.

The mean diurnal NEE cycles simulated by CLM-Ens_P and CLM-Ens_{PAI} for RO_{gc}, ME_{gc}, SE_{gc} and $WÜ_{gc}$ are shown in Figure 5.3 – Figure 5.6. For C3-crop, the mean indicates that with estimated parameters, ecosystem respiration (ER) was considerably less overestimated in

winter, given that the NEE signal at that time is mainly determined by ER. On the other hand, GPP was considerably less underestimated in spring (daytime) compared to CLM-Ref (Figure 5.4, Figure 5.5), given that relative contribution of GPP to the NEE signal at that time is higher than the relative contribution of ER. The spread of CLM-Ens$_P$ was very low for all sites, indicating that the uncertainty of simulated NEE resulting from parameter uncertainty was minor. This is however also related to the fact that parameters were already conditioned to NEE data, which reduced the parameter uncertainty. For all C3-grass and C3-crop sites and for all seasons, the ensemble spread of CLM-Ens$_{PAI}$ was considerably larger compered to CLM-Ens$_P$. The high NEE uncertainty for CLM-Ens$_{PAI}$ is also indicated by Diff$_{CI90}$ of the annual NEE sum (Table 5.6). For CLM-Ens$_{PAI}$, Diff$_{CI90}$ spans a wide range from 9.5 gC m^{-2} y^{-1} (WÜ$_{gc}$) to 718.0 gC m^{-2} y^{-1} (SE$_{gc}$). In contrast, for CLM-Ens$_P$, Diff$_{CI90}$ varied only between 0.5 gC m^{-2} y^{-1} (RO) and 10.5 gC m^{-2} y^{-1} (NZ). The standard deviation of NEE$_{sum}$ was smallest for WÜ$_{gc}$ (3.1 gC m^{-2} y^{-1}) and highest for SE$_{gc}$ in case of CLM-Ens$_{PAI}$, and notably lower in case of CLM-Ens$_P$ (0.1 – 3.4 gC m^{-2} y^{-1}). For WÜ$_{gc}$ (coniferous forest), Diff$_{CI90}$ and STD of CLM-Ens$_{PAI}$ were smallest and did not differ much from CLM-Ens$_P$. Accordingly, the ensemble spread of the mean diurnal NEE cycle for WÜ$_{gc}$ (Figure 5.6) did not differ considerably from CLM-Ens$_P$.

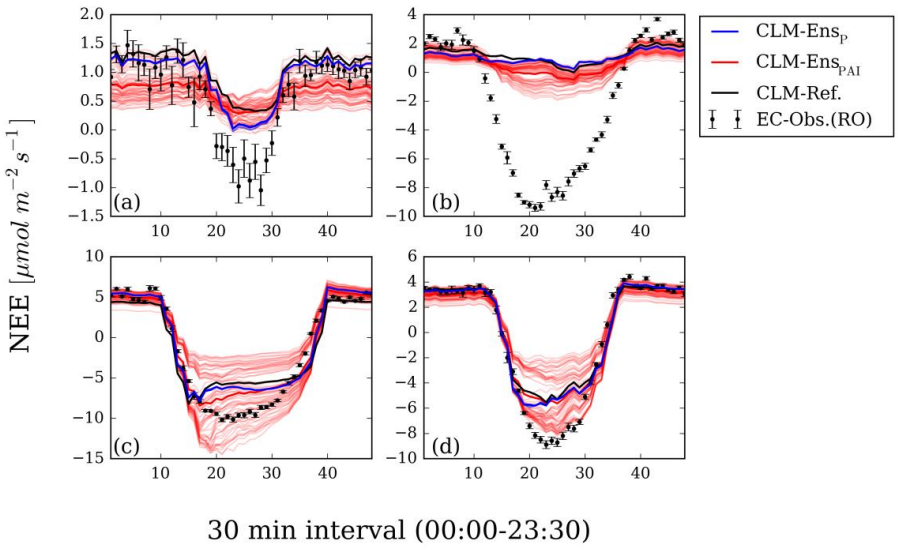

Figure 5.3: Mean diurnal course of half-hourly NEE for winter '12/'13 (a), spring 2013 (b), summer 2013 (c) and autumn 2013 (d) for the Rollesbroich site (RO). Results are shown for the 60 ensemble members of the CLM cases Ens$_P$ with estimated parameters, and Ens$_{PAI}$ with additional perturbed atmospheric forcings and perturbed initial states, in comparison to a reference run with default parameters (CLM-Ref) and EC data (EC-Obs.) (Bold lines: ensemble mean).

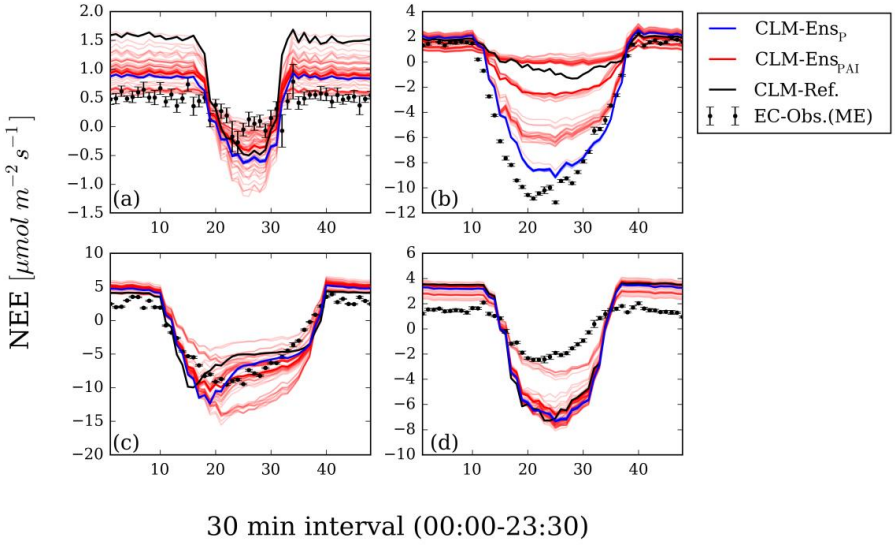

Figure 5.4: Like Figure 5.3, for the Merzenhausen site (ME).

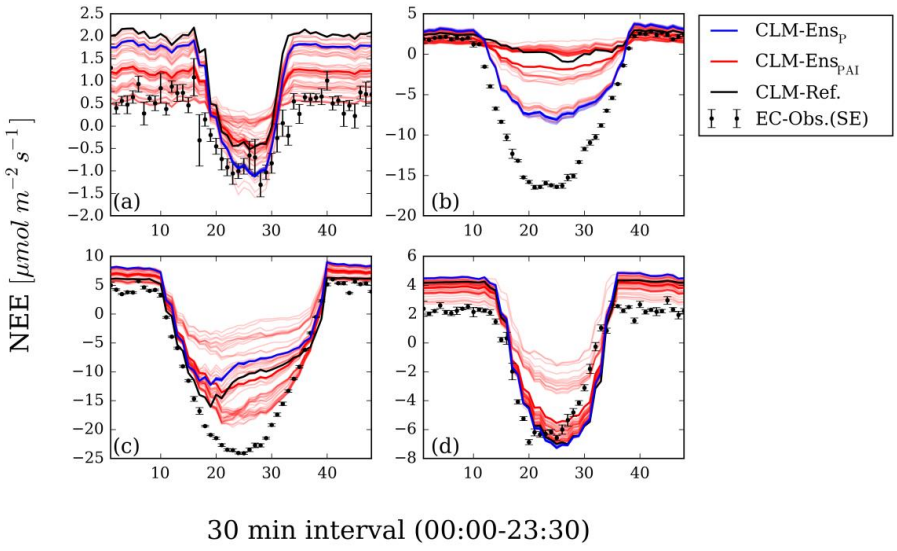

Figure 5.5: Like Figure 5.3, for the Selhausen site (SE).

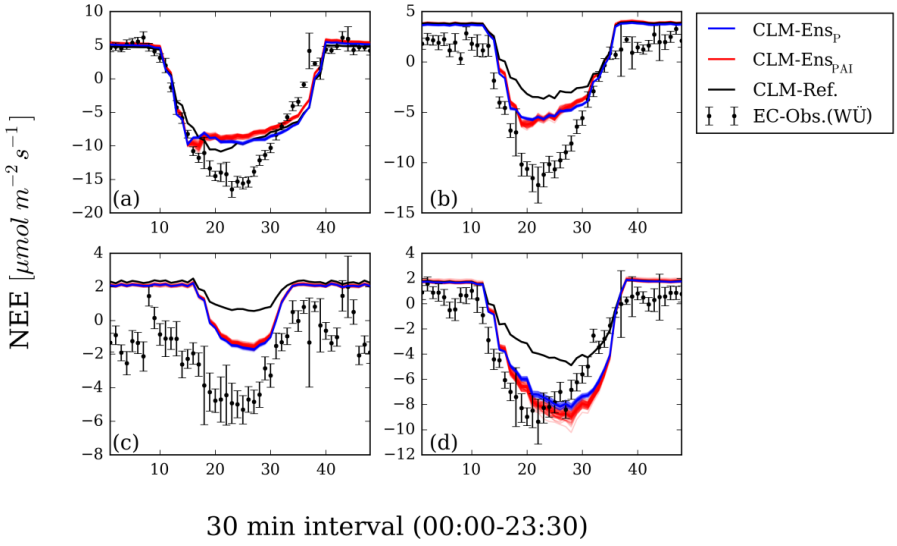

Figure 5.6: Mean diurnal course of half-hourly NEE for summer 2012 (a), autumn 2012 (b), winter '12/'13 (c) and spring 2013 (d) for the Wüstebach site (WÜ). Results are shown for the 60 ensemble members of the CLM cases Ens$_P$ with estimated parameters, and Ens$_{PAI}$ with additional perturbed atmospheric forcings and perturbed initial states, in comparison to a reference run with default parameters (CLM-Ref) and EC data (EC-Obs.) (Bold lines: ensemble mean).

In correspondence with NEE, the ensemble spread of LAI was lower for WÜ$_{gc}$ than for the other sites (Figure 5.7), except for the grid cell "RA" (Figure 5.7e), which was covered 24% by deciduous forest. For RA, the spread and the magnitude of simulated LAI differed very minor between CLM-Ens$_{PAI}$ and CLM-Ens$_P$. Results suggest that for forest, both NEE and LAI simulated by CLM4.5BGC are less sensitive to the perturbed atmospheric input data and initial conditions than C3-grass and C3-crop.

Related to the large ensemble spread, CLM-Ens$_{PAI}$ covered well most of the observations except in spring, where daytime NEE (GPP) was underestimated for C3-grass and C3-crop (Figure 5.54, Figure 5.5). The strong underestimation of GPP in spring 2013 for C3-grass and C3-crop is related to a delay of the plant onset indicated by the LAI (Figure 5.7 c,d). For ME, the beginning of plant onset in spring 2013 was indicated by the rapid increase of the daily LAI from zero to >2. For CLM-Ref and for most of the CLM-Ens$_{PAI}$ ensemble members, the onset started in May. For those model realizations, the underestimation of the mean daytime GPP in spring was highest. In contrast, for CLM-Ens$_P$ and a small proportion of CLM-Ens$_{PAI}$, the plant onset already started in March. For those cases, the underestimation of daytime GPP in spring

was notably lower. This elucidates the close link of modeled NEE and LAI and highlights that errors in the timing of plant onset can lead to substantial errors in simulated NEE.

Table 5.6: Absolute differences $Diff_{CI90}$ between the lower and upper 90% confidence interval ($CI90_{up}$, $CI90_{low}$), and standard deviation (STD) of the annual NEE sum [gC m^{-2} y^{-1}] for the seven grid cells in the Rur catchment where EC towers are located.

site	$CI90_{low}$ **Ens_P**	$CI90_{up}$ **Ens_P**	$CI90_{low}$ **Ens_{PAI}**	$CI90_{up}$ **Ens_{PAI}**	$Diff_{CI90}$ **Ens_P**	$Diff_{CI90}$ **Ens_{PAI}**	STD **Ens_P**	STD **Ens_{PAI}**
RO_{gc}	143.7	144.2	-221.3	403.6	0.5	624.9	0.1	211.9
ME_{gc}	-62.0	-66.3	-77.5	-8.0	4.3	69.5	3.4	24.8
KA_{gc}	-345.4	-338.4	-292.5	172.2	7.0	464.7	2.0	141.8
SE_{gc}	-34.2	-28.7	-218.7	499.3	5.5	718.0	1.5	225.9
NZ_{gc}	-163.8	-153.8	-205.2	91.3	10.0	296.4	2.8	99.9
EN_{gc}	-32.0	-26.9	-71.9	-9.9	5.1	62.0	1.5	24.1
$WÜ_{gc}$	-28.4	-26.8	-17.3	-7.8	1.6	9.5	0.5	3.1

*Ens_P: CLM ensemble with estimated parameters; Ens_{PAI}: CLM ensemble with estimated parameters, perturbed atmospheric forcings and perturbed initial states

Deficits in the stress deciduous phenology scheme of CLM are discussed in Dahlin et al. (2015). This phenology scheme is strongly based on various arbitrary thresholds, such as "crit_offset_swi" (water stress days for offset trigger) or "crit_onset_fdd" (critical number of freezing degree days to trigger onset). Besides deficits in plant phenology, management (harvesting, cutting, etc.) is not explicitly considered for C3-crop and C3-grass in CLM. Therefore, observed temporal LAI variations in the growing season are not well represented by CLM (Figure 5.7). We assume that the too generalized and simplified model representation of C3-crop and C3-grass is a main reason for the high uncertainty of NEE and LAI simulations as well as the irregular distribution of the CLM-Ens_{PAI} ensemble members for those PFTs. Empirical site studies (Hollinger et al., 2004; Richardson et al., 2010a, 2009) as well as modeling studies (Baldocchi and Wilson, 2001; Richardson et al., 2012) show that the growing season length can considerably alter annual net productivity (NEP) in boreal and temperate forest ecosystems. Here, it was shown that in CLM, the timing of plant onset and offset is particularly flawed for C3-grass and C3-crop. Accordingly, the finding that CLM-Ens_P provided more reliable estimates of the NEE sums for ME and SE than the reference run with default parameters (Table 5.4) was mainly related to the fact that parameter estimates shifted the plant onset ahead.

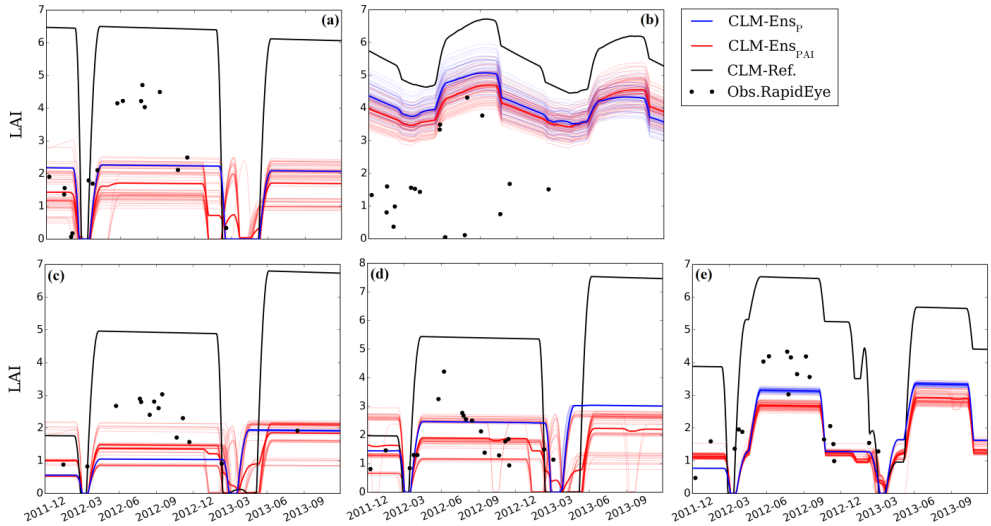

Figure 5.7: Daily leaf area indices (LAI) for five grid cells in the Rur catchment: RO$_{gc}$ (a), WÜ$_{gc}$ (b) ME$_{gc}$ (c), SE$_{gc}$ (d) and RA$_{gc}$ (e) for the period December 2011- November 2013. Results are shown for the 60 ensemble members of the CLM cases Ens$_P$ with estimated parameters, and Ens$_{PAI}$ with additional perturbed atmospheric forcings and perturbed initial states, in comparison to a reference run with default parameters (CLM-Ref) and RapidEye data (Obs.RapidEye) (Bold lines: ensemble mean).

5.4. CONCLUSIONS

NEE is a key flux and LAI is a key variable of the carbon cycle represented by CLM and similar models. Both, LAI and NEE are closely linked via common parameters such as the five parameters estimated in this study. Therefore, parameter estimation with NEE data was found suitable to improve prognostic CLM predictions of LAI. Predicted LAI with estimated parameters were not only improved in terms of the magnitude. In some cases also the timing of vegetation onset was more correct. This resulted also in an improved characterization of NEE, which was highly underestimated in spring in cases where the plant onset was delayed. This highlights the potential of DREAM-CLM parameter estimates to overcome model structural deficits in terms of a misrepresentation of plant phenology.

Constraining CLM parameters with DREAM without talking into account the uncertainty of atmospheric forcings and initial states resulted in a very low uncertainty of the predicted NEE and LAI. For example, the absolute difference of the upper and lower boundary of the 90% confidence interval for the annual NEE sum of the ensemble (Diff$_{CI90}$) only varied between 0.5

and 10.0 gC m^{-2} y^{-1}. However, for CLM-Ens_{PAI} with additional consideration of uncertainty in the initial model conditions and atmospheric input data, $Diff_{CI90}$ was 62.0 – 718.0 gC m^{-2} y^{-1} for C3-grass and C3-crop. Evergreen coniferous forest was least sensitive to the perturbed initial states and atmospheric forcings ($Diff_{CI90}$ = 9.5 gC m^{-2} y^{-1}). It is concluded that the estimated annual NEE-sum is related to a large uncertainty, due to uncertain atmospheric forcings, initial conditions and parameters. However, these uncertainties are considerable lower for evergreen needleleaf trees (and presumably also for broadleaf deciduous trees) than for C3-grass and C3-crop.

Estimated parameters reduced the relative difference between the observed and modeled NEE sum significantly for most evaluation sites compared to a reference run with default parameters. The sign of the annual NEE sum for the catchment was reversed from positive to negative with estimated parameters compared to default parameters. This elucidates the potential and relevance of thorough parameter estimation in terms of obtaining more reliable estimates of regional carbon balances.

Chapter 6: Summary

Modeling of land surface fluxes (carbon, nitrogen, water and energy) is essential to improve the understanding and predictability of feedback mechanisms between climate change, ecosystem behavior, hydrological processes and land use. In order to support future decision making in climate politics and environmental planning, it is important to implement and enhance land surface modeling at the regional level. A central goal of my PHD work was to upscale net ecosystem exchange (NEE) from the eddy covariance (EC) footprint scale to the Rur catchment domain using the Community Land Model (CLM) and updated ecosystem parameter values, which were estimated with help of measured NEE data. Such model-data fusion approaches require an accurate estimate of the measurement uncertainty, which is essential as well for a thorough evaluation of the model performance.

Therefore, first the uncertainty of eddy covariance NEE measurements was investigated for one grassland site inside the Rur catchment. The classical two-tower approach estimates the measurement uncertainty or random error based on the standard deviations of the fluxes measured simultaneously at two nearby EC towers. The random error is estimated as function of the flux magnitude with help of a linear regression equation, which allows then to estimate the random error as function of the measurement value. Because accurate uncertainty estimation is usually time consuming, regression functions like the ones published by Richardson et al. (2006) are commonly used by other scientists to obtain random error estimates of EC fluxes. Various other uncertainty estimation approaches have been developed, but up to now none is generally accepted and applied. The two-tower approach assumes statistical independence of the measured data (non-overlapping footprints) and at the same time identical environmental conditions in the footprint of both EC towers. Because these two requirements are contradictory, the definition of an appropriate tower distance is difficult and the applicability of the method limited. To solve this issue, an extension of the classical two-tower approach is presented, which corrects for systematic differences of the synchronously measured NEE data from two EC stations. It was assumed that systematic flux differences mainly arise from different environmental conditions in the footprint area of both EC stations and thus increase with the EC tower distance. The role of the EC tower distance was investigated by applying and evaluating the uncertainty estimation for five different EC tower distances ranging between 8 m and 34 km. The analysis was made for a dataset that had been filtered for similar weather conditions at the two sites, and an unfiltered one. The uncertainty estimates were compared with corresponding estimates obtained from an independent reference method presented in Mauder

et al. (2013), which is based on the auto- and cross correlations of the raw data measured at a single EC station. The proposed extension of the two-tower approach applied to weather-filtered data substantially reduced the overestimation of the two-tower based NEE measurement uncertainty for all separation distances except for 8 m, by 79% (34 km distance) to 100% (95 m distance). A major conclusion of this study is that the extension of the two-tower approach raised the applicability of the two-tower approach to more site pairs with less ideal conditions, i.e. not very similar environmental conditions. The fact that both approaches, the extended two-tower approach and statistical reference method, provided very similar uncertainty estimates enhanced confidence in both methods.

In the second study, eight key ecological parameters were identified which strongly determine the simulated carbon fluxes in CLM. Those parameters were then estimated with the Markov Chain Monte Carlo method DREAM (DiffeRential Evolution Adaptive Metropolis) separately for four sites with different land cover types: C3-grass, C3-crop, evergreen coniferous forest and broadleaf deciduous forest. Those are the most widespread plant functional types (PFTs) in the Rur catchment and cover > 90% of the vegetated catchment area. The four sites were located inside or close to the Rur catchment. From the eight estimated parameters, five are PFT-specific and three are hard-wired in the CLM source code. Hard-wired parameters such as the temperature coefficient Q_{10} do not vary among PFTs in CLM by default. However, various studies indicate that for example Q_{10} is not a constant, but varies e.g. depending on the PFT and different environmental conditions (Flanagan and Johnson, 2005; Kätterer et al., 1998; Kirschbaum, 2010; Reichstein et al., 2005). Therefore, the eight parameters were estimated jointly for each PFT. The parameters were constrained with half-hourly NEE time series measured at four EC sites. The NEE time series covered a whole year (including gaps). In addition, parameters were estimated separately for the single seasons of this one-year period in order to test if accounting for seasonal variations of the CLM parameters would improve the simulated NEE. Temporal variations of LSM parameters and its relevance for model-data fusion approaches and carbon flux predictions have already been highlighted in previous studies (e.g. Williams et al., 2005; Mo et al., 2008), but have not yet been explicitly investigated for CLM. In addition, it was investigated how strongly the CLM parameter estimates and initial states are linked. This was done by means of an additional experiment where two initial state factors for the CLM carbon-nitrogen pools were estimated jointly with the parameters. Parameter estimates obtained from DREAM were evaluated using (i) half-hourly NEE observations of an independent evaluation period, and (ii) NEE data from four FLUXNET sites situated in about 600 km distance to the original sites. To comprehensively evaluate the parameter estimates,

different evaluation indices were calculated, which express the mismatch of modeled and measured NEE data: (i) the relative difference of the annual NEE sum ($RD_{\sum NEE}$), (ii) the root mean square error for the one-year time series of half-hourly NEE data ($RMSE_m$), (iii) the mean absolute difference of the mean diurnal NEE cycle (MAD_{diur}), and (iv) the mean absolute difference of the monthly mean NEE values over the evaluation year (MAD_{ann}). Those indices were calculated and compared for the CLM runs with updated parameters and a reference run with CLM default parameters. It was shown that parameter values underlie a strong seasonal variability. Parameters that were estimated on seasonal basis outperformed the parameters that were estimated based on the whole one year period. With parameters estimated separately for the four seasons, $RD_{\sum NEE}$ was 50% lower than for the reference run, averaged over all sites. The respective MAD_{diur} and MAD_{ann} indices were reduced by a factor of 1.5 (MAD_{diur}) and 1.4 (MAD_{ann}) on average. This highlights that estimated parameters notably improved the consistency of modeled and measured NEE data as well as the model representation of the simulated mean diurnal and annual NEE cycle. The evaluation was more successful for the forest PFTs compared to C3-grass and C3-crop. Along with this result, correlations between parameters and the initial state factors were found to be higher for C3-grass and C3-crop than for the forest PFTs. It was concluded that CLM4.5 parameter estimates for evergreen needleleaf forest and broadleaf deciduous forest were best transferable and most reliable.

In a following study, DREAM-CLM parameter estimates were applied to the whole Rur catchment domain and thus used to upscale NEE data from the EC footprint scale to the catchment scale. New parameter sets were estimated using the same data and the same DREAM-CLM set-up as in the previous study, but this time only considering the five PFT-specific parameters. The CLM performance with and without updated parameters was evaluated based on NEE data of seven EC towers inside the Rur catchment. The difference between the observed and simulated NEE sum for the evaluation period (Dec. 2012 – Nov. 2013) was 23% smaller if DREAM-parameters instead of default parameters were used as input. This indicates that parameter estimates can provide a more reliable estimate of the annual NEE balance for the catchment than global default parameters. However, as expected, results suggested that parameters estimated for a particular crop type could not be transferred to grid cells where very different crops types are grown, such as sugar beet instead of winter wheat. This highlights the severe limitations of large scale carbon flux estimation with land surface models that only distinguish between very broad groups of PFTs. In addition, it was tested if parameter estimates improve the prognostically simulated LAI for the catchment. This was evaluated using LAI data obtained from remotely sensed RapidEye images. Results showed that the misfit between

modeled and observed LAI data was notably reduced if estimated parameters instead of CLM default parameters were used, particularly in case of C3-grass and C3-crop. For those PFTs, the mean absolute difference between observed and modeled LAI data (MAD_{LAI}) was about 52% lower with parameter estimates. Modeled LAI with estimated parameters was not only improved in terms of magnitude, but in some cases also in terms the beginning of plant onset in spring. This was linked to a notably reduced underestimation of GPP in spring and an improved NEE estimate for the whole year. To obtain a more comprehensive picture of model uncertainty, a second CLM ensemble was set up where perturbed meteorological input data and perturbed initial conditions were applied in addition to the estimated ecosystem parameters. The considerably lower spread of NEE and LAI for the forest PFTs compared to C3-crop and C3-grass indicated that the model uncertainty was notably higher for C3-crop and C3-grass. This agrees with findings of the previous study and highlights the potential of parameter and uncertainty estimation to support the understanding and further development of land surface models like CLM.

Chapter 7: Final conclusions and outlook

This study revealed how strongly uncertainties of CLM parameters, initial states and model structure are linked. It was highlighted that due to the correlation of carbon cycle relevant CLM parameters and initial conditions, optimal parameter values are not constant in time, but vary seasonally, which was already emphasized in previous studies with other land surface models. Thus, carbon flux estimation would benefit from the option to define temporally variable ecosystem parameters like Q_{10} (temperature sensitivity coefficient) or sla_{top} (specific leaf area at the canopy top [m^2 g^{-1} C]). Estimated values for CLM parameters like Q_{10} that are not PFT-specifically defined by default also varied among plant functional types. Thus, the representation of carbon fluxes could be further improved if a PFT-specific definition of those parameters would be enabled. DREAM parameter estimates were shown to be mutually dependent on the initial model states. This implies that estimated values of NEE-relevant key parameters are not necessarily optimal in combination with a different set of initial model conditions (e.g. another site or a different time period). This is linked to the fact that also initial model states are highly uncertain, since they underlay the steady state assumption and do not represent the real state of the ecosystem. Parameter estimation with a relaxed steady state assumption as discussed by Carvalhais et al. (2008) could therefore be beneficial. In terms of DREAM-CLM, this could theoretically be realized by estimating parameters independently for an ensemble of perturbed initial states and then summarizing the obtained joint posterior pdfs. However, this would be computationally very time consuming. An alternative approach is to estimate initial model states jointly with the model parameters as shown in Chapter 4. This way, the uncertainty of model initial states and the correlation of model states and parameters are accurately taken into account. However, this does not solve the problem that the estimated values may not be transferrable to other sites or regions. CLM4.5BGC contains hundreds of state variables that need to be spun up and are linked to ensure a closed energy and carbon balance. Substituting selected initial model states by the estimated values most likely breaks the carbon and energy balance of the model. The balance checks can be commented out in the source code, but then a basic strength of the LSM is discarded as well. The approach used here to estimate factors that are applied to all carbon or nitrogen pools (instead of estimating the absolute value of singe CN pools) is considered advantageous in terms of preserving the carbon and nitrogen balances.

With regard to the close link of CLM parameters and states, it is important to further investigate how parameter uncertainty affects the uncertainty of model initial states and vice versa. The

uncertainty of the initial model states is also influenced by the atmospheric input data used during the model spin-up. Chapter 5 showed how strongly perturbed initial states and perturbed atmospheric forcings increased the uncertainty of predicted NEE and LAI in case of C3-crop and C3-grass, compared to an ensemble with uncertain parameters only. This needs further investigation, for example by comparing results for different lengths of perturbed spin-ups.

The strong sensitivity of NEE and LAI to the perturbed initial conditions and atmospheric forcings for C3-grass and C3-crop is related to deficits in the model structure of CLM. For the characterization of LAI and NEE it was found particularly important to improve the representation of the beginning and end of the active growing season for grasses and crops, i.e. the stress deciduous phenology scheme. In case of the generic PFTs "C3-grass" and "C3-crop" defined in this study, this would involve the implementation of currently missing key processes such as senescence (observed at the winter wheat sites in the catchment). Because the growing season strongly varies for different crop types, a discretization of different crop types and the consideration of management are considered necessary. As shown here, otherwise no robust parameter estimates can be obtained via LSM-data fusion. Crop management (e.g. timing of sowing and harvesting) is partly implemented for CLM4.5, but not for the PFTs "sugar beet" and "winter wheat", the most widespread crops in the Rur catchment. Thus, the generic crop module was used in this study. In the future, new parameterizations for specific crop types should be implemented, as it is foreseen the upcoming version(s) of CLM (personal communication with Yaquiong Lu from NCAR).

It this study, NEE was used to constrain CLM via parameter estimation with $DREAM_{(zs)}$. However, the GPP component of NEE is closely linked to the latent heat flux (LE) via the process of stomatal opening and closing. Both processes are linked to the LAI, which is used to upscale photosynthesis from leaf scale to larger scales. Therefore, a multi-objective parameter estimation approach would be beneficial to improve and evaluate the overall LSM performance. Additional data like LAI, soil moisture content, fPAR (Fraction of Photosynthetically Active Radiation) and leaf C:N ratios could be assimilated to further improve the model. In order to improve respiration and C:N pool estimates, measurements of litter, soil organic matter and turnover times would be beneficial. Because such data is often limited, an extension of measurements at highly equipped site are considered very important for model-data fusion and model evaluation. Sequential data assimilation with an Ensemble Kalman Filter (EnKF) like method could be suited to integrate the multiple data sources and would be computationally less costly compared to other model-data fusion methods.

Finally, this study highlights the importance of representativeness of the EC data if used to upscale land surface fluxes via model-data fusion. Additional NEE data from EC stations available inside or close to the Rur catchment would be beneficial to improve DREAM-CLM parameter estimates for all PFTs and to adequately evaluate the reliability of the catchment scale NEE prediction. Not only the amount of available EC stations within the catchment were very limited for the evaluation of the upscaling approach, but also the length of available NEE time series for the stations available. The reduction of uncertainties in land surface flux estimates at a regional scale would therefore be enhanced with a further expansion of EC stations at representative sites.

Bibliography

Abramowitz, G., Leuning, R., Clark, M., Pitman, A., 2008. Evaluating the performance of land surface models. Journal of Climate 21, 5468–5481.

Ali, M., Montzka, C., Stadler, A., Menz, G., Thonfeld, F., Vereecken, H., 2015. Estimation and Validation of RapidEye-Based Time-Series of Leaf Area Index for Winter Wheat in the Rur Catchment (Germany). Remote Sensing 7, 2808–2831.

Allard, V., Soussana, J.-F., Falcimagne, R., Berbigier, P., Bonnefond, J.M., Ceschia, E., D'hour, P., Hénault, C., Laville, P., Martin, C., Pinarès-Patino, C., 2007. The role of grazing management for the net biome productivity and greenhouse gas budget (CO2, N2O and CH4) of semi-natural grassland. Agriculture, Ecosystems & Environment 121, 47–58.

Ammann, C., Flechard, C.R., Leifeld, J., Neftel, A., Fuhrer, J., 2007. The carbon budget of newly established temperate grassland depends on management intensity. Agriculture, Ecosystems & Environment 121, 5–20.

Anderson, J., Hoar, T., Raeder, K., Liu, H., Collins, N., Torn, R., Avellano, A., 2009. The data assimilation research testbed: A community facility. Bulletin of the American Meteorological Society 90, 1283–1296.

Anderson, M.C., Kustas, W.P., Norman, J.M., 2003. Upscaling and Downscaling—A Regional View of the Soil–Plant–Atmosphere Continuum. Agronomy Journal 95.

Andrén, O., Paustian, K., 1987. Barley straw decomposition in the field: a comparison of models. Ecology 1190–1200.

Arbeitsgruppe BK50, 2001. Allgemeine Informationen zur Bodenkarte 1 : 50 000. - 55 S.; Krefeld. Geol. Dienst Nordrh.-Westf.

Asner, G.P., Scurlock, J.M.O., A. Hicke, J., 2003. Global synthesis of leaf area index observations: implications for ecological and remote sensing studies. Global Ecology and Biogeography 12, 191–205.

Arora, V.K., Boer, G.J., Friedlingstein, P., Eby, M., Jones, C.D., Christian, J.R., Bonan, G., Bopp, L., Brovkin, V., Cadule, P., Hajima, T., Ilyina, T., Lindsay, K., Tjiputra, J.F., Wu, T., 2013. Carbon–Concentration and Carbon–Climate Feedbacks in CMIP5 Earth System Models. J. Climate 26, 5289–5314.

Aubinet, M., Vesala, T., Papale, D., 2011. Eddy Covariance: A Practical Guide to Measurement and Data Analysis. Springer Verlag.

Baatz, R., Bogena, H.R., Hendricks Franssen, H.-J., Huisman, J.A., Qu, W., Montzka, C., Vereecken, H., 2014. Calibration of a catchment scale cosmic-ray probe network: A comparison of three parameterization methods. Journal of Hydrology, Determination of soil moisture: Measurements and theoretical approaches 516, 231–244.

Baker, I.T., Prihodko, L., Denning, A.S., Goulden, M., Miller, S., Da Rocha, H.R., 2008. Seasonal drought stress in the Amazon: Reconciling models and observations. Journal of Geophysical Research: Biogeosciences (2005–2012) 113.

Baldauf, M., Förstner, J., Klink, S., Reinhardt, T., Schraff, C., Seifert, A., Stephan, K., Wetterdienst, D., 2009. Kurze Beschreibung des Lokal-Modells Kürzestfrist COSMO-DE (LMK) und seiner Datenbanken auf dem Datenserver des DWD. Deutscher Wetterdienst, Geschäftsbereich Forschung und Entwicklung, Offenbach, Germany.

Baldocchi, D.D., 2001. Assessing ecosystem carbon balance: problems and prospects of the eddy covariance technique. Annual Review of Ecology and Systematics 33, 1–33.

Baldocchi, D.D., 2003. Assessing the eddy covariance technique for evaluating carbon dioxide exchange rates of ecosystems: past, present and future. Global Change Biology 9, 479–492.

Baldocchi, D.D., Wilson, K.B., 2001. Modeling CO2 and water vapor exchange of a temperate broadleaved forest across hourly to decadal time scales. Ecological Modelling 142, 155–184.

Ball, T.J., Berry, J.A., 1982. Ci/Cs ratio: a basis for predicting stomatal control of photosynthesis. Year book-Carnegie Institution of Washington.

Ball, J.T., Woodrow, I.E., Berry, J.A., 1987. A Model Predicting Stomatal Conductance and its Contribution to the Control of Photosynthesis under Different Environmental Conditions, in: Biggins, J. (Ed.), Progress in Photosynthesis Research. Springer Netherlands, pp. 221–224.

Barr, A.G., Morgenstern, K., Black, T.A., McCaughey, J.H., Nesic, Z., 2006. Surface energy balance closure by the eddy-covariance method above three boreal forest stands and implications for the measurement of the CO2 flux. Agricultural and Forest Meteorology 140, 322–337.

Beven, K., Freer, J., 2001. Equifinality, data assimilation, and uncertainty estimation in mechanistic modelling of complex environmental systems using the GLUE methodology. Journal of Hydrology 249, 11–29.

Bilionis, I., Drewniak, B.A., Constantinescu, E.M., 2015. Crop physiology calibration in the CLM. Geosci. Model Dev. 8, 1071–1083.

Billesbach, D.P., 2011. Estimating uncertainties in individual eddy covariance flux measurements: A comparison of methods and a proposed new method. Agricultural and Forest Meteorology 151, 394–405.

blackbridge, 2015. Satellite Imagery Product Specifications. Version 6.1.

Bogena, H.R., Huisman, J.A., Meier, H., Rosenbaum, U., Weuthen, A., 2009. Hybrid Wireless Underground Sensor Networks: Quantification of Signal Attenuation in Soil. Vadose Zone Journal 8, 755–761.

Bonan, G.B., DeFries, R.S., Coe, M.T., Ojima, D.S., 2002. Land Use and Climate, in: Land Change Science; Observing, Monitoring and Understanding Trajectories of Change on the Earth's Surface. Remote Sensing and Digital Image Processing, pp. 301–314.

Bonan, G.B., Lawrence, P.J., Oleson, K.W., Levis, S., Jung, M., Reichstein, M., Lawrence, D.M., Swenson, S.C., 2011. Improving canopy processes in the Community Land Model version 4 (CLM4) using global flux fields empirically inferred from FLUXNET data. Journal of Geophysical Research 116.

Bonan, G.B., Hartman, M.D., Parton, W.J., Wieder, W.R., 2013. Evaluating litter decomposition in earth system models with long-term litterbag experiments: an example using the Community Land Model version 4 (CLM4). Global Change Biology 19, 957–974.

Bonan, G.B., Williams, M., Fisher, R.A., Oleson, K.W., 2014. Modeling stomatal conductance in the earth system: linking leaf water-use efficiency and water transport along the soil–plant–atmosphere continuum. Geosci. Model Dev. 7, 2193–2222.

Braswell, B.H., Sacks, W.J., Linder, E., Schimel, D.S., 2005. Estimating diurnal to annual ecosystem parameters by synthesis of a carbon flux model with eddy covariance net ecosystem exchange observations. Global Change Biology 11, 335–355.

Bréda, N.J.J., 2003. Ground-based measurements of leaf area index: a review of methods, instruments and current controversies. J. Exp. Bot. 54, 2403–2417.

Brovkin, V., Boysen, L., Arora, V.K., Boisier, J.P., Cadule, P., Chini, L., Claussen, M., Friedlingstein, P., Gayler, V., van den Hurk, B.J.J.M., Hurtt, G.C., Jones, C. D., Kato, E., de Noblet-Ducoudré, N., Pacifico, F., Pongratz, J., Weiss, M., 2013. Effect of Anthropogenic Land-Use and Land-Cover Changes on Climate and Land Carbon Storage in CMIP5 Projections for the Twenty-First Century. J. Climate 26, 6859–6881.

Chai, T., Draxler, R.R., 2014. Root mean square error (RMSE) or mean absolute error (MAE)?–Arguments against avoiding RMSE in the literature. Geosci. Model Dev. 7, 1247–1250.

Carvalhais, N., Reichstein, M., Seixas, J., Collatz, G.J., Pereira, J.S., Berbigier, P., Carrara, A., Granier, A., Montagnani, L., Papale, D., Rambal, S., Sanz, M.J., Valentini, R., 2008. Implications of the carbon cycle steady state assumption for biogeochemical modeling performance and inverse parameter retrieval. Global Biogeochemical Cycles 22

Carvalhais, N., Reichstein, M., Ciais, P., Collatz, G.J., Mahecha, M.D., Montagnani, L., Papale, D., Rambal, S., Seixas, J., 2010. Identification of vegetation and soil carbon pools out of equilibrium in a process model via eddy covariance and biometric constraints. Global Change Biology 16, 2813–2829.

Chen, J.M., Rich, P.M., Gower, S.T., Norman, J.M., Plummer, S., 1997. Leaf area index of boreal forests: theory, techniques, and measurements. Journal of Geophysical Research: Atmospheres (1984–2012) 102, 29429–29443.

Chen, B., Black, T.A., Coops, N.C., Hilker, T., Trofymow, J.A., Morgenstern, K., 2009. Assessing tower flux footprint climatology and scaling between remotely sensed and eddy covariance measurements. Boundary-layer meteorology 130, 137–167.

Chen, B., Coops, N.C., Fu, D., Margolis, H.A., Amiro, B.D., Black, T.A., Arain, M.A., Barr, A.G., Bourque, C.P.-A., Flanagan, L.B., Lafleur, P.M., McCaughey, J.H., Wofsy, S.C., 2012. Characterizing spatial representativeness of flux tower eddy-covariance measurements across the Canadian Carbon Program Network using remote sensing and footprint analysis. Remote Sensing of Environment 124, 742–755.

Chevallier, F., Palmer, P.I., Feng, L., Boesch, H., O'Dell, C.W., Bousquet, P., 2014. Toward robust and consistent regional CO2 flux estimates from in-situ and spaceborne measurements of atmospheric CO2. Geophys. Res. Lett. 41, 2013GL058772.

Chapin III, F.S., Matson, P.A., Mooney, H.A., 2002. Principles of terrestrial ecosystem ecology. Springer, New York, USA.

Collatz, G.J., Ball, J.T., Grivet, C., Berry, J.A., 1991. Physiological and environmental regulation of stomatal conductance, photosynthesis and transpiration: a model that includes a laminar boundary layer. Agricultural and Forest Meteorology 54, 107–136.

Collatz, G.J., Ribas-Carbo, M., Berry, J.A., 1992. Coupled photosynthesis-stomatal conductance model for leaves of C4 plants. Functional Plant Biology 19, 519–538.

Cosby, B.J., Hornberger, G.M., Clapp, R.B., Ginn, T., 1984. A statistical exploration of the relationships of soil moisture characteristics to the physical properties of soils. Water Resour. Res 20, 682–690.

Dahlin, K.M., Fisher, R.A., Lawrence, P.J., 2015. Environmental drivers of drought deciduous phenology in the Community Land Model. Biogeosciences Discussions 12, 5803–5839.

Dai, Y., Dickinson, R.E., Wang, Y.-P., 2004. A Two-Big-Leaf Model for Canopy Temperature, Photosynthesis, and Stomatal Conductance. Journal of Climate 17, 2281–2299.

Dekker, S.C., Vrugt, J.A., Elkington, R.J., 2012. Significant variation in vegetation characteristics and dynamics from ecohydrological optimality of net carbon profit. Ecohydrol. 5, 1–18.

Deng, F., Chen, J.M., Ishizawa, M., Yuen, C.-W., Mo, G., Higuchi, K., Chan, D., Maksyutov, S., 2007. Global monthly CO2 flux inversion with a focus over North America. Tellus B 59, 179–190.

Desai, A.R., Noormets, A., Bolstad, P.V., Chen, J., Cook, B.D., Davis, K.J., Euskirchen, E.S., Gough, C., Martin, J.G., Ricciuto, D.M., Schmid, H.P., Tang, J., Wang, W., 2008. Influence of vegetation and seasonal forcing on carbon dioxide fluxes across the Upper Midwest, USA: Implications for regional scaling. Agricultural and Forest Meteorology 148, 288–308.

Dijk, A.V., Moene, A.F., DeBruin, H.A.R., 2004. The principles of surface flux physics: theory, practice and description of the ECPACK library. Meteorology and Air Quality Group of Wageningen University, Wageningen.

Dragoni, D., Schmid, H.P., Grimmond, C.S.B., Loescher, H.W., 2007. Uncertainty of annual net ecosystem productivity estimated using eddy covariance flux measurements. Journal of Geophysical Research-Atmospheres 112, 1–9.

Dumont, B., Leemans, V., Mansouri, M., Bodson, B., Destain, J.-P., Destain, M.-F., 2014. Parameter identification of the STICS crop model, using an accelerated formal MCMC approach. Environmental Modelling & Software 52, 121–135.

Evensen, G., 2003. The ensemble Kalman filter: Theoretical formulation and practical implementation. Ocean dynamics 53, 343–367.

Falge, E., Baldocchi, D., Olson, R., Anthoni, P., Aubinet, M., Bernhofer, C., Burba, G., Ceulemans, R., Clement, R., Dolman, H., others, 2001. Gap filling strategies for defensible annual sums of net ecosystem exchange. Agricultural and forest meteorology 107, 43–69.

Farquhar, G.D., von Caemmerer, S. von, Berry, J.A., 1980. A biochemical model of photosynthetic CO2 assimilation in leaves of C3 species. Planta 149, 78–90.

Finkelstein, P.L., Sims, P.F., 2001. Sampling error in eddy correlation flux measurements. Journal of Geophysical Research: Atmospheres 106, 3503–3509.

Finnigan, J., 2008. An introduction to flux measurements in difficult conditions. Ecological Applications 18, 1340–1350.

Fisher, J.B., Sikka, M., Oechel, W.C., Huntzinger, D.N., Melton, J.R., Koven, C.D., Ahlström, A., Arain, A.M., Baker, I., Chen, J.M., Ciais, P., Davidson, C., Dietze, M., El-Masri, B., Hayes, D., Huntingford, C., Jain, A., Levy, P.E., Lomas, M.R., Poulter, B., Price, D., Sahoo, A.K., Schaefer, K., Tian, H., Tomelleri, E., Verbeeck, H., Viovy, N., Wania, R., Zeng, N., Miller, C.E., 2014. Carbon cycle uncertainty in the Alaskan Arctic. Biogeosciences 11, 4271–4288.

Flanagan, L.B., Johnson, B.G., 2005. Interacting effects of temperature, soil moisture and plant biomass production on ecosystem respiration in a northern temperate grassland. Agricultural and Forest Meteorology 130, 237–253.

Foereid, B., Ward, D.S., Mahowald, N., Paterson, E., Lehmann, J., 2014. The Sensitivity of Carbon Turnover in the Community Land Model to Modified Assumptions about Soil Processes." Earth Syst. Dynam. 5: 211– 221.

Foken, T., Wichura, B., 1996. Tools for quality assessment of surface-based flux measurements. Agricultural and Forest Meteorology 78, 83–105.

Foken, T., 2008. The energy balance closure problem: An overview. Ecological Applications 18, 1351–1367.

Foken, T., Wimmer, F., Mauder, M., Thomas, C., Liebethal, C., 2006. Some aspects of the energy balance closure problem. Atmospheric Chemistry and Physics 6, 4395–4402.

Garrigues, S., Allard, D., Baret, F., Weiss, M., 2006. Influence of landscape spatial heterogeneity on the non-linear estimation of leaf area index from moderate spatial resolution remote sensing data. Remote Sensing of Environment 105, 286–298.

Garrigues, S., Lacaze, R., Baret, F., Morisette, J.T., Weiss, M., Nickeson, J.E., Fernandes, R., Plummer, S., Shabanov, N.V., Myneni, R.B., Knyazikhin, Y., Yang, W., 2008. Validation and intercomparison of global Leaf Area Index products derived from remote sensing data. J. Geophys. Res. 113, G02028.

Gayler, S., Ingwersen, J., Priesack, E., Wöhling, T., Wulfmeyer, V., Streck, T., 2013. Assessing the relevance of subsurface processes for the simulation of evapotranspiration and soil moisture dynamics with CLM3. 5: comparison with field data and crop model simulations. Environmental earth sciences 69, 415–427.

Gelman, A., Rubin, D.B., 1992. Inference from iterative simulation using multiple sequences. Statistical science 457–472.

Göhler, M., Mai, J., Cuntz, M., 2013. Use of eigendecomposition in a parameter sensitivity analyisis of the Community Land Model. Journal of Geophysical research. Journal of Geophysical Research: Biogeosciences 118, 904–921.

Goulden, M.L., Munger, J.W., Fan, S.M., Daube, B.C., Wofsy, S.C., 1996. Measurements of carbon sequestration by long-term eddy covariance: Methods and a critical evaluation of accuracy. Global Change Biology 2, 169–182.

Graf, A., Bogena, H.R., Drüe, C., Hardelauf, H., Pütz, T., Heinemann, G., Vereecken, H., 2014. Spatiotemporal relations between water budget components and soil water content in a forested tributary catchment. Water Resources Research 50, 4837–4857.

Groenendijk, M., Dolman, A.J., Van der Molen, M.K., Leuning, R., Arneth, A., Delpierre, N., Gash, J.H.C., Lindroth, A., Richardson, A.D., Verbeeck, H., others, 2011. Assessing parameter variability in a photosynthesis model within and between plant functional types using global Fluxnet eddy covariance data. Agricultural and forest meteorology 151, 22–38.

Han, X., Li, X., Hendricks Franssen, H.J., Vereecken, H., Montzka, C., 2012. Spatial horizontal correlation characteristics in the land data assimilation of soil moisture. Hydrol. Earth Syst. Sci. 16, 1349–1363.

Han, X., Hendricks Franssen, H.-J., Li, X., Zhang, Y., Montzka, C., Vereecken, H., 2013. Joint assimilation of surface temperature and L-band microwave brightness temperature in land data assimilation. Vadose Zone Journal 12.

Han, X., Franssen, H.-J.H., Montzka, C., Vereecken, H., 2014. Soil moisture and soil properties estimation in the Community Land Model with synthetic brightness temperature observations. Water Resour. Res. 50, 6081–6105.

Hararuk, O., Xia, J., Luo, Y., 2014. Evaluation and improvement of a global land model against soil carbon data using a Bayesian Markov chain Monte Carlo method. J. Geophys. Res. Biogeosci. 119, 2013JG002535.

Hendricks Franssen, H.J., Stoeckli, R., Lehner, I., Rotenberg, E., Seneviratne, S.I., 2010. Energy balance closure of eddy-covariance data: A multisite analysis for European FLUXNET stations. Agricultural and Forest Meteorology 150, 1553–1567.

Herbst, M., Prolingheuer, N., Graf, A., Huisman, J.A., Weihermüller, L., Vanderborght, J., 2009. Characterization and Understanding of Bare Soil Respiration Spatial Variability at Plot Scale. Vadose Zone Journal 8, 762.

Hill, T.C., Ryan, E., Williams, M., 2012. The use of CO2 flux time series for parameter and carbon stock estimation in carbon cycle research. Global Change Biology 18, 179–193.

Hohlfeld, C., Lüers, B., Müller, B., Resch-Esser, U., Titz, S., 2012. TERENO – Finding local solutions to global change. TERENO.

Hollinger, D.Y., Aber, J., Dail, B., Davidson, E.A., Goltz, S.M., Hughes, H., Leclerc, M.Y., Lee, J.T., Richardson, A.D., Rodrigues, C., Scott, N. a., Achuatavarier, D., Walsh, J., 2004. Spatial and temporal variability in forest–atmosphere CO2 exchange. Global Change Biology 10, 1689–1706.

Hollinger, D.Y., Richardson, A.D., 2005. Uncertainty in eddy covariance measurements and its application to physiological models. Tree Physiology 25, 873–885.

Huntzinger, D.N., Post, W.M., Wei, Y., Michalak, A.M., West, T.O., Jacobson, A.R., Baker, I.T., Chen, J.M., Davis, K.J., Hayes, D.J., Hoffman, F.M., Jain, A.K., Liu, S., McGuire, A.D., Neilson, R.P., Potter, C., Poulter, B., Price, D., Raczka, B.M., Tian, H.Q., Thornton, P., Tomelleri, E., Viovy, N., Xiao, J., Yuan, W., Zeng, N., Zhao, M., Cook, R., 2012. North American Carbon Program (NACP) regional interim synthesis: Terrestrial biospheric model intercomparison. Ecological Modelling 232, 144–157.

Iizumi, T., Tanaka, Y., Sakurai, G., Ishigooka, Y., Yokozawa, M., 2014. Dependency of parameter values of a crop model on the spatial scale of simulation. J. Adv. Model. Earth Syst. 6, 527–540.

Imukova, K., Ingwersen, J., Hevart, M., Streck, T., 2015. Energy balance closure on a winter wheat stand: comparing the eddy covariance technique with the soil water balance method. Energy 12, 6783–6820.

Jenkinson, D.S., Coleman, K., 2008. The turnover of organic carbon in subsoils. Part 2. Modelling carbon turnover. European Journal of Soil Science 59, 400–413.

Kato, T., Scholze, M., Knorr, W., Veenendaal, E., Kaminski, T., Kattge, J., Gobron, N., 2012. Simultaneous assimilation of satellite and eddy covariance data for improving terrestrial water and carbon simulations at a semi-arid woodland site in Botswana. Biogeosciences Discussions 9.

Kätterer, T., Reichstein, M., Andrén, O., Lomander, A., 1998. Temperature dependence of organic matter decomposition: a critical review using literature data analyzed with different models. Biology and fertility of soils 27, 258–262.

Keenan, T.F., Baker, I., Barr, A., Ciais, P., Davis, K., Dietze, M., Dragoni, D., Gough, C.M., Grant, R., Hollinger, D., Hufkens, K., Poulter, B., McCaughey, H., Raczka, B., Ryu, Y., Schaefer, K., Tian, H., Verbeeck, H., Zhao, M., Richardson, A.D., 2012a. Terrestrial biosphere model performance for inter-annual variability of land-atmosphere CO2 exchange. Glob Change Biol 18, 1971–1987.

Keenan, T.F., Davidson, E., Moffat, A.M., Munger, W., Richardson, A.D., 2012b. Using model-data fusion to interpret past trends, and quantify uncertainties in future projections, of terrestrial ecosystem carbon cycling. Global Change Biology 18, 2555–2569.

Kessomkiat, W., Hendricks-Franssen, H.-J., Graf, A., Vereecken, H., 2013. Estimating random errors of eddy covariance data: An extended two-tower approach. Agricultural and Forest Meteorology 171, 203–219.

Kirschbaum, M.U.F., 1995. The temperature dependence of soil organic matter decomposition, and the effect of global warming on soil organic C storage. Soil Biology & Biochemistry 27, 753–760.

Kirschbaum, M.U.F., 2010. The temperature dependence of organic matter decomposition: seasonal temperature variations turn a sharp short-term temperature response into a more moderate annually averaged response. Global Change Biology 16, 2117–2129.

Knorr, W., Kattge, J., 2005. Inversion of terrestrial ecosystem model parameter values against eddy covariance measurements by Monte Carlo sampling. Global Change Biology 11, 1333–1351.

Kormann, R., Meixner, F.X., 2001. An Analytical Footprint Model For Non-Neutral Stratification. Boundary-Layer Meteorology 99, 207–224.

Korres, W., Koyama, C.N., Fiener, P., Schneider, K., 2010. Analysis of surface soil moisture patterns in agricultural landscapes using Empirical Orthogonal Functions. Hydrol. Earth Syst. Sci. 14, 751–764.

Koven, C.D., Riley, W.J., Subin, Z.M., Tang, J.Y., Torn, M.S., Collins, W.D., Bonan, G.B., Lawrence, D.M., Swenson, S.C., 2013. The effect of vertically resolved soil biogeochemistry and alternate soil C and N models on C dynamics of CLM4. Biogeosciences 10, 7109–7131.

Krinner, G., Viovy, N., de Noblet-Ducoudré, N., Ogée, J., Polcher, J., Friedlingstein, P., Ciais, P., Sitch, S., Prentice, I.C., 2005. A dynamic global vegetation model for studies of the coupled atmosphere-biosphere system. Global Biogeochemical Cycles 19.

Kukharets, V.P., Nalbandyan, H.G., Foken, T., 2000. Thermal interactions between the underlying surface and a nonstationary radiation flux. Izvestiya Atmospheric and Oceanic Physics 36, 318–325.

Kumar, S.V., Reichle, R.H., Harrison, K.W., Peters-Lidard, C.D., Yatheendradas, S., Santanello, J.A., 2012. A comparison of methods for a priori bias correction in soil moisture data assimilation. Water Resour. Res. 48, W03515.

Kuppel, S., Peylin, P., Chevallier, F., Bacour, C., Maignan, F., Richardson, A.D., 2012. Constraining a global ecosystem model with multi-site eddy-covariance data. Biogeosciences Discuss. 9, 3317–3380.

Kuppel, S., Chevallier, F., Peylin, P., 2013. Quantifying the model structural error in carbon cycle data assimilation systems. Geosci. Model Dev. 6, 45–55.

Kuppel, S., Peylin, P., Maignan, F., Chevallier, F., Kiely, G., Montagnani, L., Cescatti, A., 2014. Model–data fusion across ecosystems: from multisite optimizations to global simulations. Geosci. Model Dev. 7, 2581–2597.

Laloy, E., Vrugt, J.A., 2012. High-Dimensional Posterior Exploration of Hydrologic Models Using Multiple-Try DREAM(ZS) and High-Performance Computing. Water Resources Research 48 (1): 1–18.

Lawrence, D.M., Oleson, K.W., Flanner, M.G., Fletcher, C.G., Lawrence, P.J., Levis, S., Swenson, S.C., Bonan, G.B., 2012. The CCSM4 land simulation, 1850-2005: Assessment of surface climate and new capabilities. Journal of Climate 25, 2240–2260.

Leifeld, J., Fuhrer, J., 2005. The Temperature Response of CO2 Production from Bulk Soils and Soil Fractions is related to Soil Organic Matter Quality. Biogeochemistry 75, 433–453.

Li, K.Y., Coe, M.T., Ramankutty, N., De Jong, R., 2007. Modeling the hydrological impact of land-use change in West Africa. Journal of hydrology 337, 258–268.

Liu, H., Randerson, J., Lindfors, J., Massman, W., Foken, T., 2006. Consequences of Incomplete Surface Energy Balance Closure for CO2 Fluxes from Open-Path CO2/H2O Infrared Gas Analysers. Boundary-Layer Meteorology 120, 65–85.

Lloyd, J., Taylor, J.A., 1994. On the Temperature Dependence of Soil Respiration. Functional Ecology 8, 315. doi:10.2307/2389824

Luo, Y., Weng, E., Wu, X., Gao, C., Zhou, X., Zhang, L., 2009. Parameter identifiability, constraint, and equifinality in data assimilation with ecosystem models. Ecological Applications 19, 571–574.

Lussem, U., Waldhoff, G., 2013. Land use classification 2012 of the Rur Catchment. CRC/TR32 Database (TR32DB). Accessed from http://tr32db.uni-koeln.de/data.php?dataID=801 at 2013-09-12.

Mao, J., Ricciuto, D.M., Thornton, P.E., Warren, J.M., King, A.W., Shi, X., Iversen, C.M., Norby, R.J., 2016. Evaluating the Community Land Model in a pine stand with shading manipulations and 13CO2 labeling. Biogeosciences 13, 641–657. doi:10.5194/bg-13-641-2016.

Mauder, M., Desjardins, R.L., Pattey, E., Worth, D., 2010. An Attempt to Close the Daytime Surface Energy Balance Using Spatially-Averaged Flux Measurements. Boundary-layer meteorology 136, 175–191.

Mauder, M., Foken, T., 2011. Documentation and instruction manual of the Eddy covariance software package TK3. Univ.Bayreuth, Abt. Mikrometeorologie.

Mauder, M., Cuntz, M., Drüe, C., Graf, A., Rebmann, C., Schmid, H.P., Schmidt, M., Steinbrecher, R., 2013. A strategy for quality and uncertainty assessment of long-term eddy-covariance measurements. Agricultural and Forest Meteorology 169, 122–135.

Melaas, E.K., Richardson, A.D., Friedl, M.A., Dragoni, D., Gough, C.M., Herbst, M., Montagnani, L., Moors, E., 2013. Using FLUXNET data to improve models of springtime vegetation activity onset in forest ecosystems. Agricultural and Forest Meteorology 171–172, 46–56.

Metropolis, N., Rosenbluth, A.W., Rosenbluth, M.N., Teller, A.H., Teller, E., 1953. Equation of State Calculations by Fast Computing Machines. The Journal of Chemical Physics 21, 1087–1092.

Mitchell, S., Beven, K., Freer, J., 2009. Multiple sources of predictive uncertainty in modeled estimates of net ecosystem CO2 exchange. Ecological Modelling 220, 3259–3270.

Moffat, A.M., Papale, D., Reichstein, M., Hollinger, D.Y., Richardson, A.D., Barr, A.G., Beckstein, C., Braswell, B.H., Churkina, G., Desai, A.R., Falge, E., Gove, J.H., Heimann, M., Hui, D.F., Jarvis, A.J., Kattge, J., Noormets, A., Stauch, V.J., 2007.

Comprehensive comparison of gap-filling techniques for eddy covariance net carbon fluxes. Agricultural and Forest Meteorology 147, 209–232.

Montzka, C., Canty, M., Kreins, P., Kunkel, R., Menz, G., Vereecken, H., Wendland, F., 2008a. Multispectral remotely sensed data in modelling the annual variability of nitrate concentrations in the leachate. Environmental Modelling & Software 23, 1070–1081.

Montzka, C., Canty, M., Kunkel, R., Menz, G., Vereecken, H., Wendland, F., 2008b. Modelling the water balance of a mesoscale catchment basin using remotely sensed land cover data. Journal of Hydrology 353, 322–334.

Moore, C.J., 1986. Frequency response corrections for eddy correlation systems. Boundary-Layer Meteorology 37, 17–35.

Mo, X., Chen, J.M., Ju, W., Black, T.A., 2008. Optimization of ecosystem model parameters through assimilating eddy covariance flux data with an ensemble Kalman filter. Ecological Modelling 217, 157–173.

Oak Ridge National Laboratory Distributed Active Archive Center (ORNL DAAC). 2015. FLUXNET Web Page. Available online [http://fluxnet.ornl.gov] from ORNL DAAC, Oak Ridge, Tennessee, U.S.A. Accessed May 5, 2013.

Oleson, K., Lawrence, D.M., Bonan, G.B., Drewniak, B., Huang, M., Koven, C.D., Levis, S., Li, F., Riley, W.J., Subin, Z.M., Swenson, S., Thornton, P.E., Bozbiyik, A., Fisher, R., Heald, C.L., Kluzek, E., Lamarque, J.-F., Lawrence, P.J., Leung, L.R., Lipscomb, W., Muszala, S.P., Ricciuto, D.M., Sacks, W.J., Sun, Y., Tang, J., Yang, Z.-L., 2013. Technical description of version 4.5 of the Community Land Model (CLM).

Orchard, V.A., Cook, F.J., 1983. Relationship between soil respiration and soil moisture. Soil Biology and Biochemistry 15, 447–453.

Oren, R., Hsieh, C.-I., Stoy, P., Albertson, J., Mccarthy, H.R., Harrell, P., Katul, G.G., 2006. Estimating the uncertainty in annual net ecosystem carbon exchange: spatial variation in turbulent fluxes and sampling errors in eddy-covariance measurements. Global Change Biology 12, 883–896.

Panin, G.N., Tetzlaff, G., Raabe, A., 1998. Inhomogeneity of the land surface and problems in the parameterization of surface fluxes in natural conditions. Theoretical and Applied Climatology 60, 163–178.

Papale, D., Valentini, R., 2003. A new assessment of European forests carbon exchanges by eddy fluxes and artificial neural network spatialization. Global Change Biology 9, 525–535.

Park, S.K., Xu, L., 2013. Data Assimilation for Atmospheric, Oceanic and Hydrologic Applications (Vol. II). Springer Science & Business Media.

Parton, W.J., Stewart, J.W.B., Cole, C.V., 1988. Dynamics of C, N, P and S in grassland soils: a model. Biogeochemistry 5, 109–131.

Parton, W.J., Scurlock, J.M.O., Ojima, D.S., Gilmanov, T.G., Scholes, R.J., Schimel, D.S., Kirchner, T., Menaut, J.-C., Seastedt, T., Moya, E.G., Kamnalrut, A., Kinyamario, J.I., 1993. Observations and modeling of biomass and soil organic matter dynamics for the grassland biome worldwide. Global Biogeochemical Cycles 7, 785–809.

Peters, W., Jacobson, A.R., Sweeney, C., Andrews, A.E., Conway, T.J., Masarie, K., Miller, J.B., Bruhwiler, L.M.P., Pétron, G., Hirsch, A.I., Worthy, D.E.J., Werf, G.R. van der, Randerson, J.T., Wennberg, P.O., Krol, M.C., Tans, P.P., 2007. An atmospheric

perspective on North American carbon dioxide exchange: CarbonTracker. PNAS 104, 18925–18930.

Peylin, P., Law, R.M., Gurney, K.R., Chevallier, F., Jacobson, A.R., Maki, T., Niwa, Y., Patra, P.K., Peters, W., Rayner, P.J., others, 2013. Global atmospheric carbon budget: results from an ensemble of atmospheric CO 2 inversions. Biogeosciences Discussions 10, 5301–5360.

Piao, S., Sitch, S., Ciais, P., Friedlingstein, P., Peylin, P., Wang, X., Ahlström, A., Anav, A., Canadell, J.G., Cong, N., Huntingford, C., Jung, M., Levis, S., Levy, P.E., Li, J., Lin, X., Lomas, M.R., Lu, M., Luo, Y., Ma, Y., Myneni, R.B., Poulter, B., Sun, Z., Wang, T., Viovy, N., Zaehle, S., Zeng, N., 2013. Evaluation of terrestrial carbon cycle models for their response to climate variability and to CO2 trends. Glob Change Biol 19, 2117–2132.

Post, J., Hattermann, F.F., Krysanova, V., Suckow, F., 2008. Parameter and input data uncertainty estimation for the assessment of long-term soil organic carbon dynamics. Environmental Modelling & Software 23, 125–138.

Post, H., Hendricks Franssen, H.J., Graf, A., Schmidt, M., Vereecken, H., 2015. Uncertainty analysis of eddy covariance CO2 flux measurements for different EC tower distances using an extended two-tower approach. Biogeosciences 12, 1205–1221.

Post, H., Vrugt, J.A., Fox, A., Vereecken, H., Hendricks Franssen, 2016. Estimation of Community Land Model parameters with DREAM(zs) for an improved assessment of net carbon fluxes at European sites (under review for the JGR- Biogeosciences).

Propastin, P., Erasmi, S., 2010. A physically based approach to model LAI from MODIS 250m data in a tropical region. International Journal of Applied Earth Observation and Geoinformation 12, 47–59.

Pumpanen, J., Longdoz, B., Kutsch, W., 2009. Field measurements of soil respiration: principles and constraints, potentials and limitations of different methods, in: Soil Carbon Dynamics–An Integrated Methodology. Cambridge University Press, pp. 16–33.

Quéré, C.L., Andres, R.J., Boden, T., Conway, T., Houghton, R.A., House, J.I., Marland, G., Peters, G.P., Werf, G., Ahlström, A., 2012. The global carbon budget 1959–2011. Earth System Science Data Discussions 5, 1107–1157.

Qu, W., Bogena, H.R., Huisman, J.A., Vereecken, H., 2013. Calibration of a Novel Low-Cost Soil Water Content Sensor Based on a Ring Oscillator. Vadose Zone Journal 12, 1–10.

Qu, W., Bogena, H.R., Huisman, J.A., Martinez, G., Pachepsky, Y.A., Vereecken, H., 2014. Effects of soil hydraulic properties on the spatial variability of soil water content: evidence from sensor network data and inverse modeling. Vadose Zone Journal 13.

Rannik, Ü., Sogachev, A., Foken, T., Göckede, M., Kljun, N., Leclerc, M.Y., Vesala, T., 2012. Footprint Analysis, in: Aubinet, M., Vesala, T., Papale, D. (Eds.), Eddy Covariance, Springer Atmospheric Sciences. Springer Netherlands, pp. 211–261.

Raupach, M.R., Rayner, P.J., Barrett, D.J., DeFries, R.S., Heimann, M., Ojima, D.S., Quegan, S., Schmullius, C.C., 2005. Model-data synthesis in terrestrial carbon observation: methods, data requirements and data uncertainty specifications. Global Change Biology 11, 378–397.

Regionaler Klimaatlas Deutschland., 2015. Regionale Klimabüros der Helmholtz Gemeinschaft URL: http://www.regionaler-klimaatlas.de (28.4.2015).

Reichenau, Tim G., Wolfgang Korres, Carsten Montzka, Peter Fiener, Florian Wilken, Anja Stadler, Guido Waldhoff, and Karl Schneider. 2016. Spatial Heterogeneity of Leaf Area Index (LAI) and Its Temporal Course on Arable Land: Combining Field Measurements, Remote Sensing and Simulation in a Comprehensive Data Analysis Approach (CDAA). PLOS ONE 11 (7): e0158451. doi:10.1371/journal.pone.0158451.

Reichle, R.H., Koster, R.D., Liu, P., Mahanama, S.P.P., Njoku, E.G., Owe, M., 2007. Comparison and assimilation of global soil moisture retrievals from the Advanced Microwave Scanning Radiometer for the Earth Observing System (AMSR-E) and the Scanning Multichannel Microwave Radiometer (SMMR). J. Geophys. Res. 112, D09108.

Reichle, R.H., Kumar, S.V., Mahanama, S.P., Koster, R.D., Liu, Q., 2010. Assimilation of Satellite-Derived Skin Temperature Observations into Land Surface Models. Journal of Hydrometeorology 11.

Reichstein, M., Subke, J.-A., Angeli, A.C., Tenhunen, J.D., 2005. Does the temperature sensitivity of decomposition of soil organic matter depend upon water content, soil horizon, or incubation time? Global Change Biology 11, 1754–1767.

Reichstein, M., Beer, C., 2008. Soil respiration across scales: The importance of a model–data integration framework for data interpretation. Journal of Plant Nutrition and Soil Science 171, 344–354.

Rey, A., Pegoraro, E., Jarvis, P.G., 2008. Carbon mineralization rates at different soil depths across a network of European forest sites (FORCAST). Eur. J. Soil Sci. 59, 1049–1062.

Richardson, A.D., Hollinger, D.Y., Burba, G.G., Davis, K.J., Flanagan, L.B., Katul, G.G., William Munger, J., Ricciuto, D.M., Stoy, P.C., Suyker, A.E., Verma, S.B., Wofsy, S.C., 2006. A multi-site analysis of random error in tower-based measurements of carbon and energy fluxes. Agricultural and Forest Meteorology 136, 1–18.

Richardson, A.D., Hollinger, D.Y., Aber, J.D., Ollinger, S.V., Braswell, B.H., 2007. Environmental variation is directly responsible for short- but not long-term variation in forest-atmosphere carbon exchange. Global Change Biology 13, 788–803.

Richardson, A.D., Mahecha, M.D., Falge, E., Kattge, J., Moffat, A.M., Papale, D., Reichstein, M., Stauch, V.J., Braswell, B.H., Churkina, G., Kruijt, B., Hollinger, D.Y., 2008. Statistical properties of random CO2 flux measurement uncertainty inferred from model residuals. Agricultural and Forest Meteorology 148, 38–50.

Richardson, A.D., Hollinger, D.Y., Dail, D.B., Lee, J.T., Munger, J.W., O'keefe, J., 2009. Influence of spring phenology on seasonal and annual carbon balance in two contrasting New England forests. Tree physiology 29, 321–331.

Richardson, A.D., Black, T.A., Ciais, P., Delbart, N., Friedl, M.A., Gobron, N., Hollinger, D.Y., Kutsch, W.L., Longdoz, B., Luyssaert, S., Migliavacca, M., Montagnani, L., Munger, J.W., Moors, E., Piao, S., Rebmann, C., Reichstein, M., Saigusa, N., Tomelleri, E., Vargas, R., Varlagin, A., 2010a. Influence of spring and autumn phenological transitions on forest ecosystem productivity. Phil. Trans. R. Soc. B 365, 3227–3246.

Richardson, A.D., Williams, M., Hollinger, D.Y., Moore, D.J.P., Dail, D.B., Davidson, E.A., Scott, N.A., Evans, R.S., Hughes, H., Lee, J.T., Rodrigues, C., Savage, K., 2010b. Estimating parameters of a forest ecosystem C model with measurements of stocks and fluxes as joint constraints. Oecologia 164, 25–40.

Richardson, A.D., Anderson, R.S., Arain, M.A., Barr, A.G., Bohrer, G., Chen, G., Chen, J.M., Ciais, P., Davis, K.J., Desai, A.R., Dietze, M.C., Dragoni, D., Garrity, S.R., Gough,

C.M., Grant, R., Hollinger, D.Y., Margolis, H.A., McCaughey, H., Migliavacca, M., Monson, R.K., Munger, J.W., Poulter, B., Raczka, B.M., Ricciuto, D.M., Sahoo, A.K., Schaefer, K., Tian, H., Vargas, R., Verbeeck, H., Xiao, J., Xue, Y., 2012. Terrestrial biosphere models need better representation of vegetation phenology: results from the North American Carbon Program Site Synthesis. Glob Change Biol 18, 566–584.

Richardson, A.D., Aubinet, M., Barr, A.G., Hollinger, D.Y., Ibrom, A., Lasslop, G., Reichstein, M., 2012. Uncertainty Quantification. Eddy Covariance. A Practical Guide to Measurement and Data Analysis 173–209.

Rosolem, R., Gupta, H.V., Shuttleworth, W.J., de Gonçalves, L.G.G., Zeng, X., 2013. Towards a comprehensive approach to parameter estimation in land surface parameterization schemes. Hydrol. Process. 27, 2075–2097.

Saltelli, A., Sobol', I.M., 1995. About the use of rank transformation in sensitivity analysis of model output. Reliability Engineering & System Safety 50, 225–239.

Saltelli, A., Ratto, M., Andres, T., Campolongo, F., Cariboni, J., Gatelli, D., Saisana, M., Tarantola, S., 2008. Global sensitivity analysis: the primer. John Wiley & Sons.

Santaren, D., Peylin, P., Bacour, C., Ciais, P., Longdoz, B., 2013. Ecosystem model optimization using in situ flux observations: benefit of monte-carlo vs. variational schemes and analyses of the year-to-year model performances. Biogeosciences Discussions 10, 18009–18064.

Santaren, D., Peylin, P., Viovy, N., Ciais, P., 2007. Optimizing a process-based ecosystem model with eddy-covariance flux measurements: A pine forest in southern France. Global Biogeochem. Cycles 21, GB2013.

Scharnagl, B., Vrugt, J.A., Vereecken, H., Herbst, M., 2010. Information content of incubation experiments for inverse estimation of pools in the Rothamsted carbon model: a Bayesian perspective. Biogeosciences 7, 763–776.

Schmidt, M., Reichenau, T.G., Fiener, P., Schneider, K., 2012. The carbon budget of a winter wheat field: An eddy covariance analysis of seasonal and inter-annual variability. Agricultural and Forest Meteorology 165, 114–126.

Schulz, K., Jarvis, A., Beven, K., Soegaard, H., 2001. The Predictive Uncertainty of Land Surface Fluxes in Response to Increasing Ambient Carbon Dioxide. J. Climate 14, 2551–2562.

scilands GmbH, 2010. Digital Elevation Model 10 without anthropogenic landforms, Göttingen, Germany.

Sellers, P.J., Randall, D.A., Collatz, G.J., Berry, J.A., Field, C.B., Dazlich, D.A., Zhang, C., Collelo, G.D., Bounoua, L., 1996. A revised land surface parameterization (SiB2) for atmospheric GCMs. Part I: Model formulation. Journal of climate 9, 676–705.

Stocker, T.F., Qin, D., Plattner, G.K., Tignor, M., Allen, S.K., Boschung, J., Nauels, A., Xia, Y., Bex, B., Midgley, B.M., 2013. IPCC, 2013: climate change 2013: the physical science basis. Contribution of working group I to the fifth assessment report of the intergovernmental panel on climate change.

Stöckli, R., Lawrence, D.M., Niu, G.-Y., Oleson, K.W., Thornton, P.E., Yang, Z.-L., Bonan, G.B., Denning, A.S., Running, S.W., 2008. Use of FLUXNET in the Community Land Model development. J. Geophys. Res. 113, 1-19.

Stoy, P.C., Williams, M., Disney, M., Prieto-Blanco, A., Huntley, B., Baxter, R., Lewis, P., 2009. Upscaling as ecological information transfer: a simple framework with application to Arctic ecosystem carbon exchange. Landscape Ecology 24, 971–986.

Sus, O., Heuer, M.W., Meyers, T.P., Williams, M., 2013. A data assimilation framework for constraining upscaled cropland carbon flux seasonality and biometry with MODIS. Biogeosciences 10, 2451–2466.

Ter Braak, C.J.F., Vrugt, J.A., 2008. Differential Evolution Markov Chain with snooker updater and fewer chains. Stat Comput 18, 435–446.

Thornton, P.E., Law, B.E., Gholz, H.L., Clark, K.L., Falge, E., Ellsworth, D.S., Golstein, A.H., Monson, R.K., Hollinger, D., Falk, M., Chen, J., Sparks, J.P., 2002. Modeling and measuring the effects of disturbance history and climate on carbon and water budgets in evergreen needleleaf forests. Agricultural and Forest Meteorology 113, 185–222.

Thornton, P.E., Rosenbloom, N.A., 2005. Ecosystem model spin-up: Estimating steady state conditions in a coupled terrestrial carbon and nitrogen cycle model. Ecological Modelling 189, 25–48.

Thornton, P.E., Zimmermann, N.E., 2007. An improved canopy integration scheme for a land surface model with prognostic canopy structure. Journal of Climate 20, 3902–3923.

Thornton, P.E., Doney, S.C., Lindsay, K., Moore, J.K., Mahowald, N., Randerson, J.T., Fung, I., Lamarque, J.F., Feddema, J.J., Lee, Y.H., 2009. Carbon-nitrogen interactions regulate climate-carbon cycle feedbacks: results from an atmosphere-ocean general circulation model. Biogeosciences 6, 2099–2120.

Todd-Brown, K.E., Hopkins, F.M., Kivlin, S.N., Talbot, J.M., Allison, S.D., 2012. A framework for representing microbial decomposition in coupled climate models. Biogeochemistry 109, 19–33.

Todd-Brown, K.E.O., Randerson, J.T., Post, W.M., Hoffman, F.M., Tarnocai, C., Schuur, E.A.G., Allison, S.D., 2013. Causes of variation in soil carbon simulations from CMIP5 Earth system models and comparison with observations. Biogeosciences 10, 1717–1736.

Todd-Brown, K.E.O., Randerson, J.T., Hopkins, F., Arora, V., Hajima, T., Jones, C., Shevliakova, E., Tjiputra, J., Volodin, E., Wu, T., others, 2014. Changes in soil organic carbon storage predicted by Earth system models during the 21st century. Biogeosciences 11, 2341–2356.

Todd, R.W., Evett, S.R., Howell, T.A., 2000. The Bowen ratio-ene
estimating latent heat flux of irrigated alfalfa evaluated in a semi-arid, advective environment. Agricultural and Forest Meteorology 103, 335–348.

Tolk, L.F., Dolman, A.J., Meesters, A.G.C.A., Peters, W., 2011. A comparison of different inverse carbon flux estimation approaches for application on a regional domain. Atmos. Chem. Phys. 11, 10349–10365.

Tsubo, M., Walker, S., 2005. Relationships between photosynthetically active radiation and clearness index at Bloemfontein, South Africa. Theoretical and applied climatology 80, 17–25.

Turner, D.P., Göckede, M., Law, B.E., Ritts, W.D., Cohen, W.B., Yang, Z., Hudiburg, T., Kennedy, R., Duane, M., 2011. Multiple constraint analysis of regional land–surface carbon flux. Tellus B 63, 207–221.

Twine, T.E., Kustas, W.P., Norman, J.M., Cook, D.R., Houser, P.R., Meyers, T.P., Prueger, J.H., Starks, P.J., Wesely, M.L., 2000. Correcting eddy-covariance flux underestimates over a grassland. Agricultural and Forest Meteorology 103, 279–300.

Tyc, G., Tulip, J., Schulten, D., Krischke, M., Oxfort, M., 2005. The RapidEye mission design. Acta Astronautica, 4th IAA International Symposium on Small Satellites for Earth Observation 56, 213–219.

Verbeeck, H., Peylin, P., Bacour, C., Bonal, D., Steppe, K., Ciais, P., 2011. Seasonal patterns of CO2 fluxes in Amazon forests: Fusion of eddy covariance data and the ORCHIDEE model. Journal of Geophysical Research: Biogeosciences 116.

Vrugt, J.A., Robinson, B.A., 2007. Improved evolutionary optimization from genetically adaptive multimethod search. Proceedings of the National Academy of Sciences 104, 708–711.

Vrugt, J.A., ter Braak, C.J.F., Clark, M.P., Hyman, J.M., Robinson, B.A., 2008. Treatment of input uncertainty in hydrologic modeling: Doing hydrology backward with Markov chain Monte Carlo simulation. Water Resour. Res. 44, W00B09.

Vrugt, J.A., Ter Braak, C.J.F., Diks, C.G.H., Robinson, B.A., Hyman, J.M., Higdon, D., 2009. Accelerating Markov chain Monte Carlo simulation by differential evolution with self-adaptive randomized subspace sampling. International Journal of Nonlinear Sciences and Numerical Simulation 10, 273–290.

Vrugt, J.A., 2016. Markov Chain Monte Carlo Simulation Using the DREAM Software Package: Theory, Concepts, and MATLAB Implementation. Environmental Modelling & Software 75: 273–316.

Waldhoff, G., 2010. Land use classification of 2009 for the Rur catchment. TR32 1.

Waldhoff, G., Curdt, C., Hoffmeister, D., Bareth, G., 2012. Analysis of multitemporal and multisensor remote sensing data for crop rotation mapping. ISPRS International Archives of the Photogrammetry, Remote Sensing and Spatial Information Sciences, I-7 177–182.

Wang, G., 2007. On the latent state estimation of nonlinear population dynamics using Bayesian and non-Bayesian state-space models. Ecological Modelling 200, 521–528.

Wang, Y.-P., Leuning, R., Cleugh, H.A., Coppin, P.A., 2001. Parameter estimation in surface exchange models using nonlinear inversion: how many parameters can we estimate and which measurements are most useful? Global Change Biology 7, 495–510.

Wang, Y.P., Baldocchi, D., Leuning, R., Falge, E., Vesala, T., 2007. Estimating parameters in a land-surface model by applying nonlinear inversion to eddy covariance flux measurements from eight FLUXNET sites. Global Change Biology 13, 652–670.

Wang, Y.-P., Trudinger, C.M., Enting, I.G., 2009. A review of applications of model–data fusion to studies of terrestrial carbon fluxes at different scales. Agricultural and Forest Meteorology 149, 1829–1842.

Webb, E.K., Pearman, G.I., Leuning, R., 1980. Correction of flux measurements for density effects due to heat and water vapour transfer. Quarterly Journal of the Royal Meteorological Society 106, 85–100.

Williams, M., Schwarz, P.A., Law, B.E., Irvine, J., Kurpius, M.R., 2005. An improved analysis of forest carbon dynamics using data assimilation. Global Change Biology 11, 89–105.

Williams, M., Richardson, A.D., Reichstein, M., Stoy, P.C., Peylin, P., Verbeeck, H., Carvalhais, N., Jung, M., Hollinger, D.Y., Kattge, J., Leuning, R., Luo, Y., Tomelleri,

E., Trudinger, C.M., Wang, Y.P., 2009. Improving land surface models with FLUXNET data. Biogeosciences 6, 1341–1359.

Wilson, K., Goldstein, A., Falge, E., Aubinet, M., Baldocchi, D., Berbigier, P., Bernhofer, C., Ceulemans, R., Dolman, H., Field, C., Grelle, A., Ibrom, A., Law, B.., Kowalski, A., Meyers, T., Moncrieff, J., Monson, R., Oechel, W., Tenhunen, J., Valentini, R., Verma, S., 2002. Energy balance closure at FLUXNET sites. Agricultural and Forest Meteorology 113, 223–243.

Xiao, J.F., Davis, K.J., Urban, N.M., Keller, K., Saliendra, N.Z., 2011. Upscaling carbon fluxes from towers to the regional scale: Influence of parameter variability and land cover representation on regional flux estimates. Journal of Geophysical Research-Biogeosciences 116.

Xiao, J., Davis, K.J., Urban, N.M., Keller, K., 2014. Uncertainty in model parameters and regional carbon fluxes: A model-data fusion approach. Agricultural and Forest Meteorology 189–190, 175–186.

Xu, L., Baldocchi, D.D., Tang, J., 2004. How soil moisture, rain pulses, and growth alter the response of ecosystem respiration to temperature. Global Biogeochem. Cycles 18, GB4002.

Xu, T., White, L., Hui, D., Luo, Y., 2006. Probabilistic inversion of a terrestrial ecosystem model: Analysis of uncertainty in parameter estimation and model prediction. Global Biogeochemical Cycles 20.

Zacharias, S., Bogena, H., Samaniego, L., Mauder, M., Fuß, R., Pütz, T., Frenzel, M., Schwank, M., Baessler, C., Butterbach-Bahl, K., Bens, O., Borg, E., Brauer, A., Dietrich, P., Hajnsek, I., Helle, G., Kiese, R., Kunstmann, H., Klotz, S., Munch, J.C., Papen, H., Priesack, E., Schmid, H.P., Steinbrecher, R., Rosenbaum, U., Teutsch, G., Vereecken, H., 2011. A Network of Terrestrial Environmental Observatories in Germany. Vadose Zone Journal 10, 955–973.

Zeng, X., 2001. Global Vegetation Root Distribution for Land Modeling. J. Hydrometeorol. 2, 525–530.

Acknowledgments

First, I gratefully acknowledge my supervisor Prof. Dr. Harrie-Jan Hendricks Franssen for his great support during my doctoral studies, particularly for the many helpful conversations we had, the constant feedback he provided, and his confidence that everything will work out well at times when I was not so sure. Moreover, I am grateful to Expeer (Experimentation in Ecosystem Research), the EU project which financed my work on this topic, and facilitated a valuable cooperation and exchange with international project partners like Philippe Peylin and Natasha McBean. I also highly appreciate the support by Tim Hoar and the terrestrial science group from the National Center for Atmospheric Research (NCAR, Boulder CO, USA), and the collaboration with Andrew Fox from the National Ecological Observatory Network (NEON, Boulder CO, USA) during my research stay in Boulder (USA) and afterwards. Moreover, I am grateful for the collaboration with Jasper Vrugt, who introduced the DREAM approach to me and provided helpful support. Then, I gratefully acknowledge my colleagues from the Institute of Bio- and Geosciences at the Jülich Research Center, especially:

- The head of the institute, Prof. Dr. Harry Vereecken, for his support and feedback
- Alexander Graf and Marius Schmidt who provided the eddy covariance data for the Rur catchment sites and were always open for questions regarding that data
- Roland Baatz and Xujun Han for sharing input data and scripts to set up CLM for the Rur catchment application
- Pramod Kumbar and Guowei He for their support on high performance computing
- Carsten Montzka and Mohammed Ali for sharing the RapidEye LAI data provided by Blackbridge with the RapidEye Science Archive (RESA)

Besides, I gratefully acknowledge the TERENO and the Transregional Collaborative Research Centre 32 (TR32), for providing information and data required for this study. I also gratefully acknowledge the computing time granted on the supercomputer JUROPA at the Jülich Supercomputing Centre (JSC) and the Centre for High-Performance Scientific Computing in Terrestrial Systems: HPSC TerrSys, Geoverbund ABC/J, Leo-Brandt-Strasse, 52425 Jülich, Germany. For allocating the FLUXNET data used in this study, I am exceptionally thankful to CarboExtreme (EU-FP7) and Christian Bernhofer (DE-Tha, DE-Gri, DE-Kli) as well as CarboEuropeIP (EU-FP6) and Eric Dufrene (FR-Fon).

Band / Volume 335
Einfluss fehlpassungsinduzierter Spannungsfelder auf den Transportprozess bei ionischer Leitung
J. Keppner (2016), viii, 171 pp
ISBN: 978-3-95806-171-2

Band / Volume 336
Production and Characterization of Monodisperse Uranium Particles for Nuclear Safeguards Applications
A. Knott (2016), A-H, 123, xxviii, xiii pp
ISBN: 978-3-95806-172-9

Band / Volume 337
3D hydrological simulation of a forested headwater catchment: Spatio-temporal validation and scale dependent parameterization
Z. Fang (2016), XVII, 119 pp
ISBN: 978-3-95806-174-3

Band / Volume 338
Influence of Thermomechanical Treatment on High Temperature Properties of Laves Phase Strengthened Ferritic Steels
M. Talík (2016), xxiii, 130 pp
ISBN: 978-3-95806-175-0

Band / Volume 339
Groundwater recharge in Slovenia
Results of a bilateral German-Slovenian Research project
Mišo Andjelov, Zlatko Mikulič, Björn Tetzlaff, Jože Uhan & Frank Wendland (2016)
ISBN: 978-3-95806-177-4

Band / Volume 340
Atomic oxygen derived from SCIAMACHY O(^{1}S) and OH airglow measurements in the Mesopause region
Y. Zhu (2016), 206 pp
ISBN: 978-3-95806-178-1

Band / Volume 341
Diagnostic Mirror Concept Development for Use in the Complex Environment of a Fusion Reactor
A. Krimmer (2016), x, 123 pp
ISBN: 978-3-95806-180-4

Band / Volume 342
Long-Term Measurements of the Radiation Exposure of the Inhabitants of Radioactively Contaminated Regions of Belarus – The Korma Report II (1998 – 2015)
P. Zoriy, H. Dederichs, J. Pillath, B. Heuel-Fabianek, P. Hill, R. Lennartz (2016), ca 105 pp
ISBN: 978-3-95806-181-1

Band / Volume 343
Entwicklung und Charakterisierung von Nickel/Gadolinium-Ceroxid-basierten Anoden für die metallgestützte Festoxid-Brennstoffzelle
V. Rojek-Wöckner (2016), XVI, 136 pp
ISBN: 978-3-95806-182-8

Band / Volume 344
Reaction-diffusion modelling of hydrogen retention and release mechanisms in beryllium
M. Wensing (2016), 100 pp
ISBN: 978-3-95806-184-2

Band / Volume 345
Light Management by Intermediate Reflectors in Silicon-based Tandem Solar Cells
A. Hoffmann (2016), 199 pp
ISBN: 978-3-95806-186-6

Band / Volume 346
Design eines hocheffizienten Festoxid-Brennstoffzellensystems mit integrierter Schutzgaserzeugung
M. Engelbracht (2016), 190 pp
ISBN: 978-3-95806-189-7

Band / Volume 347
On model and measurement uncertainty in predicting land surface carbon fluxes
H. Post (2016), xviii, 135 pp
ISBN: 978-3-95806-190-3

Energie & Umwelt /
Energy & Environment
Band / Volume 347
ISBN 978-3-95806-190-3